Final Version: 6/4/21

Report of AAPM Task Group 155: Megavoltage photon beam dosimetry in small fields and non-equilibrium conditions

Indra J. Das

Department of Radiation Oncology, Northwestern Memorial Hospital, Northwest University Feinberg School of Medicine, Chicago, IL 60611, USA

Paolo Francescon

Department of Radiation Oncology, Ospedale Di Vicenza, Viale Rodolfi, Vicenza 36100, Italy

Jean M. Moran

Department of Medical Physics, Memorial Sloan-Kettering Cancer Center, New York, NY 10065, USA

Anders Ahnesjö

Medical Radiation Sciences, Department of Immunology, Genetics and Pathology, Uppsala University, 75185 Uppsala, Sweden

Maria M. Aspradakis

Institute of Radiation Oncology, Cantonal Hospital of Graubünden, Chur, Switzerland

Chee-Wai Cheng

Department of Radiation Oncology, University Hospitals Cleveland Medical Center, Cleveland, OH, 46255, USA

George X. Ding

Department of Radiation Oncology, Vanderbilt University School of Medicine, Nashville, TN 37232, USA

John D. Fenwick

Molecular and Clinical Cancer Medicine, Institute of Systems, Molecular and Integrative Biology, University of Liverpool, Liverpool L69 3BX, UK

M. Saiful Huq

Department of Radiation Oncology, University of Pittsburgh School of Medicine and UPMC Hillman Cancer Center, Pittsburgh, PA 15232, USA

Mark Oldham

Department of Radiation Oncology, Duke University Medical Center, Durham, NC 27710, USA

Chester S. Reft

Department of Radiation Oncology, University of Chicago, Chicago, IL 60637, USA

Otto A. Sauer

Department of Radiation Oncology, Klinik fur Strahlentherapie, University of Würzburg, Würzburg 97080, Germany

Conflict of interest

The Chair of the *[TG-155, Indra J Das]* has reviewed the required Conflict of Interest statement on file for each member of *[TG-155]* and determined that disclosure of potential Conflicts of Interest is an adequate management plan. Disclosures of potential Conflicts of Interest for each member of *[TG-155]* are found at the close of this document but there is no COI.

(Note: page numbers are inaccurate due to moving table and figures)

I.A. Table of Contents

ABSTRACT

Small-field dosimetry used in advance treatment technologies poses challenges due to loss of lateral charged particle equilibrium (LCPE), occlusion of the primary photon source, and the limited choice of suitable radiation detectors. These challenges greatly influence dosimetric accuracy. High profile radiation incidents have demonstrated a poor understanding of appropriate methodology for small-field dosimetry. These incidents are a cause for concern because the use of small fields in various specialized radiation treatment techniques continues to grow rapidly.

Reference and relative dosimetry in small and composite fields are the subject of the International Atomic Energy Agency (IAEA) dosimetry code of practice that has been published as TRS-483 and an AAPM summary publication.[1,2] The charge of AAPM task group 155 (TG-155) is to summarize current knowledge on small field dosimetry and to provide recommendations of best practice for relative dose determination in small megavoltage photon beams. An overview of the issue of LCPE and the changes in photon beam perturbations with decreasing field size is provided. Recommendations are included on appropriate detector systems and measurement methodologies.

Existing published data on dosimetric parameters in small photon fields (e.g. percentage depth dose, tissue phantom ratio/tissue maximum ratio, off-axis ratios, and field output factors) together with the necessary perturbation corrections for various detectors are reviewed. A discussion of errors and an uncertainty analysis in measurements is provided.

The design of beam models in treatment planning systems to simulate small fields necessitates special attention on the influence of the primary beam source and collimating devices in the computation of energy fluence and dose. The general requirements for fluence and dose calculation engines suitable for modeling dose in small fields are reviewed. Implementations in commercial treatment planning systems vary widely, and the aims of this report are to provide insight for the medical physicist and guidance to developers of beams models for radiotherapy treatment planning.

Key Words: small field, relative dosimetry, non-equilibrium dosimetry, treatment modalities, detector correction factors, photon dose modeling

II. LIST OF SYMBOLS AND ACRONYMS

AAPM	American Association of Physicists in Medicine
CPE	Charged Particle Equilibrium
$D_{\mathrm{w},Q_{\mathrm{msr}}}^{f_{\mathrm{msr}}}$	Absorbed dose to water at the reference depth z_{ref} in water in the absence of the detector in a field specified by f_{msr} and beam quality Q_{msr}.
DLG	Dosimetric leaf gap
$\%\mathrm{dd}(10)_x$	The photon component of the percent depth dose at 10 cm depth in water for a 10x10 cm^2 field
f_{clin}	Clinical (*clin*) non-reference radiation field
f_{msr}	Machine-specific reference (*msr*) field; the term is introduced for machines that cannot establish the conventional reference field (i.e. 10x10 cm^2). For example, f_{msr} in Gamma Knife, CyberKnife and TomoTherapy are 1.6 or 1.8 cm diameter, 6 cm diameter and 5x10 cm^2, respectively. Some standards laboratories provide calibration of ionization chambers in the hospitals *msr* field. This is not widely available yet
f_{ref}	Reference field (*ref*) specified in dosimetry protocols for which the calibration coefficient of an ionization chamber in terms of absorbed dose to water is provided by a standards laboratory
FWHM	Full-width at half-maximum
IAEA	International Atomic Energy Agency
ICRU	International Commission on Radiation Units and Measurements
IMRT	Intensity-modulated radiation therapy
GUM	Guide to the expression of Uncertainty in Measurements.
LCPE	Lateral charged particle equilibrium
$k_{Q,Q_0}^{f_{ref}}$	Correction factor that accounts for the differences between the response of a detector in field f_{ref} in a beam of quality Q and reference beam quality Q_0 as defined in TRS-483.[1]
$k_{Q_{clin},Q_{msr}}^{f_{clin},f_{msr}}$	The detector-specific correction factor that accounts for the difference between the responses of the detector in fields f_{clin} in a beam of quality Q_{clin} and in fields f_{msr} in beam of quality Q_{msr} as defined by Alfonso et al.[3]
k_{Q,Q_0}	The beam-quality correction factor, which corrects for the differences between the response of an ionization chamber in the reference beam of quality Q_o used for calibrating the chamber and the beam of quality Q (defined as $k_{Q,}$ in TG-51[4])
$(\bar{L}/\rho)_{air}^{w}$	Restricted mass collision stopping power ratio of water to air
$M_{Q_{msr}}^{f_{msr}}$	Detector reading in field f_{msr} and beam quality Q_{msr} corrected for influence of changes in pressure and temperature, incomplete charge collection, polarity effect and electrometer correction factor (TRS-483[1])
$(\overline{\mu_{en}}/\rho)$	Spectrum-averaged mass energy-absorption coefficient

MU	Monitor unit
N_{D,w,Q_0}	This is $N_{D,w}$ in TG-51,[4] and defined as the calibration coefficient in terms of absorbed dose to water for an ionization chamber at a reference beam of quality, Q_0 and field size f_{ref}
$N_{D,w,Q_0}^{f_{ref}}$	Calibration coefficient in terms of absorbed dose to water for an ionization chamber at a reference beam quality Q_0 in the conventional reference field f_{ref}.
OAR	Off-Axis Ratio
$\Omega_{Q_{clin},Q_{msr}}^{f_{clin},f_{msr}}$	Field Output factor that converts the absorbed dose to water for the machine-specific reference field f_{msr} to the absorbed dose to water for the clinical field f_{clin}.
PDD	Percent Depth Dose
P_{eff}	Effective point of measurement (EPOM)
pf_{clin}	Detector perturbation correction factor in clinical field, f_{clin}.
pf_{msr}	Detector perturbation factor in machine-specific reference field, f_{msr}.
Q_0	The reference beam quality in in a standards lab, usually ^{60}Co.
Q_{clin}	The beam quality of the clinical non-reference radiation field, f_{clin}.
Q_{msr}	The beam quality of the machine-specific reference field, f_{msr}.
Q_{ref}	The beam quality of the conventional reference field, f_{ref}.
r_{LCPE}	The minimum photon beam radius required to achieve *LCPE*
SBRT	Stereotactic body radiation therapy
$S_{\underline{clin}}$	Equivalent field size defined in terms of *FWHM*
SFD	Stereotactic Photon Diode
SRS	Stereotactic radiosurgery
SSD	Source-to-Surface Distance
TMR	Tissue Maximum Ratio
TPR	Tissue Phantom Ratio
TPR_{10}^{20}	The tissue phantom ratio in water at depth of 20 and 10 cm for a field size of 10x10 cm2 defined at a source to detector distance of 100 cm
VMAT	Volumetric modulated arc radiotherapy

III. INTRODUCTION

The use of small photon fields has grown rapidly with the implementation of modern specialized radiation treatment techniques, compared to traditional field sizes ranging from 4x4 cm^2 to 40x40 cm^2 typically used in radiation therapy.[5] Documents providing guidance and the implementation of stereotactic radiotherapy (SRT), stereotactic radiosurgery (SRS)[6,7] and stereotactic body therapy (SBRT)[8] have been published with limited coverage of small field dosimetry. The International Commission on Radiation Units and Measurements (ICRU) published Report 91[9] on prescribing, recording and reporting of stereotactic treatments with small photon beams which covers principles of small field dosimetry and small field treatment planning dose calculation algorithms. In linear accelerator-based SRS/SRT/SBRT, field sizes are defined by secondary/tertiary collimators (multileaf collimators (MLCs) and cones). Cones are divergent and are used to define circular fields with diameters typically varying from 0.5 cm to 4 cm.[10] Detailed information on SRS/SRT dedicated systems can be found in various references.[6,7,11] Table I summarizes the smallest collimator settings available on such radiotherapy delivery systems.

In intensity-modulated radiotherapy (IMRT), the intensity of a radiation beam is varied either through multiple static MLC segments (step-and-shoot technique) or MLC leaves moving continuously as radiation is delivered (sliding window technique).[12,13] Volumetric modulated arc therapy (VMAT) technology[14-16] is used to more efficiently deliver highly conformal dose distributions as an alternative to sliding window and step-and-shoot IMRT.[17] These techniques invariably use combinations of a large number of small fields. Dosimetric aspects specific to sliding window IMRT,[14] the physical and dosimetric aspects of a dynamic MLC, and the variation on dose output have been extensively studied.[18,19] The task groups TG-135 and TG-120 provide detailed discussion on the dosimetric tools and techniques for SRS and IMRT.[11,20]

In the context of small fields, lateral charged particle equilibrium (LCPE)[1] (earlier referred as lateral electronic equilibrium, LEE[21]) is not established in the region of a radiation detector. The loss of LCPE indicates that electrons traveling laterally out of the region are not replaced by electrons moving laterally into it.[22-24] The loss of LCPE occurs in the penumbra region, the interior portion of narrow fields, and regions with media of different densities (low density and interfaces).[24-27] The sensitive volume of a detector, its density, and atomic composition can strongly influence dosimetric accuracy when LCPE is lost. In very narrow fields (such as 1 x 5 cm^2), LCPE is not established even on the central axis; consequently small field conditions exist in these fields even when using detectors with very small sensitive volumes and width of 1-2 mm. Under small field conditions, the degree of LCPE on-axis and the output factor decrease rapidly with decreasing field size.[28,29] Beam output is reduced further as the beam collimating system starts to occlude the primary radiation source.[30,31] Electrons travel greater

distances in low-density media such as lung and air, causing LCPE to break down and further complicating dosimetry.[32,33]

Detectors of appropriate size, composition, and construction are needed for accurate dosimetric measurements in small fields. Many detectors are too large and cannot resolve penumbra widths of the beam profiles. Detector elemental composition impacts response in small fields to a lesser extent than the density.[23,27,34-37] Numerous experimental and Monte Carlo (MC) studies have investigated the suitability of detectors for the determination of dosimetric parameters, such as percentage depth dose (PDD), tissue maximum and phantom ratio (TMR, TPR) and field output factors (Ω), in small photon fields.[3,21,36,38-50] The consensus has been that suitable detectors must be considerably smaller than the field size as it impacts detector readings when CPE breaks down around the sensitive volumes of detectors.[3,51,52]

Studies from the early 2000's indicated the existence of substantial problems with the determination of absorbed dose and machine output in small fields. In the wake of prominent cases of misadministration of radiation therapy in Europe and North America, several organizations commissioned working groups to systematically address small field dosimetry. These included the British Society, Institute of Physics and Engineering in Medicine (IPEM), the AAPM, the International Atomic energy Agency (IAEA), the International Commission of Radiation Units and Measurements (ICRU) as well as other national organizations around the world. The IPEM summarized the challenges associated with the dosimetry of small fields and provided an early extensive review on detectors and their merits in small fields in IPEM Report 103.[30] The IPEM Report also includes recommendations on good practice in small field dosimetry. Around 2007, within the AAPM two initiatives emerged in parallel. One initiative, in collaboration with the International Atomic Energy Agency (IAEA) and termed here the IAEA-AAPM initiative, focused on the aspect of reference dosimetry in linac beams that could not realize the standard TG-51 conditions as well as small-field linac output. A parallel initiative emerged in 2007, was approved as TG-155 and focused on the details of small-field relative dose measurements and small-field aspects impacting treatment planning dose calculations.

The IAEA-AAPM initiative led to a formalism, commonly known as the 'Alfonso formalism', for reference dosimetry of small and nonstandard radiation fields[3]. Based on this formalism, IAEA-AAPM report TRS-483[1] (henceforth referred to as TRS-483) was developed that addresses calibration in nonstandard reference fields and linac output in static small fields. TRS-483 provides a code of practice for reference dosimetry for two specific sets of devices for which the conventional reference field conditions such as a 10 x10 cm^2 field size and 100 cm source-to-surface distance (SSD) or source-to-axis distance (SAD) are not applicable: (1) the specialized treatment devices such as Gamma Knife, TomoTherapy, and CyberKnife and (2) linear accelerators with small fields with configurations that do not satisfy the reference calibration conditions defined in existing dosimetry protocols.[4,53] TRS-483 provides calibration guidelines for absorbed dose in water traceable to a primary standard laboratory

using a reference ion chamber. The report introduces the concept of the machine specific reference (*msr*) field as many of the systems are unable to achieve the reference field size of 10x10 cm^2. For the determination of output in small static fields, the TRS-483 also presents compiled field output correction factors for detectors based on published literature at the time of publication.

While advanced guidance was being developed for small field dosimetry, there was an increase in the availability of machines with flattening filter free (FFF) beams on the latest design c-arm or robotic linacs which are being used to deliver SRS, SBRT, IMRT, and VMAT.[54] Lechner et al[55] have investigated small field dosimetry in such beams (FFF). The TRS-483[1] report and other guidance documents[56,57] provide physicists with information on the impact on measurements of the very high dose rates and non-flat profiles in FFF beams. Additionally, very small beams with millimeter widths are being used for animal irradiation but mainly with kilovoltage beams (e.g. 220 kVp with Cu filter).[58] Their dosimetry is beyond the scope of this report and will not be addressed here.

The purpose of the present TG-155 report is to describe the framework for applying detector-specific correction factors and the practical aspects of relative dosimetry of small fields. The report provides guidance and recommendations on the various types of active and passive detectors as well as guidance on measuring beam profiles, PDD, TMR/TPR in small radiation fields for beams from accelerating potential of 6 MV or lower since they are most often employed for specialized treatment procedures utilizing small fields. ICRU-91[9] contains a section on small field dosimetry and treatment planning systems (TPS) without referencing individual manufacturers. For several reasons such as the greater range of secondary electrons, possible limitations in the accuracy of dose calculation algorithms, as well as neutron production, ICRU-91 recommends not using energies above 10 MV for small fields.[9] Sources of errors in dosimetric measurements of small fields are analysed, and estimates are provided of expected uncertainties with 1 σ in measured beam profiles, PDDs, TMRs, and field output factors.

The input of data in a TPS measured with an inappropriately chosen detector has been one of the root causes of significant dosimetric errors which have resulted in patient harm reported in the media.[59-62] Solberg et al[63] provided an executive summary of these major incidences in SRS and SBRT. Care has been taken to ensure that the report by TG-155 is complementary and consistent with several important international reports while minimizing overlap of information. In this task group report, we provide a general overview of photon beam models used in dose calculation algorithms implemented in TPSs and in independent monitor unit (MU) verification software tools. Emphasis is placed on treatment planning dose calculation modeling in the case of narrow radiation fields. Many TPSs were originally designed and commissioned to describe fields larger than 3x3 cm^2, and an understanding of beam modeling is important when commissioning those systems to extend their use to small static or composite fields.[64] Additionally, key algorithm parameters influencing doses calculated in small fields are highlighted, and the importance of well measured dosimetric small field data is emphasized. This report also emphasizes

the importance and methodology to accurately measure dosimetric data used for the configuration of dose calculation models.

IV. BRIEF OUTLINE OF IAEA/AAPM FORMALISM

IV.A. Reference Dosimetry

The IAEA and the AAPM jointly published a new code of practice (CoP) for reference and relative dosimetry of small static photon fields used in external beam radiotherapy published as IAEA Technical Report Series TRS-483[1] and summarized in a paper by Palmans et al.[2] Although Alfonso et al.[3] provided options for calibration of static field as well as composite fields like IMRT, only static field recommendations are made in the TRS-483[1] protocol and Palmans et al[2]. The formalism for reference dosimetry in small static photon fields is a slightly modified version of the formalism recommended by Alfonso et al.[3] and essentially provides an extension to existing protocols for reference dosimetry.[4,53] It is based on the use of an ionization chamber that has been calibrated by a standards laboratory in a reference beam of quality Q_0. It defines the formalism and the necessary factors to account for possible changes in detector response to determine the absorbed dose to water under non-standard reference conditions, where the reference field size of 10×10 cm^2 cannot be realized, as illustrated in Figure 1. According to the formalism, the absorbed dose to water at the reference depth in the absence of the detector, $D_{w,Q_{\mathrm{msr}}}^{f_{\mathrm{msr}}}$ in a field size f_{msr} of beam quality Q_{msr} is given by:

$$D_{w,Q_{msr}}^{f_{msr}} = M_{Q_{msr}}^{f_{msr}} N_{D,w,Q_0}^{f_{ref}} k_{Q_{msr},Q_0}^{f_{msr},f_{ref}} \qquad (1a)$$

$$D_{w,Q_{msr}}^{f_{msr}} = M_{Q_{msr}}^{f_{msr}} N_{D,w,Q_0}^{f_{ref}} k_{Q,Q_0}^{f_{ref}} k_{Q_{msr},Q}^{f_{msr},f_{ref}} \qquad (1b)$$

where, subscripts and superscripts are defined in the section with the list of symbols. Briefly, the notation "*msr"* stands for the machine specific reference as shown in Table 1. *M* is the measurement reading by the detector (corrected for variations in ambient conditions, polarity, leakage, stem and recombination effects). The notation f_{ref} denotes the conventional reference field in dosimetry protocols. The calibration coefficient of an ionization chamber in terms of absorbed dose to water is provided by an Accredited Dosimetry Calibration Laboratory (ADCL) for the beam quality Q_o for a specific field size f_{ref}. The f_{msr} is the machine-specific-reference field, $N_{D,\mathrm{w,Qo}}$ is the chamber-specific calibration coefficient in terms of absorbed dose to water for ^{60}Co in f_{ref}, and $N_{D,w,Q_0}^{f_{ref}}$ is the chamber-specific beam-quality correction factor. The last factor in Eq. 1, $k_{Q_{\mathrm{msr}},Q}^{f_{\mathrm{msr}},f_{\mathrm{ref}}}$ is a correction factor that accounts for the detector´s difference in calibration coefficient between the conventional reference field and the actual f_{msr} field due to differences in field geometry, phantom material, and beam quality. The Eq 1(b) is used when no generic correction factor for the *msr* is available. The term $k_{Q,Q_0}^{f_{ref}}$ represents the difference

between the response of the ionization chamber between beam quality Q and Q_o at a standard laboratory.[2]

IV.B. Relative Dosimetry

Relative dosimetry typically refers to the determination of ratio of absorbed doses which may either be in reference or non-reference conditions. Dosimetric quantities such as PDD, TMR, OAR, and field output factor are, by definition, ratios of doses and fall under relative dosimetry. Following the IAEA-AAPM task group's formalism, the ratio of detector signal under non-reference conditions can be related to the ratio of absorbed doses through a detector-specific corrrection factor. This factor accounts for the difference in the detector response between the arbitary, non-reference, irradiation geometry and the reference irradiation geometry. Thus, absorbed dose to water at a point in a phantom in the absence of the detector for an arbitrary clinical field f_{clin} of beam quality Q_{clin} is expressed as:

$$D_{\mathrm{w},Q_{\mathrm{clin}}}^{f_{\mathrm{clin}}} = D_{\mathrm{w},Q_{\mathrm{msr}}}^{f_{\mathrm{msr}}} \Omega_{Q_{\mathrm{clin}}Q_{\mathrm{msr}}}^{f_{\mathrm{cli}n},f_{\mathrm{msr}}} \tag{2}$$

where $\Omega_{Q_{\mathrm{clin}}Q_{\mathrm{msr}}}^{f_{\mathrm{clin}}f_{\mathrm{msr}}}$ is the field output factor that converts the absorbed dose to water per monitor unit (MU) for the machine-specific reference field to the absorbed dose to water in the clinical field per MU.[1] This in essence is the traditional output factor or the in-water output ratio in TG-74[52] but it is emphasized that the field output factor is a ratio of absorbed doses and not a ratio of detector readings. This is made explicit by writing the field output factor as

$$\Omega_{Q_{clin},Q_{msr}}^{f_{clin},f_{msr}} = \frac{D_{w,Q_{clin}}^{f_{clin}}}{D_{w,Q_{msr}}^{f_{msr}}} = \left[\frac{M_{Q_{clin}}^{f_{clin}}}{M_{Q_{msr}}^{f_{msr}}}\right] k_{Q_{clin},Q_{msr}}^{f_{clin},f_{msr}} \tag{3}$$

and recognizing that a field output *correction* factor given by,

$$\mathrm{k}_{Q_{\mathrm{clin}},Q_{\mathrm{msr}}}^{f_{\mathrm{clin}},f_{\mathrm{msr}}} = \frac{\left(D_{\mathrm{w},Q_{\mathrm{clin}}}^{f_{\mathrm{clin}}}\right)/\left(M_{Q_{\mathrm{clin}}}^{f_{\mathrm{clin}}}\right)}{\left(D_{\mathrm{w},Q_{\mathrm{msr}}}^{f_{\mathrm{msr}}}\right)/\left(M_{Q_{\mathrm{msr}}}^{f_{\mathrm{msr}}}\right)}, \tag{4}$$

must be involved in determining the field output factor. This correction factor is involved for dose determination in small fields realized on specialized systems (such as Gamma Knife, TomoTherapy, CyberKnife, etc.) as well as for small fields defined on conventional linacs. The correction factor $k_{Q_{\mathrm{clin}},Q_{\mathrm{msr}}}^{f_{\mathrm{clin}},f_{\mathrm{msr}}}$ provides a link to dose based on ratios of detector readings as defined in Eq. 4 and differs from unity for the majority of the detectors.[1]

The calculation of $k_{Q_{\mathrm{clin}},Q_{\mathrm{msr}}}^{f_{\mathrm{clin}},f_{\mathrm{msr}}}$ for several detectors in small fields has been the subject of many investigations.[50,55,70-92] For air-filled ionization chambers, $k_{Q_{\mathrm{clin}},Q_{\mathrm{msr}}}^{f_{\mathrm{clin}},f_{\mathrm{msr}}}$ can theoretically be expressed as the

ratio of the product of the field size-dependent water-to-air restricted stopping-power ratios, $[\bar{L}/\rho]^{w}_{air}$, and the overall chamber perturbation correction factor, p, for the clinical (f_{clin}) and the machine-specific reference (f_{msr}) field sizes, respectively, as shown in Eq. 5.[93]

$$k^{f_{clin},f_{msr}}_{Q_{clin},Q_{msr}} = \frac{\left[\left(\frac{\bar{L}}{\rho}\right)^{w}_{air} \cdot P_{fl} \cdot P_{gr} \cdot P_{stem} \cdot P_{cell} \cdot P_{wall}\right]_{f_{clin}}}{\left[\left(\frac{\bar{L}}{\rho}\right)^{w}_{air} \cdot P_{fl} \cdot P_{gr} \cdot P_{stem} \cdot P_{cell} \cdot P_{wall}\right]_{f_{msr}}} \quad (5)$$

$P_{gr} \equiv P_{\rho} \cdot P_{vol}$ accounts for the perturbation due to mass density and volume effects.[93] Although an expression as in Eq. (5) can provide insight in the detector-associated physical reasons for the sometimes substantial correction factors in small field dosimetry, most calculated datasets are determined by using direct Monte Carlo calculations of the double ratio expressed in Eq. (4). The mean values of $k^{f_{\text{clin}},f_{\text{msr}}}_{Q_{\text{clin}},Q_{\text{msr}}}$ averaged over full-width at half-maximum (FWHM) and energy for various microdetectors have been provided for Siemens, Elekta and Varian machines by several investigators.[77,81,94]

Alternatively, the $k^{f_{\text{clin}},f_{\text{msr}}}_{Q_{\text{clin}},Q_{\text{msr}}}$ can be derived by experimentally comparing the detectors' response to that of a reference detector with known response in varying field sizes.[82,95,96] For the same nominal energy, the $k^{f_{\text{clin}},f_{\text{msr}}}_{Q_{\text{clin}},Q_{\text{msr}}}$ factor mostly depends on the field size, expressed by the FWHM of the dose profile at the depth of measurement, and the type of detector. It is less dependent on the linac model, the radial FWHM of the primary electron source or the energy of the primary electron source, the distance between the exit window, and the target. Therefore, it has been suggested that a mean value of $k^{f_{\text{clin}},f_{\text{msr}}}_{Q_{\text{clin}},Q_{\text{msr}}}$ could be used with an acceptable uncertainty.[77,81,94] Thus, the numerical values of $k^{f_{\text{clin}},f_{\text{msr}}}_{Q_{\text{clin}},Q_{\text{msr}}}$ cannot be applied to other types of detectors and machines of differing nominal energies. Of all these parameters the field size at the point of measurements, f_{clin}, is critical and needs to be determined experimentally. In TRS-483, all field output correction factors are specified as a function of the field size expressed by the parameter S_{clin} which is determined by explicitly measuring the FWHM of the profiles both in-plane (x) and cross-plane (y) direction at the depth of output determination as given in Eq. 6.

$$S_{clin} = \sqrt{FWHM(x) \bullet FWHM(y)} \quad (6)$$

Please note that this definition is applicable only in small fields whereas in broad beams, the equivalent square field is chosen such that it provides equal photon scatter contribution. Additionally, this definition is not fully verified and need additional investigations. For specialized machines like Gamma Knife, CyberKnife and TomoTherapy, users should refer to specific data collection using other types of detectors for which the detector-specific correction factor is known, such as reported by TRS-

483.[1] A number of other investigators have provided data available in the published literature for comparison and reference[74,76,78,81,94,97-102] that continues to be an active area of investigation.

V. SMALL FIELDS: DEFINITION OF FIELD SIZE

Small radiation fields have been defined as those that satisfy one or more of the following conditions: (1) LCPE lost on the beam axis, (2) collimating devices partially occlude the primary photon source in the beam axis, or (3) the detector size is large or similar to the beam dimensions.[1,30,31,51] The definition of a small radiation field is also subject to the detector characteristics with respect to the lateral range of the charged particles produced in the photon beam. Due to electronic disequilibrium, there is a reduction in dose at the center of the beam with decreasing field sizes[28,29,103]as shown in Figure 2.[104] Source occlusion or blocking of the direct beam source leads to a reduction of the primary fluence resulting in a drop in beam output and the overlap of penumbras formed from opposing collimating jaws (Figure 3). The dimension of the primary photon beam source (also known as the focal spot) is on the order of millimeters and varies with machine type and accelerating potential. Figure 4 shows a wide range of source sizes determined for older machine types and for new machines.[105] On the modern machines such as the Varian TrueBeam, the focal spot has been shown to be relatively constant (< 1.0 mm) for most energies and to have sub-millimeter (0.7-0.9 mm) dimensions in the x and y directions, as shown in Fig 4.[106]

The size of the focal spot of a linear accelerator can be determined by several methods and the interested reader is referred to the information provided in the references.[105-115] However, as subsequently noted, it is not critical in clinical practice and it is not necessary to measure the focal spot for clinical applications.

The signal measured by the detector in a small field depends predominantly on the size of the detector's active volume in relation to the field's dimensions, its construction, the densities of its active volume and other components.[116] As a result, perturbation of charged particle fluence can lead to an incorrect interpretation of the measured data.[116] Li et al.[21] demonstrated that complete LCPE could be achieved if the photon beam radius is greater than the range of secondary electrons to achieve lateral electronic equilibrium (r_{LCPE}), and provided a relationship between the beam quality index in terms of TPR_{10}^{20} and r_{LCPE} in water. If $\%dd(10)_x$ is used as the quality index as defined in TG-51,[4] the approach by Kalach and Rogers[117] can be used to convert TPR_{10}^{20} to $\%dd(10)_x$. Table II shows values of r_{LCPE} for the typical photon energies used in radiation therapy based on equation provided by Li et al.[21] The values in Table II may differ from more advanced calculations as provided by Papaconstadopoulos[118] and adopted in TRS-483[1] for r_{LCPE} as given in equation 7 in terms of TPR and equation 8 in terms of

$\%dd(10)_x$. It is noted that the value of r_{LCPE} will be slightly different (~1 mm) between these 2 equations.

$$r_{LCPE}\ (\text{cm}) = 8.369 \times \text{TPR}_{20,10} - 4.382 \quad (7)$$

$$r_{LCPE}\ (\text{cm}) = 77.97\text{x}10^{-3} \times \%dd(10)_x - 4.112 \quad (8)$$

It should also be noted that Equations 7 and 8 are meant to provide an approximate value of r_{LCPE} for a flattened beam, for the purposes of estimating when a beam is small and should be used with caution when FFF beams are considered. For FFF beams, the %*dd* and TPR values are substantially lower in comparison with the filtered beams of the same nominal MV value, while their r_{LCPE} is similar to that of a flattened beam at the same nominal accelerating potential.

Equations 7 and 8 can be further simplified when TCPE exists, e.g. where dose in water (D_w) and collision kerma (K_{coll}) are identical. Given these approximations for clinical radiation therapy applications, the range of r_{LCPE} values can then be represented in terms of d_{max} of the beam for a clinical physicist:

$$r_{LCPE}\ (\text{cm}) \approx 0.67\ d_{max} \pm 0.2 \quad (9)$$

where d_{max} is the depth of maximum dose in cm for the 10 x 10 cm^2 reference field. The range of the lateral travel of secondary electrons and its relation to LCPE becomes more prominent in inhomogeneous media, especially in a low-density medium such as lung.[116,119-121]

In summary, a photon field should be considered a small field when the distance from the central axis to the field edge is smaller than the lateral range for charged particle equilibrium. In practice this distance should be measured with respect to the outside dimension of the detector. As this task group provides recommendations on dosimetry in 6 MV photon beams, fields ≤ 3x3 cm^2 are typically considered as small fields. A field should be considered a small field if any of the following are true:

i) Field size (diameter) < $2*r_{LCPE}+d$, where d is the maximum detector outside dimension[1]

ii) Detector's view of the primary photon source is obstructed by the primary collimator

iii) The detector composition, size, or design is unsuitable for optimal readings in the measurement conditions (Section V)

VI. DETECTORS

The value of the r_{LCPE} greatly restricts the physical dimensions of the detectors that can be used for the experimental determination of small field dosimetric parameters such as field output factors (Ωs), beam profiles, PDD, TMR, or TPR.[34,37,122,123] When used for measurements in small fields, a detectors' reading must be adjusted for perturbation of particle fluence caused by the physical size, densities of the active volume, surrounding components, and non-water equivalence of the dosimeter.[124-126]

The Proceedings of the AAPM Summer School 2009[127] include a comprehensive discussion on various radiation detectors; however, these are not specific to small field measurements. Specific guidance on the choice of detectors for use in small field dosimetry can be found in IPEM Report 103;[30] AAPM Report TG-120[20] and ICRU-91[9], which include a list of detectors and their characteristics in small field and IMRT dosimetry. A comprehensive summary on detectors applicable for small field reference and relative dosimetry is included in the TRS-483 report.[1]

The characteristics of a detector including the value of $k_{Q_{\text{clin}},Q_{\text{msr}}}^{f_{\text{clin}},f_{\text{msr}}}$ and its constancy near unity is desirable as a function of clinical conditions but this is hard to achieve. There are only a few detectors (plastic scintillators, microDiamond, some diodes and Gafchromic films) that are suitable for small field dosimetry and have a near-unity $k_{Q_{\text{clin}},Q_{\text{msr}}}^{f_{\text{clin}},f_{\text{msr}}}$ factor. The characteristics of these detectors have been summarized in the literature.[128-130] This section presents a brief summary of the most relevant detectors and gel dosimeters for current and future applications.

Ionization chambers are the most commonly used detectors in radiation dosimetry due to their favorable characteristics (high precision, linearity, stability). However, small-volume ionization chambers experience low signal-to-noise ratios and in some cases high polarity effects. Solid-state dosimeters such as diodes and metal-oxide-semiconductor field-effect transistor (MOSFET) have smaller sensitive volumes. However, these dosimeters are not water-equivalent and exhibit a differential energy dependence with respect to water. Thus, their response with field size and the possible effects of beam hardening at the measurement depth must be considered. References[124,131-134] showed that for small fields the dose absorbed by the detector's sensitive volume depends upon its density. High-density detectors over-respond while low density detectors under-respond.[135] Correction factors are often required to convert the measured detector signal to an absorbed dose. As no single detector ensures accurate dose (± 2%) determination for field sizes ranging from 0.4x0.4 to 3x3 cm^2, the current consensus recommends making a careful comparison using at least two types of acceptable detectors.[43,131,132]

VI.A. Real time detectors

VI.A.1. Ionization chambers

Air-filled ionization chambers are most commonly used for dosimetric measurements because of their high sensitivity, long-term stability, reproducibility, and robustness. These characteristics enable ionization chambers to have calibration coefficients that are traceable to national standards. Two types of ionization chambers should be distinguished: cylindrical (known as "thimble" chambers) and plane-parallel. The sensitivity of air-filled ionization chambers varies in direct proportion to its sensitive volume. Very small-volume chambers produce very small ionization currents. Despite this limitation, small-volume ionization chambers have been used successfully for dosimetric measurements with substantial correction factors [38,40,50,122,136] for fields down to 1x1 cm^2.

VI.A.1.a. Signal-to-noise ratio and charge leakage

Small-volume ionization chambers are used to improve the spatial resolution of the measurements. The central electrode (0.55 to 0.16 mm in diameter) has been sometimes constructed from an electrode of high atomic number (Z) material (e.g., steel) in order to increase the signal from their small cavity. Monte Carlo simulations in a broad field and at depths down to 20 cm in water have shown that the high-Z material in the chamber creates perturbations up to 3% relative to detectors having a central electrode made of a low-Z material.[137] In the case of narrow fields, such perturbations have been shown to be significant. For this reason, in small field dosimetry the use of chambers with high-Z material should be avoided,[20,136] whereas ionization chambers with an aluminium central electrode do not exhibit large perturbation effects.

Due to the low sensitivity of small volume ionization chambers, a measurement that does not consider leakage can result in an error in absorbed dose of up to 16%, depending on the irradiation technique.[138] The magnitude of the leakage for the chamber-electrometer combination can be measured, assuming that the leakage current is constant and does not change when the beam is on. However, the background signal while the beam is on could be an issue when using a microchamber as shown by Sarkar et al.[139] In general, for small microchambers background readings that would be collected over the same time as the irradiation time should be subtracted. The extracameral signal increases with the length of irradiated cable in most chambers.[5,136] Leakage current introduced by the cable, connectors, and electrometer can have a larger effect on small-volume ionization chambers due to their smaller signal-to-noise ratios than for the larger volume Farmer type ionization chambers.

Another approach to overcome the challenge of low signal-to-noise ratio and to increase the sensitivity of small-volume chambers is to replace the air cavity with a dielectric fluid. Liquid-filled ionization chambers (LICs) have lower perturbation effects due to the near water equivalence of the dielectric liquids.[140,141] These enable the acquisition of measured datasets of higher spatial resolution (<0.1 mm). However, corrections for ion recombination effects are substantial, and the standard method of correcting ionization recombination does not apply to liquid-filled cavities because the collected charge does not increase linearly with voltage and only saturates at voltages too high that are suitable

for the insulators used in the detector.[142-145] Chung et al[146] have proposed an accurate method to correct for the general recombination in this detector. Nevertheless, liquid-filled ionization chambers,[77,142,147,148] despite being promising for small field dosimetry applications, are no longer commercially available.

VI.A.1.b. Volume averaging

Depending on the field size and dimensions of the ionization chamber, the detector's signal may need to be corrected for volume averaging. The correction value can be calculated using the beam profiles at the measurement point in the radiation field. It is determined by taking the ratio of absorbed dose to water at the point of measurement without the detector to the absorbed dose to water in the phantom averaged over the detector's sensitive volume without the detector. Profiles acquired for treatment planning commissioning should be corrected for volume averaging, or, preferably, use a small enough detector with minimum perturbation such that volume averaging is unnecessary

VI.A.2. Solid State Detectors

The high sensitivity of diodes permits their construction with very small dimensions, a favorable characteristic for use in small field dosimetry. The active volume of a diode is determined by the depletion region, which usually ranges between 20 and 80 μm. Diodes may need additional corrections for the following characteristics: dose rate dependence, variation of response with accumulated dose (up to 10%), temperature dependence (~0.3 %/^{0}C), contact material, energy, and angular dependence.[149]

The restricted mass collision stopping-power ratio of water to silicon, $[\bar{L}/\rho]_{Si}^{w}$ in small fields can be assumed to be close to the values at the reference field (10 x 10 cm^2), but this is not the case for the spectrum-averaged mass energy-absorption coefficient ratio of water to silicon $[\bar{\mu}_{en}/\rho]_{Si}^{w}$.[41,150] The atomic number and density of silicon are different from that of water thus greatly affecting the fractional response due to photoelectric interactions. This effect is prominent in large fields as the low-energy photon scatter is substantially contributing to the spectrum, but this is relevant for small-field dosimetry field output factors as detector readings are normalized to those in the reference (large) field. In small fields, an additional opposing effect is due to the presence of silicon, which introduces an overresponse in small fields due to a fluence perturbation that is not negligible.[151,152] A possible solution is to use the intermediate field method, sometimes referred to as the daisy chain technique[153-155] (cross calibration of diode against the chamber in an intermediate field to connect measurements in large fields to small fields) to measure field output factors normalized to a 10x10 cm^2 field. Although this technique accounts for the energy dependence of large fields, it does not consider the electron fluence perturbation due to the high density of silicon in small fields. A multi-institutional investigation from Japan for small field dosimetry with high definition MLC demonstrated large variations in the dosimetric parameters, for 5mm square fields and it was attributed to measurement errors due to selection of detectors.[156] It should

be noted that even with the use of the intermediate field method, each of the detectors involved in the process must be corrected for the appropriate field output correction factors.

Mobit et al[151] showed that Spencer-Attix cavity theory underestimate dose in high density cavity and provided Monte Carlo modeling of the energy response of the diodes in the detector cavity which included an energy dependent factor to compensate for the lack of local charged particle equilibrium that account for depth and field size dependence of the diode. Scott *et al*.[124] demonstrated with the Monte Carlo method that diodes could be used to determine the dosimetric parameters of small fields down to 1x1 cm^2. Simulations and measurements showed up to 4.5% differences in fields smaller than 1x1 cm^2, and they were attributed to the source occlusion and the difficulty of accurately modeling the focal spot.

VI.A.2.a. Diode Types

Three common types of silicon diode designs are commercially available: an unshielded diode (such as the PTW-60017) generally recommended for electron beams; a shielded diode (such as the PTW-60016) containing a tungsten-epoxy filter to decrease the fluence of low-energy photons, and an unshielded stereotactic photon diode (such as the IBA SFD) specifically designed for measurements in stereotactic beams. Details on the characteristics of recommended diode detectors are provided in TRS-483[1] and IPEM report 103.[30] Numerous publications recommend not using the shielded diode detectors for small field measurements because the shielding introduces additional scatter and increased directional dependence.[127,151,152,157] In contrast, several other publications reported <1% correction factors for a shielded diode in small fields.[158-160] Due to the conflicting published information regarding the use of a shielded diode in small field measurements, this report recommends the use of either a stereotactic or an unshielded diode since these latter diodes yield similar results in small field measurements (see data from TRS-483[1]). In any situation, correction factors are required when the fields are small for most diodes.

Recently a new unshielded silicon diode detector (PTW-60023) known as microSilicon detector with very small dimension (0.032 mm^3 with 1.5 mm diameter) with an epoxy density of 1.15 g/cm^3 was introduced and was found to have very suitable characteristics for small field dosimetry for both linear accelerators and CyberKnife.[161-164] Even the new shielded diode (PTW-60022) showed a very good characteristics and superior results in very small photon fields.[165]

VI.A.3. Diamond Detectors

Diamond detectors have been well characterized.[45,166-172] One of the main advantages with natural diamond detector for measurements in small fields is that it is nearly tissue equivalent due to the low atomic number, Z=6, which is close to that of water, Z=7.4. It offers relatively high spatial resolution with high sensitivity. Considerations hindering their widespread use are: (1) the mass density of diamond, 3.5 g/cm^3, is higher than that of water; (2) detector dimensions (including the materials around

the active layer) can be relatively large for use in very small fields such as 1x1 cm^2; (3) natural diamond detectors are very expensive; (4) diamond detectors have a dose rate dependent response;[166,169-171] (5) there is large variability in the dimensions of the active layer among detectors of the same type; and (6) as a result, correction factors are specimen dependent.[168,173] Thus, a single, universal, correction cannot be recommended for all diamond detectors of the same type. The issues mentioned above appear to be overcome with the introduction of synthetic chemical vapor deposited diamonds (CVD).[174] However, as in the case of solid-state detectors, in small field sizes (less than 1 x 1 cm^2) a CVD would also introduce photon fluence perturbations due to the difference of its mass density from that of water and would require appropriate corrections. Detectors with the early design using a natural diamond should be used only with proper Monte Carlo simulations or published and inter-compared $k_{Q_{\text{clin}}Q_{\text{msr}}}^{f_{\text{clin}}f_{\text{msr}}}$ factors.

With advances in crystal design, a single crystal diamond detector (known as the microdiamond detector) is commercially available. Due to its tissue equivalence and very small size, this detector has been shown to measure dose with only a small perturbation for very small field sizes. Several groups have shown that $k_{Q_{\text{clin}}Q_{\text{msr}}}^{f_{\text{clin}}f_{\text{msr}}}$ can be treated as unity in small fields.[78,81,101,175,176] However, data presented in the TRS-483[1] report show small correction factors below 1.5 cm^2, whereas for the natural diamond detector the correction factor is close to unity (±1%) for very small fields. De Coste et al[83] systematically characterized the PTW microDiamond field output factors. To better understand its response in small fields and to investigate its suitability for reference dosimetry, ten microDiamonds were calibrated under ^{60}Co irradiation. The field output factors measurements were performed in 6 MV photon beams from different manufacturer (CyberKnife, Varian, Elekta) linacs. They demonstrated that the detector response for field sizes larger than approximately 1 x 1 cm^2 did not require corrections, since $k_{Q_{\text{clin}}Q_{\text{msr}}}^{f_{\text{clin}}f_{\text{msr}}}$ is within 1% of unity. Das and Francescon[177] indicated that for very small fields (≤0.75 cm) $k_{Q_{\text{clin}}Q_{\text{msr}}}^{f_{\text{clin}}f_{\text{msr}}}$ may differ from the values published by Azangwe et al[82] which was adopted in TRS-483.[1] A recent publication by Casar et al[178] measured field output factors for a microDiamond and six other diode detectors and reported a systematic over-response of the microDiamond detector for fields ≤ 1x1 cm^2 which differed from the data provided in TRS-483.[1] It was suggested that correction factors for this detector depend upon the type of linac, beam energy, and collimation used. The behavior of correction factors for the microDiamond in very small field sizes (≤ 1x1 cm^2) was shown to depend on the combination of volume averaging and perturbation effects in the detector material. These two relevant effects compensate each other very well in the microDiamonds dosimeter, leading to relatively small overall output correction factors. As a result, correction factors lower than 1.5% were evaluated for beam sizes down to 5 mm in all linacs.[83] Because similar curves of $k_{Q_{\text{clin}}Q_{\text{msr}}}^{f_{\text{clin}}f_{\text{msr}}}$ were observed for the three different linacs used in this study, a single empirical function was calculated that provides output

correction factors within 0.5% from the MC values derived for all three linacs, down to fields as small as 4.6 mm in size. This maximum deviation was shown to be comparable to the intrinsic repeatability for the very small field sizes obtained by linacs using jaws and/or MLCs. Because of the conflicting data, users of the microDiamond dosimeter are encouraged to evaluate the detector performance and to compare it to the newly published data[83,84,91,177,179-182] that may differ from that of TRS-483.[1] Also, as recommended in TRS-483, at least one other suitable small field detector should be used to compare with the microDiamond measurements.

VI.A.4. Plastic Scintillators

Plastic scintillators have a number of favorable dosimetric characteristics for small field dosimetry, such as their relative tissue equivalence, angular independence, stable photon energy response, small size, density similar to water, and high sensitivity.[95,183-189] Morin et al.[188] compared small field measurements with plastic scintillators and various diodes for a CyberKnife. They reported good agreement between the scintillator measurements and Monte Carlo calculations. Due to their unique characteristics, this dosimeter can be used for small field dosimetry without any correction factors.[1,190] However, the development and clinical implementation of plastic scintillators are still a work-in-progress. There is only one such detector (PSD-W1) available from a single manufacturer (Standard Imaging, Middleton, WI). The use of the detector is not as straightforward as with other detector systems. Its use requires a certain irradiation geometry in a solid phantom, use of a specific type of readout system, and corrections to account for the additional signal (light) that is generated by the system itself (Cerenkov radiation in the light fiber).[191] Even though, $k_{Q_{\text{clin}}Q_{\text{msr}}}^{f_{\text{clin}}f_{\text{msr}}}$ is 1.0 for most field sizes as reported in TRS-483, the literature is not uniform about W1 being a problem free detector. This is due to Cherenkov radiation in the fiber in the commercial W1 as the calibration procedure involves a particular irradiation geometry of the fiber that does not necessarily account for a small-field application. The specific angular distribution of the Cherenkov radiation during irradiation in small fields, with the detector oriented vertically, led to systematic effects on the data in the smallest fields.[89,189] This behavior prevents the use of the W1 for scanning. To overcome some of the problem associated with W1, Standard imaging introduced PSD-W2 in 2019 with the added capability for using it in a scanning system. The PSD-W2 has a better system to counteract and mitigate the Cerenkov radiation. The charactersitics of the W2 are identical to that of W1 as has been reported by Galavis et al.[192] In addition to the W1 and W2 plastic scintillators, inorganic scintillator detector of about 200 μm diameter are being studied that could be used for ultra-high resolution dosimetry as shown by Debnath et al.[193]

VI.B. Passive Detectors

VI.B.1. Passive Detectors -2D

Radiochromic films[128,194-197] provide two-dimensional dosimetric information, not available immediately following irradiation; and for this reason they are referred to as 2D passive detectors. Because of their superior spatial resolution compared to other detectors, they can provide unsurpassed results for beam profiles and FWHM measurements. Radiochromic film can be used as well for field output factor measurements. Radiochromic film has an effective atomic number and density similar to water. It exhibits an approximately linear dose response and does not require chemical processing.[194] Detailed information on radiochromic film is available in the book by Das.[128] The optical density changes with time post-irradiation and its spatial non-uniformity can produce a position dependent variation in its radiation response.[47,198] The readout system could be relatively expensive, although inexpensive flat-bed color scanners can be used, provided that stringent protocols are followed in the readout procedure.[194] Numerous publications[198-201] have reported dose accuracy within ±2-3% in small fields. However, the dosimetric characteristics must be assessed when the manufacturer makes a significant change in the emulsion formula and it becomes a new product. This re-characterization may be time consuming for clinical use. For small fields, there are many controversial statements made for its handling and usage as reported in various publications.[202-206] In view of this controversy, it is advisable to strictly adopt all the precautions needed for radiochromic film dosimetry.[128,197]

V.B.2. Luminescent Dosimetry

Thermoluminescent detectors (TLDs), radio-photoluminescent glass (RPG), and optically stimulated luminescent detectors (OSLDs) are passive detectors that can be used only for point dose measurements.[207] TLDs come in various sizes and shapes such as powder, chips, rods, and microcubes. Depending on the composition of the TLD, they have a wide dose range and are nearly water-equivalent.[208] Their response is relatively energy independent for megavoltage photons and electrons, and they exhibit only a small angular dependence. However, unless individual detector sensitivities are determined, they have a relatively large uncertainty, about ±3%, and measurements are labor-intensive.[209] The uncertainty for relative measurements can be reduced to 1.0% by carefully determining individual relative sensitivities by calibrating them in a uniform radiation field and maintaining good quality control on the readout method.[210,211] Regardless, TLDs have been used for small field measurements.[39,198] Massilion et al.[201] showed that with proper care, TLDs can be used for small field measurements. Published studies[82,212] report that TLDs, especially 1x1x1 mm^3 microcubes, can be used with about a 1% correction factor for field sizes down to 0.6x0.6 cm^2. Detectors such as RPG[48,213-215] and OSLD[216,217] have dosimetric characteristics similar to TLDs for megavoltage photon and electron radiation except that light is used instead of heat to eject the trapped electrons to recombine with holes to emit light. RPGs and OSLDs have a similar linear dose response and are easier to handle compared to TLDs. They can be re-read since the radio-photo luminescent centers remain constant for RPGs, and each readout procedure of the OSLD detectors decreases the signal by only about 0.05%. However,

unlike TLDs, optical bleaching of OSLDs does not eliminate all of the radiation-induced effects. For accumulated doses greater than 20 Gy, there is an increase in the detector sensitivity and background signal. As with TLDs, the response is relatively independent of megavoltage photon and electron beam energies and exhibits only a small angular dependence.[48,215,218,219] They can be readout 10 minutes after irradiation. Commercially available OSLD using Al_2O_3:C can be placed in water for up to three hours without any degradation in its properties. However, it must be shielded from light, which can reduce the radiation-induced signal. These types of dosimeters as well as their specialized readout systems have recently become available and their dosimetric properties appear promising for use in small field dosimetry.[216] As with TLDs, individual relative sensitivities should be determined to reduce the measurement uncertainty to ±2.0%. Since the mass collision stopping-power and the mass energy-absorption coefficient ratios of water to LiF or Al_2O_3 are relatively constant for energies between 0.1 MeV and 10 MeV, it is expected that perturbation effects would be negligible for small detectors. However, the higher density of these detectors, especially OSLDs, causes electron fluence perturbation in small fields. The AAPM TG-191[207] has compiled guidance and recommendations on the clinical use of these detectors including their potential use for small field dosimetry. Correction factors for TLD microcubes and chips are also provided in the TRS-483 report.[1]

VI.B.2. Polymer Gel Dosimetry

Gel could be potentially useful for small field dosimetry because the following common sources of error can be eliminated or reduced: errors arising from aligning small detectors to small fields at all depths, volume averaging, and directional dependency. Furthermore, complex corrections to account for changes in media are not required. However, use of this techniques has been largely confined to academic institutions to date. Two main categories of 3D dosimetry systems are described below. Due to the limited number of clinical users, this class of detectors has not been described in recent international reports.[1,2,9]

Polymer gel dosimeters consist of a firm gelatine gel doped with a monomer compound. They respond to radiation by a polymerization reaction which forms polymer microparticles in proportion to the delivered dose.[220] The polymer microparticles remain fixed in position within the gel matrix and the distribution of particles can be imaged by MRI, optical-computed-tomography (optical-CT), or x-ray CT to provide information on delivered dose.[221,222] For small field dosimetry, optical techniques have an advantage of high spatial resolution and better signal-to-noise ratio compared to MRI readouts.[223] The polymer gel dosimeters (MGS Research Inc., Madison, CT) with Z_{eff} of 7.4 and density of 1.02 g/cm^3 provide an excellent medium for water-equivalent measurement. Polymer gels are used for a wide range of dosimetry measurements in radiation therapy including small field dosimetry.[95,224,225] With careful attention to readout and calibration procedures as outlined by Baldock et al,[222] isotropic 1 mm 3D dosimetry is feasible within ±3% uncertainty.

VI.B.3. Radiochromic Gel or Plastic Dosimetry

Two types of radiochromic 3D dosimeters are in current use: radiochromic plastic (PRESAGE®, Heuris Pharma, Skillman, NJ)[226-228] and radiochromic gels (e.g. Fricke or Fricke-Xylenol-Orange, FBX gels).[229,230] Both materials have good tissue equivalence, provide a linear optical response to radiation, and can be read out using optical-CT techniques. These materials lead to less scattered light compared with previous gel formulations which can enable a more accurate and faster readout.[221] A key concern of FBX gels is the significant fading (1-20 hours) due to the time dependent diffusion of ferrous or ferric ions in the gel. Thus, the dose distribution in FBX gels needs to be imaged shortly after capture of the signal. Fricke gels are considered relatively easy to manufacture and are used successfully. The PRESAGE® material does not suffer from diffusion, but it is not readily manufactured outside a specialized laboratory. PRESAGE® is insensitive to oxygen and exposure to the atmosphere and its hard plastic substrate negates the need for an external container (thus reducing edge artefacts) and facilitates moulding and shaping of various sizes and shapes of dosimeter. Several authors[226,230] have demonstrated measurement of small field output factors, PDD, and dose profiles with radiochromic gels and plastic. Good agreement is reported between these modalities at the ±1-3% level for small square fields above 5 mm in dimension. Agreement within 4% has been reported for ultra-small fields down to 1 mm.[231]

The current methods of 3D dosimetry are considered relative, and require a calibration procedure to convert the measured parameter to dose, although linear relationships have been widely reported for both polymer and radiochromic gels, and radiochromic plastic dosimeters. A good understanding of the performance and characteristics of the scanning system (either MRI or optical-CT) is also critical to achieve accurate results with all of the methods discussed above.[232] For small field commissioning measurements, the absolute dose delivered to the dosimeter can be tailored to maximize signal-to-noise ratio and dynamic range of the scanner.[233] For optical-CT readout, this dose should not exceed the range where scatter and cross artefacts have been observed.[221] Since gel dosimetry is still an active area of research and requires specialized readout equipment, further validation is needed to determine its appropriateness for small field dosimetry.

VII. RELATIVE DOSE PARAMETERS AND MEASUREMENTS

VII.A. Percentage Depth Dose (PDD)

PDD data are used as input for the configuration of beam models in TPSs and for second check MU calculation software. To directly measure PDDs for small fields, the most suitable detectors are micro-ionization cylindrical and parallel-plate chambers, typically with a sensitive volume less than 0.02 cm^3. TRS-483[1] has provided detailed discussion on the suitability of micro-ionization chambers in terms of their leakage, polarity effect, and P_{eff} for these measurements. Additional details are also available in various references for several beam energies.[122,234,235] Shielded and unshielded diodes,

including the smallest of the unshielded stereotactic photon diodes (SFDs), have also been suggested to be suitable for this measurement.[134,236] However, the use of a shielded diode is discouraged because its tungsten-epoxy layer below the silicon chip, which corrects for the high-Z response of the diode to low-energy photons at large fields, introduces measurement artefacts in small fields.[184] Also, radiochromic film is suitable for PDD measurements as it does not pose problems due to volume averaging or non-water equivalence.[131,237,238] However, the parallel irradiation of the Gafchromic™ EBT films is discouraged by Fontanarosa et al.[239] who observed unacceptable under dosage in PDD at depths greater than 15 cm (about 5% at 20 cm). In general, the detectors that have smallest $k_{Q_{\text{clin}},Q_{\text{msr}}}^{f_{\text{clin}},f_{\text{msr}}}$ factor (microdiamond, microslicon, plastic scintillator, EBT film)[83,90,102,128,161,163,191-193,197,240-242] are preferred to avoid the need to correct the PDD. If the institution is unable to justify acquisition of at least one of these systems, the method described by Francescon et al[243] and as described in Fig 5 could be adopted.

The methodology for the experimental determination of PDDs in broad fields is discussed extensively in TG-106.[5] The PDD has traditionally been calculated as a ratio of the ionization readings, and this method is generally valid for large (>3 x 3 cm^2) fields, where there is no need to correct for varying perturbation effects at varying depths. However, using the ratio of the readings to determine the PDD for small fields might not be valid if perturbation corrections indeed vary with depth and field size and requires accounting for the variation in the measurements. Therefore, with the choice of an appropriate detector, the detector-specific correction factor, $k_{Q_{\text{clin}},Q_{\text{msr}}}^{f_{\text{clin}},f_{\text{msr}}}$, where the field size at the position of the measurement increases is required. Francescon et al[243] showed that the largest corrections are in the build-up region where microchambers under-respond by up to 10% and diodes over-respond by up to 3%. Beyond the build-up region, stereotactic diodes and microdiamond detectors reproduce the PDD in water to within 2% up to a depth of 30 cm.[243] Microchambers over-respond for the PDD at deeper depths. This effect is greater if the stem axis is perpendicular to the beam axis because the chamber in the plane perpendicular to the beam axis occupies a greater area. Microchambers can be used for PDD measurements for field sizes greater than 10 mm without applying a correction factor.[1,90,91,244] If a microchamber is used, PDD measurements should be repeated with both positive and negative polarities and the results averaged. Also, the chamber leakage should be accounted for at various depths.[5,245] Figure 5 provides PDD data from two acceptable detectors for CyberKnife small field dosimetry. The data in the inset demonstrates that the PSD-W1 scintillator detector requires minimal corrections.

Seven major challenges need to be addressed for accurate PDD measurements of small beams: (1) choice of an appropriate detector, (2) alignment and orientation of the detector with central axis, (3) alignment of the detector axis to the beam's central axis at all depths, (4) positional accuracy defining the field, (5) placement of the reference detector within a small field, (6) monitoring machine output fluctuations, and (7) the physical size of a detector since it may not correspond to the size and position

of its sensitive volume. Therefore, a beam profile must be measured to find the position where the detector signal is maximum as described by Dietrich and Sherouse[153]. The effective detector size and central axis should be determined by scanning before measuring PDD or TMR. Also, the size of detector should be relatively small: its outer diameter should be less than half the field dimension to provide accurate data, as described in TG-120.[11]

The choice of detector (item 1) for specific clinical needs has been discussed in the AAPM TG-106 report.[5] The smallest unshielded stereotactic diode is recommended for these PDD measurements.[134,184] To address the issue of detector alignment for small field dosimetry (item 2), detector centering can be verified in a scanning water phantom by checking the symmetry of both orthogonal profiles at two different depths. Small-volume detectors (PinPoint, diamond, A-14 and stereotactic diode SFD) should be centered in a 1x1 cm^2 field as shown by Dieterich and Sherouse.[153] An offset of 0.5 mm in the detector alignment can be easily detected in the depth profiles, either visually or by the symmetry of the profiles. Any correction to detector position with respect to central axis needs to be verified with additional orthogonal profiles. In general, the detector position can be aligned with the central axis to within a fraction of a millimeter. This method has been successfully employed in the determination of the zero-field TMR.[246,247] Another method has been developed as well for detector alignment but may be more challenging to implement.[248] Finally, the orientation of the detector for scanning and PDD measurements can be important. TG-106[5] and the TRS 483[1] reports recommend alignment of the detectors for these measurements. For ionization chambers the effective point of measurements will depend on the orientation of the chamber. Because of the small dimensions of the recommended ionization chambers for small field measurements, the effective point of measurement shift will only have a minimal effect except in the build-up region with its high dose gradient.

The detector must be located along the beam's central axis for all depths so that the PDD is correctly measured. The effects of detector misalignment from the central axis (item 3) can be estimated by systematically shifting the center of the depth profiles in 0.2 mm steps in one direction for a 1x1 cm^2 field and examining the change in symmetry of the profiles and the relative dose values of the profiles after the shift. The dose profile symmetry indicates whether or not the detector is aligned with the central axis. For example, the change in the relative dose is $\leq$0.5% for the 1x1 cm^2 field within 1 mm of misalignment of the detector axis with central axis.[246] To reduce errors from possible misalignment of the detector with the central axis, one can use the serpentine method to reconstruct a PDD curve from the maximum signal of narrow beam profiles measured at several depths as is performed in TomoTherapy.[249]

The effects of the accuracy of jaw settings (item 4) can be estimated by repeating the dosimetry measurements and calculations for a range of field sizes (e.g. increments of 2 mm; range 1x1 cm^2 to 4x4 cm^2 fields). For example, with a field size change of negative 2 mm, the zero-field PDD is found

to increase by about 0.5% - 2% over the range of depths 5-30 cm. However, a field size change of +2 mm results in a lower zero-field PDD by about 0.5% - 1.0%.[246,247] If measurements are made with a scanning system, the collimator settings can be verified by measuring dose profiles along the two major axes. For other systems, radiographic or radiochromic film can be used to verify the collimator settings and FWHM.

Placing a reference detector in a small field is a challenging task and should not be attempted during beam scanning (item 5). Transmission chambers are commonly available from most vendors (Stealth chamber: IBA, T-Ref: PTW; SNC-600C: Sun Nuclear)[250,251] that can be used without any perturbations in small field scanning. If such a device is not available, the physicist should scan either without a reference chamber or with it placed at the bottom of the water tank with the gain increased to achieve a suitable signal. To monitor the machine output (item 6), measurements can be made with the detector under reference conditions at various time intervals to verify that the dosimeter response is reproducible over time or with a transmission chamber in the head under the collimator.

Monte Carlo simulations showed that the PDD is dependent on focal spot size.[111,243] A smaller focal size beam gives a higher PDD for the same depth and field size than that of a larger focal spot beam, but the PDD remains almost unchanged without effect on focal size for fields ≥ 5 mm diameter. Spot size has not been shown to affect dosimetric parameters in many modern machines (manufactured after 2005) having a sub-millimeter spot size.[252] The PDDs for a 5 mm diameter field, determined from measurements with diodes which have been corrected for dependencies and perturbations, were in good agreement (within 5%) with data from Monte Carlo simulations.[111] In fact, the dosimetric protocols for photons have no correction factor for PDDs. TRS 483[1] and Francescon et al[243] also confirmed that the effect of energy dependence is very small for small fields.

VII.B. Tissue Phantom Ratio (TPR)/Tissue Maximum Ratio (TMR)

TPR/TMR measurements are generally not required as input in advanced algorithms (kernel-based convolution/superposition, Monte Carlo-based, or direct solvers of the Boltzmann transport equation). However, such data are useful for verifying calculations with these algorithms as well as to use as input in many MU check software tools. TPR/TMR can be directly measured with the same detector systems as used for the direct measurement of PDDs.[10,39,47,131,253,254] TPR/TMR measurements have an advantage for beam modeling in that there are no inverse square law effects to be considered. Direct measurement of TPR/TMR solves some additional problems related to PDD measurements: (a) the detector axis remains aligned with the beam axis at different depths because the detector is not moved; and (b) the ratio between the dimensions of the detector and the field dimensions is constant when the depth increases so the correction to readings remains constant, that is, $k_{Q_{\text{clin}},Q_{\text{msr}}}^{f_{\text{clin}},f_{\text{msr}}}$ remains constant. Various approaches using standard water phantoms (such as PTW, Standard Imaging, IBA),

innovative scanning systems (such as ARM Inc, Port Saint Lucie, FL), and direct measurement using automated couch movements of modern linear accelerator with 1-D tank[255] can be used for the TPR/TMR measurements. The CyberKnife TPS system requires as input TMR data that can be obtained by mounting the detector in a birdcage fixed to the linac head and then moving the linac head along the z axis.

It has been shown that stereotactic diode and microchamber measured data are in good agreement with MC simulated data for very small fields (<2x2 cm^2).[243] The simulation shows that the TMR measured with a stereotactic diode and a microchamber reproduces data within 1% of the TMR in water (excluding factors that cannot be considered by MC simulation such as dose rate dependence, polarity effect, etc.).

VII.C. Conversion between PDD and TPR/TMR

TMRs have been calculated for small fields from PDDs measured with stereotactic diodes and from measured phantom scatter factors.[43,246,247,256-260] To determine TPR data for smaller fields (< 3 x 3 cm^2), Cheng et al[246] fitted the measured TPR data with a third-order polynomial and extrapolated the zero-field TPR values. The fitted data deviated by <1.5% from Monte Carlo calculated data for most depths. Xiao et al[260] used a two-step fitting process on measured TPR data to derive a function whose results differ by about 1% from the measured TPR data. Yang and Pino[261] proposed an analytical method for converting PDD measurements to TMR data for very narrow fields by parameterizing primary and scatter components. The calculated TMRs agreed within 2.0% with measured TMRs beyond the depth of maximum build-up. Several other methods,[130,262-264] have been proposed to account for non-equilibrium conditions and to convert PDD measurements to TMR data within 1% in field sizes down to 0.5 cm diameter. The conversion formulas are based on equivalent field size. The scatter ratios assume full LCPE and the conversion requires S_{cp} (total scatter factor) and S_p (phantom scatter factor) data for very small field sizes. To avoid the issues related to the lack of LCPE, an empirical method was developed by Ding and Krauss.[264] The empirical method can be used to obtain TPRs accurately from measured PDD curves for small fields down to a 4 mm diameter cone. Most of these methods are time consuming to apply in practice due to the analytical approach and have limited accuracy. It is recommended that any method adopted for small field TPR/TMR should be verified against the measurements, at least for a set of sampled points at various depths and field sizes.

VII.D. Profiles

The acquisition of beam profiles in small fields and the determination of the FWHM which specifies the f_{clin} parameter, needed to look up small field output correction factors typically involve the measurements of line doses at orthogonal directions (gun-target and left-right) at a variety of depths and a variety of field sizes down to 0.5 x 0.5 cm^2. Much of the discussion in the previous sections also

applies to the measurement of profiles. Primarily, it is recommended that the detector must be correctly mounted and precisely aligned (±0.01 mm) and oriented to the central axis of the beam at all depths. Use of a small-volume detector is extremely important for profile measurements to avoid incorrect determination of the width of the beam penumbra.[5,246,248] Figure 6 shows small field profiles for a 6 MV beam and the effects of source size and field diameter. In this example, measurements with a diode detector are compared against the data calculated with the Monte Carlo method. Good agreement is observed for fields of diameter as small as 5 mm with larger deviations seen for smaller fields. Volume averaging effects caused by detectors can greatly influence the quality of the measured dose profiles in terms of how well the detector can faithfully resolve the changes in the profile shape. Deconvolution methods that require knowledge about the effective area of the detector, which is modified by fluence perturbation[5,265-268] can be used to correct the detector signal accordingly but it mitigates the volume effect alone. However, the energy dependence is also important and needs to be accounted. To account for energy response variation along a profile, Wegener and Sauer[269] have proposed the convolution of the signals from 2 detectors of different types to resolve this issue in small field. A more accurate profile is shown for a smaller focal spot.[111] Therefore, small field profiles should be measured with the smallest, least perturbing tissue equivalent detectors[81,90,91,102,128,130,176,270] or radiochromic film.[128]

Figure 6 adapted from Sham et al[111] compares Monte Carlo data with diode-corrected data for relatively small fields. It also shows the effect of the focal spot size, with very good agreement found between calculations and corrected measurements down to 5 mm diameter fields. The differences increase in smaller fields (Figure 6). Monte Carlo simulations show that none of the detectors can exactly reproduce the profile due to perturbation by the detector materials in water. Additionally, Figure 7 shows profile (OAR) data from various detectors for a 6 MV beam for a 5 mm^2 field. When the perturbation factor is unknown, a detector with minimum perturbation should be used such as PSD (W2), microSilicon, and microdiamond.

Figure 8 shows the effect of detector materials on profile data.[77] The differences in diode and microLion profiles are relatively higher only in the tail, where the doses are very low. Therefore, the profiles obtained with these two types of detectors can be considered a good approximation of the profiles in water. The data for the microchamber demonstrates poorer performance compared to the other two detectors, even in the penumbra region of the profile. When diodes are used, one ought to verify that the dose rate dependence does not change with distance from the central axis. When detectors with a directional asymmetry (e.g. ionization chambers) are used, they can be mounted vertically (parallel to the beam axis), which can minimize the magnitude of penumbral blurring in both lateral and in-plane profiles. The user should first verify any significant stem effect or polarity effect. Additionally, the resolution of scanning in small fields should be kept to the limit of scanner motion which is typically 0.1 mm.

Radiochromic film may be used to compare with the detector-scanned profiles. This comparison requires adequate care to ensure careful film handling,[20,195,196] energy, and temporal responses for the radiochromic film.[271,272] The potential penumbral blurring associated with the film scanner may also need to be taken into account.

VII.E. Smoothing and Data Processing

When the PDD and profile data are acquired with the appropriate measurement equipment and a careful experimental set-up, extended post-processing to the acquired data may not be necessary. Nevertheless, it may be reasonable to use a modest low-pass filtering technique (or smoothing) to remove any high frequency noise components (abrupt spikes, wiggles etc). Most beam data acquisition system software provides a number of data smoothing options using a wide range of algorithms. Regardless of the filtering/smoothing technique that is used, it is imperative that the original dataset is retained to ensure that there are no unintended changes to the data such as artificial penumbral blurring or altering the peak of the profile. These considerations are especially important for scanned data for narrow field sizes. Typically, median filters are well suited for smoothing profile data, as the original data points are preserved. Median filtering should be applied to well-sampled profiles (i.e. with high point density or good resolution (0.01 cm)). The restrictions on PDD smoothing are less critical, and median or least-square fitting or other approaches may be sufficient. There is no general rule for how much smoothing can be applied to the data. Any post-processing to the data should not distort dose gradients present in the profiles, namely doses in the build-up region and/or the penumbra region. The originally scanned, raw data must always be saved as reference.

VII.F. Field Output Correction Factors

A sample of representative field output correction factors for various detectors is shown in Figure 9. More comprehensive tabulated data for wide range of detectors can be acquired from TRS-483[1] and from recent publications. Figure 9 demonstrates the wide variation of $k_{Q_{\text{clin}},Q_{\text{msr}}}^{f_{\text{clin}},f_{\text{msr}}}$ correction factors for different detectors for small fields.

Figure 10 (a) shows the difference of $k_{Q_{\text{clin}},Q_{\text{msr}}}^{f_{\text{clin}},f_{\text{msr}}}$ from 1.0 plotted on the y axis versus various types of detector for beams from a Varian accelerator (Das et al).[129] Similar data for CyberKnife is shown in Fig 10 (b). As one can see, there are certain detectors where the difference is relatively large and should not be used. Therefore, only detectors such as plastic scintillator, microdiamond, and Lion are suitable due to their smaller $k_{Q_{\text{clin}},Q_{\text{msr}}}^{f_{\text{clin}},f_{\text{msr}}}$ values. As shown by Liu et al 2014[273], the measured small field data for a 6 MV beam is relatively insensitive of the machine manufacturer for a given detector.

Even among the best detectors, there is a large variation in the correction factors as shown in Figure 11 when the field sizes are <1x1 cm^2. For fields < 1x1 cm^2, accurate measurement results require that an appropriate correction factor is chosen. For fields ≥ 1x1 cm^2, the correction factor would be smaller in magnitude making it more straightforward to accurately measure the dose as long as a proper detector is chosen. This is reflected in 0.8% variation for 1x1 cm^2 fields for most detectors as shown in caption.

VIII. DOSE MODELING IN TREATMENT PLANNING

Treatment planning system (TPS) dose calculations represent a critical link in the chain of clinical dosimetry events that determines the accuracy of the dose given to a patient. There are several guidance documents providing recommendations regarding commissioning and verification of TPS dose calculations.[274-276] TG-105[277] provided a detailed discussion on treatment planning based on Monte Carlo simulation, but it did not go into detail on small field modeling or dosimetry. ICRU Report 91[9] provides some basic principles relevant to TPS performance in small fields, however, there is as yet no dedicated recommendation focusing on small field TPS commissioning and verification. The goal of this section is to briefly summarize a number of important elements implicated in the commissioning of a TPS for dose calculations in small fields. It does not address the clinical process from simulation to treatment planning and delivery for small fields.

To accurately model the fluence for a small field, all causes of gradients need to be accurately modeled, including source occlusion, collimator leaf tip leakage, and collimator setting corrections. The modeling freedom for clinical physicists is often limited because TPSs commonly require the same set of beam model parameters for all field sizes. A workaround to mitigate insufficient modeling is to use different sets of parameters for different field size ranges in order to minimize resulting dose errors. Multiple field size ranges lead, however, to challenges in the clinical environment with respect to limiting choices, issues with plans that include both small and medium-sized fields, and the risk for using an incorrect beam model for a given patient's treatment plan.

The smaller a limiting field size is set, the more critical is the consistency and interplay between beam modeling, delivery, and measurements since errors in any of these may cause discrepancies. This approach can be further complicated by competing needs for SRS and SBRT programs and IMRT and VMAT plans. It is clear that tools for handling and verification of small field modeling are critical for TPS functionality.

VIII.A. Treatment planning dose calculations

Dose calculation algorithms used for treatment planning are generally classified as factor-based algorithms or model-based algorithms. According to ICRU Report 91[9], factor-based models are

inappropriate for use with very small fields when the irradiated medium deviates significantly from the homogeneous water medium in which the input basic dosimetric data are measured. Since this represents the majority of the important clinical applications, the remainder of section VIII will only address model-based calculations. Model-based dose calculations involve two separate steps: modeling based on field settings gives the energy fluence exiting the treatment machine, and modeling of the dose deposition resulting from irradiating a patient/phantom with that fluence. The energy fluence modeling is independent of the patient geometry and can thus be independently verified. A normalization versus a calibration measurement of absolute dose per monitor unit for a reference geometry is commonly done to yield dose per monitor unit from the TPS. The energy fluence per MU in air in the beam's isocenter plane can be viewed as composed of fluence of the direct source and fluence from different scatter sources such as flattening filter and collimators normalized to the monitor signal consisting of particles moving forward as well as those that are backscattered. For small fields, the scatter distributions from the flattening filter and collimators are relatively small without large variations so the major contributor to the overall energy fluence is the direct source. Hence, the size and shape of the direct beam source, collimator geometry, and the transmission through the MLC leaf tips are the most critical phenomena in modeling small field fluence for subsequent accurate dose calculation. This can become quite involved and various approximations are often used to simplify implementation or speed up calculations. Unfortunately, the applicability range of approximations is not always well known, challenging the clinical physicists for verification.

VIII.B. Direct Beam Source Size and Shape

Occlusion and partial attenuation of the primary source by the collimator leaf ends are the single most important processes that drive the small field characteristics of a linac. Most TPSs represent the primary source by a 2D Gaussian, occasionally with different widths in the in-plane and cross-plane directions. Even a point monodirectional electron beam is likely to result in a Gaussian-shaped photon source model due to multiple scattering in the target. Direct experimental determination of the size and shape of the direct source[105,106,108,112,278-280] reveals that it indeed varies with linac design and/or with energy on the same linac. Some bending magnet arrangements tend to yield prolonged, elliptical source shape profiles. The FWHM can vary over several mm in range, and eccentricities up to 3 mm (Fig 3).[105,106] Furthermore, the shape of the focal spot for fields smaller than 2x2 cm^2 also affects the shape of the depth dose curves.[74,111,234] Measurements of source sizes are not part of common clinical routine, although their critical role for small field output modeling deserves more attention. The source size is often used as a fitting parameter during commissioning of TPS algorithms by fitting calculated dose profiles for large fields to their measured counterpart. Small field output factors are particularly sensitive to source size settings because of the overlap of penumbral influences from any nearby field borders. While beam fitting based on small fields provides more sensitivity for source modelling, this method is

rarely recommended by TPS vendors to their users due to uncertainties in the small field measurements. However, carefully measured small field output factors should be used for verification of the field sizes considered for clinical use.[74,111,234]

VIII.C. Collimator Geometry and Fluence Modeling

After source occlusion, beam shaping is affected by the leakage profile through the rounded ends of MLC leaves (when present). In principle, the fluence modeling needs to trace individual rays from different parts of the source all through the MLC leaf ends to all positions in a beam exit plane as to ensure full accuracy of the result. Some TPSs do that, but approximations are common. Modeling the leaf attenuation profile as a shift in collimator position proportional to the effective gap offset defined by Losasso et al[281] (in later literature called the dosimetric leaf gap (DLG)[282]) has been shown to be insufficient.[283] A workaround for such TPSs has been suggested[283] through use of values optimized to minimize deviation over ranges of field sizes rather than use the directly measured dosimetric gap. The measured DLG for IMRT is unidirectional (either left to right or right to left), whereas it is bidirectional for VMAT which imposes challenges in beam modeling.[284,285] More accurate modeling can be achieved by combining explicit leaf tip projection corrections with a modulated transition region which may be beneficial for clinical use.[286] Using the IROC-Houston head phantom, Brandon et al[285] provided data on the error in treatment planning commissioning associated with the MLC offset setting. It was noted that for the PTV the coverage varied from -2% to +10% and for spinal cord -12% to +20% for values ranging from -2 mm to +2 mm of the MLC offset, respectively. It is also observed that there is a strong dependence on the PTV size with the largest differences for higher DLG.[284]

It follows that validation of the TPS interpretation of the collimator geometry is pertinent[51] but may not be sufficient due to the approximations. If several layers of collimators are aligned, the resulting source occlusion will be sensitive also to alignment errors. Thus, accelerator operating modes that retract the backup collimators from the field edges are preferable to ensure robust collimating conditions. The broadening of the fluence penumbra due to source occlusion will be larger when the collimator is higher up in the beam path. Collimator positioning is critical for verification. Central axis position offsets [287,288] should be considered and checked as these normally are included in the linac software. However, for small fields, aperture sizes estimated from FWHM may not map linearly to collimator settings due to non-equilibrium conditions that may cause bias leading to field size overestimation.[281,289]

VIII.D. Energy Fluence Mapping and Verification

During the commissioning process, it is helpful to review fluence maps with an adequate resolution (e.g. 0.1-0.2 cm) for a qualitative evaluation of the modeling of penumbra details, tongue-and-groove effects, and interleaf leakage. The energy fluence should be given in a normalization mode which is fully linkable to head scatter factors to facilitate verification.[64] For patient plans, viewing the

fluence map may be helpful when IMRT or VMAT is used for MLC-based delivery systems. The complexity of a field can then be analysed as a precursor to measurement-based QA for patients' treatment with VMAT to multiple spatially separated targets.[290,291] This information can be used to determine if a plan may need to be modified prior to measurements. This has value because the patient population often requires to be treated as quickly as possible and delays due to failed measurements would hinder patient care.

VIII.E. Dose Calculation Considerations

For small fields, model approximations play an important role when the dose calculation engine of a TPS calculates the resulting dose distribution from an energy fluence distribution.[292] With increasing beam energy, the lateral range of secondary electrons also increases. At higher beam energies (>6 MV), electron transport dominates the penumbra shaping, while at energies around 6 MV, both electron transport and source occlusion contribute to the penumbra shaping.[225,293]

Detailed descriptions of different algorithms and their expected performance in different situations are given in several references.[121,283,286,294] Algorithms such as pencil beam convolution (PBC) are not suitable in small fields due to many factors especially the poor lateral electron transport.[295] Even in the larger fields used in SRS/SBRT, dosimetric discrepancies between PBC and collapsed cone (CC) algorithms have been shown to be as high as 16%.[296,297] Numerous investigations have demonstrated its applicability to calculate dose under disequilibrium conditions, provided it is correctly configured, but statistical noise is associated with its use. Because of a large amount of lung in the field, the thorax region is challenging and presents difficulty in dose calculations due to the lateral disequilibrium where PBC approaches fail and are inadequate. Point kernel superposition/convolution models perform well for lung densities (with the exception of small deviations close to interface regions) if the kernels are correctly scaled to take into account lateral electron transport due to locally varying heterogeneities. Models intermediate between pencil and point based kernel also exist (e.g., the AAA model which is a pencil based model that includes an approximation for lateral electron scattering). In summary, for homogeneous, near-water-like tissue densities, a PBC model's final accuracy mostly depends on the accuracy of the beam model.[74,104,116,283,286,292,298] However, in heterogeneous calculations, PBC is not recommended in small field applications. For these reasons, Monte Carlo is often used to benchmark the implementation of different algorithms[119,120,298,299] and in some TPS systems, it is also directly used for patient dose calculations. Monte Carlo dose calculations explicitly account for full coupled photon and electron transport.

Besides approximations of the physical processes involved in dose deposition, discretization effects depend on the numerical implementation in the TPS algorithm and will influence the final dose accuracy. The common collapsed cone approximation for speeding up point kernel computations discretizes the directions to a limited set in which the radiant energy is spread from a primary point of

interaction.[292,300] Although the electron transport significantly blurs the dose deposition pattern, resolving small targets and organs-at-risk may still require a high resolution for the dose calculation. In particular, for non-Monte Carlo algorithms an isotropic grid of 2 mm is recommended while for Monte Carlo algorithms, voxel sizes between 1-2 mm on a side are considered appropriate (AAPM TG-101[8], AAPM TG-105[271], ICRU Report 91[9]).

VIII.F. TPS Configuration and Verification for Small Field Modeling

The configuration of the fluence and dose engines for model-based TPS algorithms, i.e. convolution/superposition or Monte Carlo simulations, requires the linac head geometry data as well as a set of measured dosimetric data (depth functions, profiles and output factors). The data are commonly used in an iterative process to set certain beam model parameters, such as the energy spectrum, the shape of the primary energy fluence distribution, and the width of the focal spot.[64,301-304] Errors in the measured data can therefore lead to an inappropriate choice of modeling parameters implemented in the TPS. The choice of the focal spot size in particular is of importance for small fields.[74,111,131] A value for this focal spot size may lead to the TPS performing optimally for broad beams, but less well for narrower beams. Source size model also has an impact on the penumbra of larger fields (e.g. 5x5 cm^2) that many physicist's tune to fit the data. Figure 12 shows how the calculated output ratio can vary with source size in a beam model and also illustrates how measurements with an inappropriate detector can affect the beam modeling. In the case of deviations, TPS model parameters may need to be adjusted appropriately. Some vendors have recommended instead that a separate beam model (treatment machine) be defined in the TPS for use with small fields (usually collimated to less than 1x1 cm^2). This strategy can be an impractical work around for IMRT planning if optimization engines result in a mixture of beam segments with small and large sizes.

In addition to the standard practice of verifying the modeling of small fields for homogeneous water medium, a model should preferably be tested in inhomogeneities, in particular for low density materials.[275,306] While making such measurements in inhomogeneous materials are delicate, point dose measurements are worthwhile to verify inhomogeneity corrections, as performed by Tang et al.[307] and Saxena et al.[308] Evaluation of calculations for inhomogeneous media is important and recommended by multiple AAPM guidance documents[13,65,306] These reports as well as guidance from ASTRO[309,310] also stress the value of testing a system from the beginning (often CT simulation) to the end (treatment delivery) which is also referred to as an end-to-end test. There are several commercial phantoms that include heterogeneous media that can be used with film or OSLDs. In addition, an independent evaluation such as available from IROC-Houston (http://irochouston.mdanderson.org/RPC/home.htm) provide invaluable information on the accuracy of the dose calculation and the entire treatment process.[311,312]

Published results that are custom to small fields use low-density media, such as lung-equivalent plastic, styrofoam, cork, or balsa wood could be used as an example.[298,313,314] As some commercial treatment planning systems made Monte Carlo (MC) algorithms available, these low-density media should first be investigated for conventional field sizes to validate the beam model.[119,120,298,315-319] As noted above, either a commercial phantom could be used or a phantom-by-mail service such as from IROC-Houston. When a TPS will be used in small photon fields, the characterization and modeling of the beam sources and collimating devices should be particularly checked for the following:

- Source size setting by verification of small field output for central and off-axis fields (see, e.g., Figure 12);
- MLC interleaf leakage and leaf-side modeling
- Jaw and leaf-end field edge positioning and transmission at different off-axis positions
- Backup jaw and MLC leaf-edge interaction (position of jaw with respect to MLC)
- Collimator intraleaf leakage modeling
- Penumbras, and full profile when penumbras overlap

In low-density media, widening of penumbra, build-down and re-build-up for beam passages through low-density regions are important considerations. A difficulty lies in validation of IMRT fields or VMAT arcs, which are composed of many small fields in this media. While most models may work well for IMRT if the MLC parameters (such as transmission, tongue and groove etc) are accurately modeled, the same algorithm may fail or be less optimal for VMAT treatment plans.[320]

IX. UNCERTAINTY

This section deals with uncertainty in field output and profiles. A detailed analysis of type A and B uncertainties for small field measurements is provided in TRS-483[1]. It is been shown that measurement uncertainty increases from ± 0.2% for fields >10 x10 mm^2 to 3.3% for 5x5 mm^2. An uncertainty analysis framework has been universally adopted from the Joint Committee.[321] Sources of these uncertainties include:

- Misalignment of the detector axis with respect to the beam central axis
- Deviation of the vertical motion of the scan arm from the central axis
- Inaccuracy in the collimator jaw settings
- Spectral changes with field size resulting in incorrect mass stopping-power ratios, especially for linear accelerators operating without a flattening filter
- Incorrect or unknown correction factors to convert detector signal to dose

- Incorrect SSD or measurement depth.

A detailed analysis of the uncertainties related to the relative output measurements of small beams is reported in various references [71,72,75,77,94,322,323] and has been estimated to be about 0.7% at one standard deviation (SD) in a small field in a homogeneous medium. The analysis that considers both type A and type B uncertainties on the correction factor $k_{Q_{\text{clin}},Q_{\text{msr}}}^{f_{\text{clin}},f_{\text{msr}}}$, indicates that this quantity can be provided by MC simulations with an overall uncertainty lower than 0.7% (1 SD).[77] Type A uncertainties are obtained through statistical methods. Conversely, type B uncertainties are related to non-statistical quantities such as errors in the underlying cross-section data and geometry approximations used in modeling the detector which are not influenced by the user but are obtained through other methods. From these considerations, the field factor defined in Eq. 3, has an associated overall uncertainty that depends on field size and detector but is about 1% (1 SD), considering the contribution of uncertainties of output measurements and $k_{Q_{\text{clin}},Q_{\text{msr}}}^{f_{\text{clin}},f_{\text{msr}}}$ by MC calculation. However, this is dependent on the detector and the field size. TRS-483[1] has provided detailed analysis and data for various detectors that varies from 0.7% to 3%.

The uncertainty of the profile measurements can be estimated by using the GUM (Guide to the expression of Uncertainty in Measurements) report.[321] The contributing uncertainties that should be considered are:

- Source-surface distance within 1.0 mm
- Horizontal position of the phantom within 0.2 degree
- Depth of the detector within 0.15 mm
- Position of the detector in the x, y directions within 0.1 mm is clinically acceptable, even though uncertainties of 0.05 mm and 0.01 mm are reported in the literature
- Reproducibility of the detector response is truly achievable at the <1% level or better at least in central region of a profile.[20,94,323] With modern detectors and electrometers, where conditions can leverage with a high signal to noise ratio (nC to pC, giving 1000 folds advantage e.g. 0.1%), this can even be achieved within 0.1%-0.2%.

For the profile the uncertainty is variable as the detector moves along the axis. It increases and has a maximum value where the gradient of the dose profile is maximum. A total uncertainty on $OF_{det}^{f_{clin}}$ measurements for the smallest field (0.5x0.5 cm^2) was found to be 0.7% at 1 standard deviation as reported by Francescon et al.[77] . The uncertainties calculated by separating the contributions to the uncertainty into the three main components, that is detector positioning, field size reproducibility due to the mechanical tolerances of MLC and output fluctuations of the accelerator were 0.2, 0.6, and 0.4%,

respectively, and when summed in quadrature gave a total relative uncertainty on $OF_{det}^{f_{clin}}$ of 0.75% (1σ). The two results, obtained with two different procedures, the first one providing directly the total uncertainty by measurements and the second one calculating the contributions of the different sources of uncertainties, provide a very similar and consistent result. By the analysis of the three separate uncertainties which contribute to the total uncertainty on $OF_{det}^{f_{clin}}$, we can see that the main source of uncertainty is due to the reproducibility of the field size due to the mechanical tolerance of MLC, assuming the uncertainty due to detector positioning is negligible due to high precision of most water tank systems.

The estimation of Monte Carlo uncertainties (type A and type B) of $OF_{det}^{f_{clin}}$ and of $k_{Q_{clin}Q_{10x10}}^{f_{clin}f_{10x10}}$ for several detectors and for the smallest field (0.5 x 0.5 cm^2) is also reported.[77] For larger fields, the geometrical uncertainty is expected to be lower and comparable to the values calculated by Wulff et al. [324] The total uncertainty (type A and B) due to the Monte Carlo calculations of $OF_{det}^{f_{clin}}$ and of $k_{Q_{clin}Q_{10x10}}^{f_{clin}f_{10x10}}$ is less than 0.7%.[94,323]

The uncertainties can be composed in a geometric mode as discussed in GUM[321] by using the MC procedure as proposed in several references[77,93,324-326] and shown in Figure 13. The uncertainties, largely dominated by the dose gradient and the detector sensitive volume. Additionally, it is usually greater for the y profile (lower jaws) compared to the x profile collimated by the upper jaws.

X. KEY RECOMMENDATIONS AND SUMMARY

These recommendations apply to small fields. A small field is defined as one in which lateral charged particle equilibrium cannot be established (see Table II). The definition of a small field depends on the beam energy. In general, fields ≤ 3x3 cm^2 can be treated as small for most photon energies (Section IV). It is reported that a few microchambers can be used without correction factor on the determination of output factors for fields > 1.5x1.5 cm^2 or diameter > 1.5 cm^2.[190] Such detectors can be used both with the stem axis parallel or perpendicular to the beam axis. For fields <1.5 cm^2, it is recommended that these are placed with the stem parallel to the beam axis with specific correction factors to convert the reading to dose as shown in TRS-483.[1]

X.A. Detector choice considerations

- For fields less than 1x1 cm^2, the interplay of source occlusion and detector dimensions demands careful selection of the detector. (Section VII F, Fig 11)
- Select a small-volume detector with minimal energy, dose, and dose rate dependence (Section IV).

- A detector with a known $k_{Q_{clin},Q_{msr}}^{f_{clin},f_{msr}}$ factor that is preferably close to one[129] should be selected, and proper measurement methods should be used (Section VII F). The values of $k_{Q_{clin},Q_{msr}}^{f_{clin},f_{msr}}$ for various detectors are provided in the TRS-483 that could be used unless a revised value from recent literature is available as shown in reference for microDiamond.[129,181,182]
- Unshielded stereotactic and electron diodes, plastic scintillators, microdiamonds and microSilicon are suitable detectors for measurements in small fields (Section VII F, Fig 10).
    - The advantages of plastic scintillator detectors (W1 and W2) are their small size, tissue equivalence, angular independence, and density similar to water.
    - The W1 plastic scintillator may have difficulty discriminating spectral sensitivity in small fields (Section V).
- For field sizes ≤ 1x1 cm^2 (Section V.A.2.a), an unshielded stereotactic diode, electron diode, plastic scintillator, and single crystal microdiamond are recommended.
- For field sizes > 1x1 cm^2, very small ionization chambers (micro-ionization chambers)[5] (excluding those with high-Z electrode) are suitable.
    - The response of an ion chamber is less affected by variations in low-energy photon fluence than diodes.
    - The selected detector should be evaluated for the signal-to-noise ratio and the measurements corrected for any polarity effects[327] and volume averaging (Section V.A.1).
- To use radiochromic film as one of the dosimeters, a flatbed scanner should be commissioned for dosimetry applications and a robust program with respect to the handling and processing of the film as described in TG-235[197] (Section V.B.3).

X.B. Measurement considerations

- For fields less than 1 x 1 cm^2, the interplay of source occlusion and detector choice demands precise positioning of the detector.
- The resolution of the scanning measurement should be smallest possible to the limit of device usually 0.1 mm.
- Dosimetric measurements should be performed with more than one detector system.
- Strategies to minimize variations in measurements among users should be tested, utilized, and shared (Section V).

- The daisy chain approach[153-155,328] can be used to determine output factors for the complete range of field sizes needed clinically. However, it should be remembered that this method normalizes the response increase in large fields, it does not account for the fluence perturbation effect that may require a correction. It is emphasized that if better detectors are available, they should be purchased and used so one does not need to over-rely on the daisy-chain method (Section V.A.2).
    - In this situation, unshielded stereotactic diodes can be used to measure the output in field sizes ≤ 3x3 cm^2 and small ionization chambers be used to measure the output from 3x3 cm^2 to 10x10 cm^2 reference field.
- While the changes in energy spectrum may be significant for small fields, the effect on the changes in mass stopping-power ratios is negligible (< 0.5%).[36,150,329,330] Hence, the actual factors that contribute to $k_{Q_{clin},Q_{msr}}^{f_{clin},f_{msr}}$ are the various perturbation factors as shown in Eq.5. (Section IV B)
- The electrometer and triaxial cables as well as any connector and additional cables need to be of a high quality to measure signals in the 10^{-12}-10^{-13}C range. The effect of leakage current should be evaluated and then corrected in the measurement when necessary (Section V.A.1.a).

X.C. TPS commissioning considerations

- Measured data that are required as input for treatment planning system (TPS) configuration and beam modeling need to strictly adhere to the requirements of the TPS manufacturer (Section VII.H).
- Measured data should be compared with specific published data from a similar machine. If a difference between published and measured data is observed, the sources of the discrepancies must be understood in the context of source size, measurement and uncertainties, as described.[105,107-109,280] Significant discrepancies should be resolved prior to clinical use (Section VII.H).
- The TPS performance should be validated with corrected measurements from two recommended detectors when used for treatment planning with small fields.
- Although pencil beam dose engines are expected to perform reasonably well in homogeneous media, their use in inhomogeneous medium is not recommended. Dose engines based on the Monte Carlo method, Boltzmann equation solvers, or point kernel convolution/superposition are the most accurate method for modeling dose from small fields within inhomogeneous media.
- A fine calculation grid size (such as ≤ 1 mm) should be used for small field applications (Section VII.G).

X.D. Independent checks

- Small field dosimetric measurements should be verified independently, either through measurements or through an independent external audit, such as that carried out by IROC-Houston[331,332] or in European countries with postal dosimetry services as described by del Mar Espinosa et al[333] referring to published data would also be helpful.
- A phantom test from CT simulation through treatment delivery, known as an end-to-end test, should be performed and may involve an independent assessment of the delivered dose (Section VII.G).

As noted in the introduction, there are a number of guidelines and recommendations related to small field dosimetry. This report focused on relative dose measurements with respect to detector choice and the importance of more than one appropriate detector for these measurements. Important considerations for the measurement setup were defined as well as some limited information regarding TPS calculations for small fields.

XI. ACKNOWLEDGMENTS

We are thankful to the many reviewers from the Work Group on Radiation Dosimetry, the Radiation Dosimetry and Treatment Planning Subcommittee, the Therapy Physics Committee and the Science council. We would like to thank to various professional editor such as Ms Deborah Skinner Nolan and to Katherine Molnar-Kimber, Ph.D. (Kimnar Group LLC, Worcester, PA) for their editorial assistance during many versions of the Task Group. Finally, our special thanks to Sonja Dieterich and Jan Seuntjens for their untiring support in many iterations of the review process.

Disclosure Statement (inserted at the close of the document)

The members of *[TG-155]* listed below attest that they have no potential Conflicts of Interest related to the subject matter or materials presented in this document.

Indra J. Das

Paolo Francescon

Jean M. Moran

Anders Ahnesjö

Maria M. Aspradakis

Chee-Wai Cheng

George X. Ding

John D. Fenwick

M. Saiful Huq

Mark Oldham

Chester S. Reft

Otto A. Sauer

Figure Captions

Figure 1. Schematic overview of the dosimetry of small static fields with reference field, according to the formalism proposed by Alfonso et al.[3] the flow chart indicates the process in achieving dose in f_{msr}. The figure was adapted from Alfonso et al.[3] for the static field calibration process.

Figure 2. Comparison between Monte Carlo simulated and experimentally measured dose profiles for 6 MV at 1.5 cm depth in water. Note the reduction in dose at the central axis as the field size is reduced. The reference beam (10×10 cm^2) was calibrated according to the AAPM TG-51[4] dosimetry protocol to give 1 cGy/MU at 100 source-to-surface distance (SSD) at a depth of 1.5 cm. The Monte Carlo simulation was also normalized to provide 1cGy/MU for the same reference condition. For a large field, the magnitude is 100% (not shown in the figure) whereas for a small field (shown in the figure), the output is low (55%). Reproduced from Ding et al.[104]

Figure 3. Source size and detector size with respect to collimator setting. Left: When the field size is reduced, it obstructs the source and limits the photon fluence. Right: As the field size is reduced, the penumbrae from opposing jaws overlap and the dose drops at the center of the field. As a result, the FWHM of the dose profile is no longer equal to the collimator setting. (Adapted from Das et al.[51]).

Figure 4. Iso-intensity and focal spots of Varian and Siemens accelerators. (a) Iso-intensity plots of the focal spots from Varian and Siemens accelerators. The intensity distribution shown corresponds to 90%, 70%, 50%, 30% and 10% intensities. The 90% intensity corresponds to the innermost line and the 10% intensity corresponds to the outermost line with other intensity lines in between. (i) Varian 2100C, 6 MV, (time point 1); (ii) Varian 2100C, 6 MV, (time point 2 after 2 years); (iii) Varian 2100C, 18 MV, (time point 1); (iv) Varian 2100C, 18 MV, (time point 2 after 2 years); (v) Siemens KD-2, 6 MV; and (vi) Siemens KD-2, 23 MV. The square grid size is 1x1 mm^2. Additional focal spot images can be viewed in the reference by Jaffray et al.[105] (b) Focal spot from three True Beams (T1, T2, T3) for 6 and 10 MV with and without FFF. The dimensions in x and y directions are noted. Modern machines such as the Varian TrueBeam have sub-millimeter focal spot sizes in both dimensions.[106] Image reproduced from Sawkey et al.[106]

Figure 5. PDD of CyberKnife for 2 cones with two detectors. Inset is difference plot in dose compared with PSD detector that does not require correction. Adapted from Francescon et al.[243]

Figure 6. The influence of varying source sizes FWHM of a Gaussian focal spot distribution approximating the actual focal spot) on the off-axis ratio**.** Comparison of the calculation of small field profiles with the Monte Carlo method with corrected diode data (symbol). (Reproduced from Sham et al[111] with permission).

Figure 7. Beam profiles showing the OAR of the 5-mm collimator measured at a depth of 10 cm with the Exradin W1 PSD scintillator detector, PTW 60012 diode, and PTW 31014 microchamber with the stem axis parallel to the beam axis before and after applying the correction factor for 5-mm collimator from CyberKnife. Adapted from Francescon et al.[77]

Figure 8. Monte Carlo simulated ratios of the off-axis ratio (OAR) with and without consideration of detector in water for the 5x5 mm^2 field for 6 MV beam (modified from Francescon et al[77]). The detector configuration is explicitly included in the simulation to obtain the most accurate results when compared with experimental profiles. For diode and microLion detectors, the differences are relatively higher only in the tail region. Therefore, the profiles obtained with these two detectors can be considered a good approximation to the profiles in water. The PinPoint detector on the other hand shows worse results for the profile than the other two detectors, even in the penumbra region of the profile, due to its characteristics including the material composition. The field edge is indicated by the line at 2.5 mm.

Figure 9. Effect of field size on the detector-specific correction factors. $k_{Q_{clin},Q_{msr}}^{f_{clin},f_{msr}}$ was calculated as the mean over all the values obtained by changing the linac models, (Siemens Primus and Elekta Synergy 6 MV), the radial FWHM and energy of the electron source as presented by Francescon et al.[77] These values can also be used with caution for Varian 6 MV machines. The maximum statistical uncertainty is ±0.003 (1 σ). Data from TRS-483[1] for various detectors at 10 cm depth differed for small fields. The differences between studies could be due to variations in depth (d_{max} vs 10 cm) in the Monte Carlo simulations.

Figure 10. Variation in the detector-specific correction factor induced by different detectors. (a), The variation of $k_{Q_{clin},Q_{msr}}^{f_{clin},f_{msr}}$ from unity for 5x5 mm^2 field is plotted for a wide range of detectors for a Varian IX machine and (b) for a CyberKnife unit with a 5 mm diameter cone. Adapted from Das et al.[129]

Figure 11. Variation of $k_{Q_{clin},Q_{msr}}^{f_{clin},f_{msr}}$ versus field size for four suitable detectors (courtesy of Indra J. Das). Please see that the variation is larger for smaller fields.

Figure 12: Illustration of variation in the calculated output factor with different effective source diameters used in the beam modeling of Helax-TMS treatment planning system. A diameter of 2.5 mm, which gave the best match in field output factors at d_{max} (S_{cp}) between measurement and calculation for collimator settings greater than 3.0 cm, was used to configure the TPS for use with broader beam sizes greater than 3.0 cm. Adapted from Aspradakis et al.[305] with permission.

Figure 13. Fractional uncertainties (1σ) for a dose profile at 10 cm depth of a 5x5 mm^2 nominal field size of an Elekta Synergy 6 MV machine along the y direction (lower diaphragm). The uncertainties considered are: Total = total combined uncertainty, Depth = depth of the detector, Position = position

of the detector in the y direction, Alignment = misalignment of the detector axis with respect to the beam central axis. Statistics = fluctuations of the machine output, Detector = sensitivity of the detector. Conservatively, the statistical distribution is considered uniform. (Figure courtesy of Paolo Francescon).

(References may be out of order due to elimination of table and figure from the text, please check)

XII. REFERENCES

1. IAEA TRS 483. *Dosimetry of small static fields used in external beam radiotherapy: An IAEA-AAPM International Code of Practice for reference and relative dose determination, Technical Report Series No. 483.* Vienna, Austria: International Atomic Energy Agency;2017.
2. Palmans H, Andreo P, Huq MS, Seuntjens J, Christaki KE, Meghzifene A. Dosimetry of small static fields used in external photon beam radiotherapy: Summary of TRS-483, the IAEA-AAPM international Code of Practice for reference and relative dose determination. *Med Phys.* 2018;45(11):e1123-e1145.
3. Alfonso P, Andreo P, Capote R, et al. A new formalism for reference dosimetry of small and nonstandard fields. *Med Phys.* 2008;35:5179-5186.
4. Almond PR, Biggs PJ, Coursey BM, et al. AAPM's TG-51 protocol for clinical reference dosimetry of high-energy photon and electron beams. *Med Phys.* 1999;26(9):1847-1870.
5. Das IJ, Cheng CW, Watts RJ, et al. Accelerator beam data commissioning equipment and procedures: Report of the TG-106 of the therapy physics committee of the AAPM. *Med Phys.* 2008;35(9):4186-4215.
6. Schell MC, Bova FJ, Larson DA, et al. *Sterotactic Radiosurgery: Report of the Task Group 42, RadiationTherapy Committee, AAPM Report No. 54* New York, NY: American Insitute of Physics; 1995.
7. Goetsch S, Alvarez PE, Bednarz G, et al. Gamma Stereotactic Radiosurgery Dosimetry and Quality Assurance (TG 178). *Med Phys.* 2021;(under review).
8. Benedict SH, Yenice KM, Followill D, et al. Stereotactic body radiation therapy: the report of AAPM Task Group 101. *Med Phys.* 2010;37(8):4078-4101.
9. ICRU Report 91. *Prescribing Recording, and Reporting of Stereotactic Treatments with Small Photon Beams.* Bethesda, MD: International Commission on Radiation Units and Measurements;2017. ICRU Report 91.
10. Das IJ, Downes MB, Corn BW, Curran BJ, Wasik MW, Andrews DW. Characteristics of a dedicated linear accelerator-based stereotactic radiosurgery-radiotherapy unit. *Radiother Oncol.* 1996;38:61-68.
11. Dieterich S, Cavedon C, Chuang CF, et al. Report of AAPM TG 135: Quality assurance for robotic radiosurgery. *Med Phys.* 2011;38(6):2914-2936.
12. IMRT Collaborative Working Group. Intensity-modulated radiotherapy: current status and issues of interest. *Int J Radiat Oncol Biol Phys.* 2001;51(4):880-914.
13. Ezzell GA, Galvin JM, Low D, et al. Guidance document on delivery, treatment planning, and clinical implementation of IMRT: report of the IMRT Subcommittee of the AAPM Radiation Therapy Committee. *Med Phys.* 2003;30(8):2089-2115.
14. Verbakel WF, Cuijpers JP, Hoffmans D, Bieker M, Slotman BJ, Senan S. Volumetric intensity-modulated arc therapy vs. conventional IMRT in head-and-neck cancer: a comparative planning and dosimetric study. *Int J Radiat Oncol Biol Phys.* 2009;74(1):252-259.
15. Otto K. Volumetric modulated arc therapy: IMRT in a single gantry arc. *Med Phys.* 2008;35(1):310-317.
16. Ling CC, Zhang P, Archambault Y, Bocanek J, Tang G, Losasso T. Commissioning and quality assurance of RapidArc radiotherapy delivery system. *Int J Radiat Oncol Biol Phys.* 2008;72(2):575-581.

17. Palma D, Vollans E, James K, et al. Volumetric modulated arc therapy for delivery of prostate radiotherapy: comparison with intensity-modulated radiotherapy and three-dimensional conformal radiotherapy. *Int J Radiat Oncol Biol Phys.* 2008;72(4):996-1001.

18. Litzenberg DW, Moran JM, Fraass BA. Verification of dynamic and segmental IMRT delivery by dynamic log file analysis. *J Appl Clin Med Phys.* 2002;3(2):63-72.

19. Wu Q, Arnfield M, Tong S, Wu Y, Mohan R. Dynamic splitting of large intensity-modulated fields. *Phys Med Biol.* 2000;45(7):1731-1740.

20. Low DA, Moran JM, Dempsey JF, Dong L, Oldham M. Dosimetry tools and techniques for IMRT. *Med Phys.* 2011;38(3):1313-1338.

21. Li XA, Soubra M, Szanto J, Gerig LH. Lateral electron equilibrium and electron contamination in measurements of head-scatter factors using miniphantoms and brass caps. *Med Phys.* 1995;22:1167-1170.

22. Attix FH. *Introduction to Radiological Physics and Radiation Dosimetry.* New York: John Wiley & Sons; 1986.

23. Zhu TC, Bjarngard BE, Shackford H. X-ray source and the output factor. *Med Phys.* 1995;22(6):793-798.

24. Bouchard H, Seuntjens J, Palmans H. On charged particle equilibrium violation in external photon fields. *Med Phys.* 2012;39(3):1473-1480.

25. Kumar S, Fenwick JD, Underwood TS, Deshpande DD, Scott AJ, Nahum AE. Breakdown of Bragg-Gray behaviour for low-density detectors under electronic disequilibrium conditions in small megavoltage photon fields. *Phys Med Biol.* 2015;60(20):8187-8212.

26. Fenwick JD, Kumar S, Scott AJ, Nahum AE. Using cavity theory to describe the dependence on detector density of dosimeter response in non-equilibrium small fields. *Phys Med Biol.* 2013;58(9):2901-2923.

27. Bouchard H. A theoretical re-examination of Spencer-Attix cavity theory. *Phys Med Biol.* 2012;57(11):3333-3358.

28. Nyholm T, Olofsson J, Ahnesjo A, Karlsson M. Photon pencil kernel parameterisation based on beam quality index. *Radiother Oncol.* 2006;78:347-351.

29. Nyholm T, Olofsson J, Ahnesjo A, Karlsson M. Modeling lateral beam quality variations in pencil kernel based photon dose calculations. *Phys Med Biol.* 2006;51(16):4111-4118.

30. Aspradakis MM, Bryne JP, Palmans H, et al. *Report No 103: Small Field MV dosimetry.* York, England: Institute of Physics and Engineering in Medicine, IPEM; 2010.

31. Charles PH, Cranmer-Sargison G, Thwaites DI, et al. A practical and theoretical definition of very small field size for radiotherapy output factor measurements. *Med Phys.* 2014;41(4):041707.

32. Bouchard H, Kamio Y, Palmans H, Seuntjens J, Duane S. Detector dose response in megavoltage small photon beams. II. Pencil beam perturbation effects. *Med Phys.* 2015;42(10):6048-6061.

33. Bouchard H, Seuntjens J, Duane S, Kamio Y, Palmans H. Detector dose response in megavoltage small photon beams. I. Theoretical concepts. *Med Phys.* 2015;42(10):6033-6047.

34. Das IJ, Downes MB, Kassaee A, Tochner Z. Choice of radiation detector in dosimetry of stereotactic radiosurgery-radiotherapy. *J Radiosurg.* 2000;3(4):177-185.

35. De Vlamynck K, Palmans H, Verhaegen F, De Wagter C, De Neve W, Thierens H. Dose measurements compared with Monte Carlo simulations of narrow 6 MV multileaf collimator shaped photon beams. *Med Phys.* 1999;26(9):1874-1882.

36. Araki F. Monte Carlo study of a CyberKnife stereotactic radiosurgery system. *Med Phys.* 2006;33(8):2955-2963.

37. Wu A, Zwicker RD, Kalend AM, Zheng Z. Comments on dose measurements for a narrow beam in radiosurgery. *Med Phys.* 1993;20(3):777-779.

38. Rice RK, Hansen JL, Svensson GK, Siddon RL. Measurements of dose distributions in small beams of 6 MV x-rays. *Phys Med Biol.* 1987;32:1087-1099.

39. Francescon P, Cora S, Cavedon C, Scalchi P, Reccanello S, Colombo F. Use of a new type of radiochromic film, a new parallel-plate micro-chamber, MOSFETs, and TLD 800 microcubes in the dosimetry of small beams. *Med Phys.* 1998;25(4):503-511.

40. Bjärngard BE, Tsai J-S, Rice RK. Doses on the central axes of narrow 6-MV x-ray beams. *Med Phys.* 1990;17(5):794-799.

41. Capote R, Sanchez-Doblado F, Leal A, Lagares JI, Arrans R, Hartmann GH. An EGSnrc Monte Carlo study of the microionization chamber for reference dosimetry of narrow irregular IMRT beamlets. *Med Phys.* 2004;31(9):2416-2422.

42. Lee H-R, Pankuch M, Chu J. Evaluation and characterization of parallel plate microchamber's functionalities in small beam dosimetry. *Med Phys.* 2002;29(11):2489-2496.

43. McKerracher C, Thwaites DI. Assessment of new small-field detectors against standard-field detectors for practical stereotactic beam data acquisition. *Phys Med Biol.* 1999;44(9):2143-2160.

44. McLaughlin WL, Soares CG, Sayeg JA, et al. The use of a radiochromic detector for the determination of stereotactic radiosurgery dose characteristics. *Med Phys.* 1994;21(3):379-388.

45. Rustgi SN. Evaluation of the dosimetric characteristics of a diamond detector for photon beam measurements. *Med Phys.* 1995;22(5):567-570.

46. Sanchez-Doblado F, Capote R, Leal A, et al. Micro ionization chamber for reference dosimetry in IMRT verification: clinical implications on OAR dosimetric errors. *Phys Med Biol.* 2005;50(5):959-970.

47. Zhu XR, Allen JJ, Shi J, Simon WE. Total scatter factors and tissue maximum ratios for small radiosurgery fields: comparison of diode detectors, a parallel-plate ion chamber, and radiographic film. *Med Phys.* 2000;27(3):472-477.

48. Araki F, Ikegami T, Ishidoya T, Kubo HD. Measurements of Gamma-Knife helmet output factors using a radiophotoluminescent glass rod dosimeter and a diode detector. *Med Phys.* 2003;30(8):1976-1981.

49. Klein DM, Tailor RC, Archambault L, Wang L, Therriault-Proulx F, Beddar AS. Measuring output factors of small fields formed by collimator jaws and multileaf collimator using plastic scintillation detectors. *Med Phys.* 2010;37(10):5541-5549.

50. Tyler M, Liu PZ, Chan KW, et al. Characterization of small-field stereotactic radiosurgery beams with modern detectors. *Phys Med Biol.* 2013;58(21):7595-7608.

51. Das IJ, Ding GX, Ahnesjö A. Small fields: Non-equilibrium radiation dosimetry. *Med Phys.* 2008;35(1):206-215.

52. Zhu TC, Ahnesjö A, Lam KL, et al. Report of AAPM Therapy Physics Committee Task Group 74: in-air output ratio, Sc, for megavoltage photon beams. *Med Phys.* 2009;36(11):5261-5291.

53. IAEA TRS 398. *Absorbed Dose Determination in External Beam Radiotherapy: An International Code of Practice for Dosimetry Based on Standards of Absorbed Dose to Water.* Vienna, Austria: International Atomic Energy Agency;2000.

54. Akino Y, Mizuno H, Isono M, Tanaka Y, Masai N, Yamamoto T. Small-field dosimetry of TrueBeam(TM) flattened and flattening filter-free beams: A multi-institutional analysis. *J Appl Clin Med Phys.* 2020;21(1):78-87.

55. Lechner W, Palmans H, Solkner L, Grochowska P, Georg D. Detector comparison for small field output factor measurements in flattening filter free photon beams. *Radiother Oncol.* 2013;109(3):356-360.

56. Xiao Y, Kry SF, Popple R, et al. Flattening filter-free accelerators: a report from the AAPM Therapy Emerging Technology Assessment Work Group. *J Appl Clin Med Phys.* 2015;16(3):5219.

57. Budgell G, Brown K, Cashmore J, et al. IPEM topical report 1: guidance on implementing flattening filter free (FFF) radiotherapy. *Phys Med Biol.* 2016;61(23):8360-8394.

58. Prezado Y, Martínez-Rovira I, Thengumpallil S, Deman P. Dosimetry protocol for the preclinical trials in white-beam minibeam radiation therapy. *Med Phys.* 2011;38(9):5012-5020.

59. Bogdanich W, Rebelo K. A Pinpoint Beam Strays Invisibly, Harming Instead of Healing. *The New York Times.* Dec 28, 2010, 2010.

60. Bogdanich W, Ruiz RR. Radiation Errors Reported in Missouri. *The New York Times.* February 24, 2010, 2010.

61. Bogdanich W. Radiation Offers New Cures, and Ways to Do Harm. *The New York Times.* January 10, 2010, 2010.

62. Derreumaux S, Boisserie G, Brunet G, Buchheit I, Sarrazin T. *Concerns in France about the dose delivered to the patients in stereotactic radiation therapy.* Vienna 2011.

63. Solberg TD, Balter JM, Benedict SH, et al. Quality and safety considerations in stereotactic radiosurgery and stereotactic body radiation therapy: Executive summary. *Pract Radiat Oncol.* 2012;2(1):2-9.

64. Ahnesjö A, Weber L, Murman A, Saxner M, Thorslund I, Traneus E. Beam modeling and verification of a photon beam multisource model. *Med Phys.* 2005;32(6):1722-1737.

65. Ezzell GA, Burmeister JW, Dogan N, et al. IMRT commissioning: multiple institution planning and dosimetry comparisons, a report from AAPM Task Group 119. *Med Phys.* 2009;36(11):5359-5373.

66. Lightstone AW, Benedict SH, Bova FJ, Solberg TD, Stern RL. Intracranial stereotactic positioning systems: Report of the American Association of Physicists in Medicine Radiation Therapy Committee Task Group no. 68. *Med Phys.* 2005;32(7):2380-2398.

67. Glide-Hurst C, Bellon M, Foster R, et al. Commissioning of the Varian TrueBeam linear accelerator: a multi-institutional study. *Med Phys.* 2013;40(3):031719.

68. Langen KM, Papanikolaou N, Balog J, et al. QA for helical tomotherapy: report of the AAPM Task Group 148. *Med Phys.* 2010;37(9):4817-4853.

69. Vandervoort E, Patrocinio H, Chow T, Soisson E, Nadeau DB. COMP Report: CPQR technical quality control guidelines for CyberKnife(R) Technology. *J Appl Clin Med Phys.* 2018;19(2):29-34.

70. Caprile P, Hartmann GH. Development and validation of a beam model applicable to small fields. *Phys Med Biol.* 2009;54(10):3257-3268.

71. Chung E, Bouchard H, Seuntjens J. Investigation of three radiation detectors for accurate measurement of absrobed dose in nonstandard fields. *Med Phys.* 2010;37(6):2404-2413.

72. Pantelis E, Moutsatsos A, Zourari K, et al. On the implementation of a recently proposed dosimetric formalism to a robotic radiosurgery system. *Med Phys.* 2010;37(5):2369-2379.

73. Rosser KE, Bedford JL. Application of a new dosimetry formalism to volumetric modulated arc therapy (VMAT). *Phys Med Biol.* 2009;54(23):7045-7061.

74. Sterpin E, Hundertmark BT, Mackie TR, Lu W, Olivera GH, Vynckier S. Monte Carlo-based analytical model for small and variable fields delivered by TomoTherapy. *Radiother Oncol.* 2010;94(2):229-234.

75. Cranmer-Sargison G, Weston S, Evans JA, Sidhu NP, Thwaites DI. Implementing a newly proposed Monte Carlo based small field dosimetry formalism for a comprehensive set of diode detectors. *Med Phys.* 2011;38(12):6592-6602.

76. Cranmer-Sargison G, Weston S, Sidhu NP, Thwaites DI. Experimental small field 6MV output ratio analysis for various diode detector and accelerator combinations. *Radiother Oncol.* 2011;100(3):429-435.

77. Francescon P, Cora S, Satariano N. Calculation of k(Q(clin),Q(msr)) (f(clin),f(msr)) for several small detectors and for two linear accelerators using Monte Carlo simulations. *Med Phys.* 2011;38(12):6513-6527.

78. Gago-Arias A, Antolin E, Fayos-Ferrer F, et al. Correction factors for ionization chamber dosimetry in CyberKnife: machine-specific, plan-class, and clinical fields. *Med Phys.* 2013;40(1):011721.

79. Czarnecki D, Zink K. Monte Carlo calculated correction factors for diodes and ion chambers in small photon fields. *Phys Med Biol.* 2013;58(8):2431-2444.

80. Charles PH, Crowe SB, Kairn T, et al. Monte Carlo-based diode design for correction-less small field dosimetry. *Phys Med Biol.* 2013;58(13):4501-4512.

81. Benmakhlouf H, Sempau J, Andreo P. Output correction factors for nine small field detectors in 6 MV radiation therapy photon beams: A PENELOPE Monte Carlo study. *Med Phys.* 2014;41(4):041711.

82. Azangwe G, Grochowska P, Georg D, et al. Detector to detector corrections: a comprehensive study of detector specific correction factors for beam output measurements for small radiotherapy beams. *Med Phys.* 2014;41(7):072103.

83. De Coste V, Francescon P, Marinelli M, et al. Is the PTW 60019 microDiamond a suitable candidate for small field reference dosimetry? *Phys Med Biol.* 2017;62(17):7036-7055.

84. O'Brien DJ, Leon-Vintro L, McClean B. Small field detector correction factors kQclin,Qmsr (fclin,fmsr) for silicon-diode and diamond detectors with circular 6 MV fields derived using both empirical and numerical methods. *Med Phys.* 2016;43(1):1035-1044.

85. Barrett JC, Knill C. Monte Carlo calculated correction factors for the PTW microDiamond detector in the Gamma Knife-Model C. *Med Phys.* 2016;43(3):1035-1044.

86. Huet C, Moignier C, Barraux V, et al. Study of commercial detector responses in non-equilibrium small photon fields of a 1000MU/min CyberKnife system. *Phys Med.* 2016;32(6):818-825.

87. Aland T, Kairn T, Kenny J. Evaluation of a Gafchromic EBT2 film dosimetry system for radiotherapy quality assurance. *Australas Phys Eng Sci Med.* 2011;34(2):251-260.

88. Pantelis E, Moutsatsos A, Zourari K, et al. On the output factor measurements of the CyberKnife iris collimator small fields: Experimental determination of the k(Q(clin),Q(msr)) (f(clin),f(msr)) correction factors for microchamber and diode detectors. *Med Phys.* 2012;39(8):4875-4885.

89. Papaconstadopoulos P, Archambault L, Seuntjens J. Experimental investigation on the accuracy of plastic scintillators and of the spectrum discrimination method in small photon fields. *Med Phys.* 2017;44(2):654-664.

90. Russo S, Masi L, Francescon P, et al. Multicenter evaluation of a synthetic single-crystal diamond detector for CyberKnife small field size output factors. *Phys Med.* 2016;32(4):575-581.

91. Masi L, Russo S, Francescon P, et al. CyberKnife beam output factor measurements: A multi-site and multi-detector study. *Phys Med.* 2016;32(12):1637-1643.

92. Francescon P, Kilby W, Noll J, Masi L, Satariano N, Russo S. Monte Carlo simulated corrections for beam commissioning measurements with circular and MLC shaped fields on the CyberKnife M6 system: a study including diode, microchamber, point scintillator, and synthetic microdiamond detectors. *Phys Med Biol.* 2017;62(3):1076-1095.

93. Bouchard H, Seuntjens J, Carrier JF, Kawrakow I. Ionization chamber gradient effects in nonstandard beam configurations. *Med Phys.* 2009;36(10):4654-4663.

94. Francescon P, Kilby W, Satariano N, Cora S. Monte Carlo simulated correction factors for machines specific reference field dose calibration and output factor measurement using fixed and iris collimators on the CyberKnife system. *Phys Med Biol.* 2012;57:3741-3258.

95. Ralston A, Liu P, Warrener K, McKenzie D, Suchowerska N. Small field diode correction factors derived using an air core fibre optic scintillation dosimeter and EBT2 film. *Phys Med Biol.* 2012;57(9):2587-2602.

96. Sauer OA, Wilbert J. Measurement of output factors for small photon beams. *Med Phys.* 2007;34(6):1983-1988.

97. Kawachi T, Saitoh H, Inoue M, Katayose T, Myojoyama A, Hatano K. Reference dosimetry condition and beam quality correction factor for CyberKnife beam. *Med Phys.* 2008;35(10):4591-4598.

98. Sterpin E, Mackie TR, Vynckier S. Monte Carlo computed machine-specific correction factors for reference dosimetry of TomoTherapy static beam for several ion chambers. *Med Phys.* 2012;39(7):4066-4072.

99. Sterpin E, Salvat F, Cravens R, Ruchala K, Olivera GH, Vynckier S. Monte Carlo simulation of helical tomotherapy with PENELOPE. *Phys Med Biol.* 2008;53(8):2161-2180.

100. Thomas SJ, Aspradakis MM, Byrne JP, et al. Reference dosimetry on TomoTherapy: an addendum to the 1990 UK MV dosimetry code of practice. *Phys Med Biol.* 2014;59(6):1339-1352.

101. Chalkley A, Heyes G. Evaluation of a synthetic single-crystal diamond detector for relative dosimetry measurements on a CyberKnife. *Br J Radiol.* 2014;87(1035):20130768.

102. Underwood TS, Rowland BC, Ferrand R, Vieillevigne L. Application of the Exradin W1 scintillator to determine Ediode 60017 and microDiamond 60019 correction factors for relative dosimetry within small MV and FFF fields. *Phys Med Biol.* 2015;60(17):6669-6683.

103. Looe HK, Delfs B, Poppinga D, Jiang P, Harder D, Poppe B. The "cutting away" of potential secondary electron tracks explains the effects of beam size and detector wall density in small-field photon dosimetry. *Phys Med Biol.* 2017;63(1):015001.

104. Ding GX, Duggan DM, Coffey CW. A theoretical approach for non-equilibrium radiation dosimetry. *Phys Med Biol.* 2008;53(13):3493-3499.

105. Jaffray DA, Battista JJ, Fenster A, Munro P. X-ray sources of medical linear accelerators: Focal and extra-focal radiation. *Med Phys.* 1993;20(5):1417-1427.

106. Sawkey D, Constantin M, Mansfield S, et al. Measurement of electron spots on TrueBeam. *Med Phys.* 2013;40(6):332 (abstr).

107. Lutz WR, Maleki N, Bjarngard BE. Evaluation of a beam-spot camera for megavoltage x rays. *Med Phys.* 1988;15(4):614-617.

108. Munro P, Rawlinson JA, Fenster A. Therapy imaging: source sizes of radiotherapy beams. *Med Phys.* 1988;15(4):517-524.

109. Gambaccini M, Cardarelli P, Taibi A, et al. Measurement of focal spot size in a 5.5 MeV linac. *Nucl Instr Meth Phys Res B.* 2011;269(10):1157-1165.

110. Loewenthal E, Loewinger E, Bar-Avraham E, Barnea G. Measurement of the source size of a 6- and 18-MV radiotherapy linac. *Med Phys.* 1992;19(3):687-690.

111. Sham E, Seuntjens J, Devic S, Podgorsak EB. Influence of focal spot on characteristics of very small diameter radiosurgical beams. *Med Phys.* 2008;35(7):3317-3330.

112. Sharpe MB, Jaffray DA, Battista JJ, Munro P. Extrafocal radiation: a unified approach to the prediction of beam penumbra and output factors for megavoltage x-ray beams. *Med Phys.* 1995;22(12):2065-2074.

113. Wang LL, Leszczynski K. Estimation of the focal spot size and shape for a medical linear accelerator by Monte Carlo simulation. *Med Phys.* 2007;34(2):485-488.

114. Yeboah C. Characterization of linear accelerator X-ray source size using a laminated beam-spot camera. *J Appl Clin Med Phys.* 2011;12(3):3463.

115. Zhu TC, Manbeck K. CT reconstruction of x-ray source profile of a medical accelerator. *Proc SPIE.* 1994;2132:242-253,.

116. Ding GX, Duggan DM, Lu B, et al. Impact of inhomogeneity corrections on dose coverage in the treatment of lung cancer using stereotactic body radiation therapy. *Med Phys.* 2007;34(7):2985-2994.

117. Kalach NI, Rogers DW. Which accelerator photon beams are "clinic-like" for reference dosimetry purposes? *Med Phys.* 2003;30(7):1546-1555.

118. Papaconstadopoulos P. *On the detector response and the reconstruction of the source intensity distribution in small photon fields*, Ph.D. Thesis, McGill University, Montreal; 2016.

119. Jones AO, Das IJ. Comparison of inhomogeneity correction algorithms in small photon fields. *Med Phys.* 2005;32(3):766-776.

120. Jones AO, Das IJ, Jones FL. A Monte Carlo study of IMRT beamleats in homogeneous media. *Med Phys.* 2003;30(3):296-300.

121. Papanikolaou N, Battista JJ, Boyer AL, et al. *Tissue inhomogeneity corrections for megavoltage photon beams: AAPM Report N0. 85.* Madison, Wi: Medical Physics Publishing; 2004.

122. Stasi M, Baiotto B, Barboni G, Scielzo G. The behavior of several microionization chambers in small intensity modulated radiotherapy fields. *Med Phys.* 2004;31(10):2792-2795.

123. Westermark M, Arndt J, Nilsson B, Brahme A. Comparative dosimetry in narrow high-energy photon beams. *Phys Med Biol.* 2000;45(3):685-702.

124. Scott AJ, Kumar S, Nahum AE, Fenwick JD. Characterizing the influence of detector density on dosimeter response in non-equilibrium small photon fields. *Phys Med Biol.* 2012;57(14):4461-4476.

125. Underwood TS, Winter HC, Hill MA, Fenwick JD. Detector density and small field dosimetry: integral versus point dose measurement schemes. *Med Phys.* 2013;40(8):082102.

126. Underwood TS, Winter HC, Hill MA, Fenwick JD. Mass-density compensation can improve the performance of a range of different detectors under non-equilibrium conditions. *Phys Med Biol.* 2013;58(23):8295-8310.

127. Rogers DWO, Cyglar JE, eds. *Clinical Dosimetry Measurements in Radiotherapy.* Madison, WI: Medical Physics Publishing; 2009. Proceedings of the American Association of Physicists in Medicine, Summer School, Colorado Springs, Co June 21-25, 2009.

128. Das IJ. *Advances in Radiochromic Film for Radiation Dosimetry: Role and Clinical Applications.* Boca Raton, FL: CRC press| Taylor & Francis Group; 2017.

129. Das IJ, Moralles J, Francescon P. Small field dosimetry: What have we learnt? *AIP Conference Proceedings.* 2016;1747:060001.

130. Zhu TC. Small Field: dosimetry in electron disequilibrium region. *J Phys: Conf Ser.* 2010;250:012056.

131. Francescon P, Cora S, Cavedon C. Total scatter factors of small beams: A multidetector and Monte Carlo study. *Med Phys.* 2008;35(2):504-513.

132. Francescon P, Cora S, Cavedon C, Scalchi P. Application of a Monte Carlo-based method for total scatter factors of small beams to new solid state micro-detectors. *J Appl Clin Med Phys.* 2009;10(1):147-152.

133. Yin FF, Zhu J, Yan H, et al. Dosimetric characteristics of Novalis shaped beam surgery unit. *Med Phys.* 2002;29(8):1729-1738.

134. Scott AJ, Nahum AE, Fenwick JD. Using a Monte Carlo model to predict dosimetric properties of small radiotherapy photon fields. *Med Phys.* 2008;35(10):4671-4684.

135. Benmakhlouf H, Andreo P. Spectral distribution of particle fluence in small field detectors and its implication on small field dosimetry. *Med Phys.* 2017;44(2):713-724.

136. Martens C, De Wagter C, De Neve W. The value of the PinPoint ion chamber for characterization of small field segments used in intensity-modulated radiotherapy. *Phys Med Biol.* 2000;45(9):2519-2530.

137. Muir BR, Rogers DW. The central electrode correction factor for high-Z electrodes in small ionization chambers. *Med Phys.* 2011;38(2):1081-1088.

138. Leybovich LB, Sethi A, Dogan N. Comparison of ionization chambers of various volumes for IMRT absolute dose verification. *Med Phys.* 2003;30(2):119-123.

139. Sarkar V, Wang B, Zhao H, et al. Percent depth-dose distribution discrepancies from very small volume ion chambers. *J Appl Clin Med Phys.* 2015;16(2):432-442.

140. Wickman G. A liquid ionization chamber with high spatial resolution. *Phys Med Biol.* 1974;19(1):66-72.

141. Wickman G, Nyström H. The use of liquids in ionization chambers for high precision radiotherapy dosimetry. *Phys Med Biol.* 1992;37:1789-1812.

142. Johansson B, Wickman G. General collection efficiency for liquid isooctane and tetramethylsilane used as sensitive media in a parallel-plate ionization chamber *Phys Med Biol.* 1997;42(1):133-145.

143. Andersson J, Johansson E, Tölli H. On the property of measurements with the PTW microLion chamber in continuous beams. *Med Phys.* 2012;39(8):4775-4787.

144. Andersson J, Tölli H. Application of the two-dose-rate method for general recombination correction for liquid ionization chambers in continuous beams. *Phys Med Biol.* 2011;56(2):299-314.

145. Tölli H, Sjogren R, Wendelsten M. A two-dose-rate method for general recombination correction for liquid ionization chambers in pulsed beams. *Phys Med Biol.* 2010;55(15):4247-4260.

146. Chung E, Davis S, Seuntjens J. Experimental analysis of general ion recombination in a liquid-filled ionization chamber in high-energy photon beams. *Med Phys.* 2013;40(6):062104.

147. Dasu A, Lofroth PO, Wickman G. Liquid ionization chamber measurements of dose distributions in small 6 MV photon beams. *Phys Med Biol.* 1998;43(1):21-36.

148. Wagner A, Crop F, Lacornerie T, Vandevelde F, Reynaert N. Use of a liquid ionization chamber for stereotactic radiotherapy dosimetry. *Phys Med Biol.* 2013;58(8):2445-2459.

149. Jursinic PA. Angular dependence of dose sensitivity of surface diodes. *Med Phys.* 2009;36(6):2165-2171.

150. Sanchez-Doblado F, Andreo P, Capote R, et al. Ionization chamber dosimetry of small photon fields: a Monte Carlo study on stopping-power ratios for radiosurgery and IMRT beams. *Phys Med Biol.* 2003;48(14):2081-2099.

151. Mobit P, Sandison G. A Monte Carlo based development of a cavity theory for solid state detectors irradiated in electron beams. *Radiat Prot Dosimetry.* 2002;101(1-4):427-429.

152. Mobit PN, Sandison GA, Nahum AE. Electron fluence perturbation correction factors for solid state detectors irradiated in megavoltage electron beams. *Phys Med Biol.* 2000;45(2):255-265.

153. Dieterich S, Sherouse GW. Experimental comparison of seven commercial dosimetry diodes for measurement of stereotactic radiosurgery cone factors. *Med Phys.* 2011;38(7):4166-4173.

154. Sharma DS, Chaudhary RK, Sharma SD, et al. Experimental determination of stereotactic cone size and detector specific output correction factor. *Br J Radiol.* 2016;90:20160918.

155. Lam SE, Bradley DA, Khandaker MU. Small-field radiotherapy photon beam output evaluation: Detectors reviewed. *Radiat Phys Chem.* 2021;178:108950.

156. Akino Y, Mizuno H, Tanaka Y, Isono M, Masai N, Yamamoto T. Inter-institutional variability of small-field-dosimetry beams among HD120() multileaf collimators: a multi-institutional analysis. *Phys Med Biol.* 2018;63(20):205018.

157. Eklund K, Ahnesjö A. Spectral perturbations from silicon diode detector encapsulation and shielding in photon fields. *Med Phys.* 2010;37(11):6055-6060.

158. Saini AS, Zhu TC. Temperature dependence of commercially available diode detectors. *Med Phys.* 2002;29(4):622-630.

159. Saini AS, Zhu TC. Dose rate and SDD dependence of commercially available diode detectors. *Med Phys.* 2004;31(4):914-924.

160. Rikner G, Grusell E. Effects of radiation damage on p-type silicon detectors. *Phys Med Biol.* 1983;28(11):1261-1267.

161. Schönfeld AB, Poppinga D, Kranzer R, et al. Technical Note: Characterization of the new microSilicon diode detector. *Med Phys.* 2019;46(9):4257-4262.

162. Francescon P, Kilby W, Noll JM, Satariano N, Orlandi C. Small field dosimetry correction factors for circular and MLC shaped fields with the CyberKnife M6 System: evaluation of the PTW 60023 microSilicon detector. *Phys Med Biol.* 2019. doi: 10.1088/1361-6560/ab6154.

163. Akino Y, Fujiwara M, Okamura K, et al. Characterization of a microSilicon diode detector for small-field photon beam dosimetry. *J Radiat Res.* 2020;61(3):410-418.

164. Weber C, Kranzer R, Weidner J, et al. Small field output correction factors of the microSilicon detector and a deeper understanding of their origin by quantifying perturbation factors. *Med Phys.* 2020;47(7):3165-3173.

165. Akino Y, Okamura K, Das IJ, et al. Technical Note: Characteristics of a microSilicon X shielded diode detector for photon beam dosimetry. *Med Phys. 2021; 48(4):2004-2009*.

166. Hoban PW, Heydarian M, Beckham WA, Beddoe AH. Dose rate dependence of a PTW diamond detector in the dosimetry of a 6 MV Photon beam. *Phys Med Biol.* 1994;39:1219-1229.

167. De Angelis C, Onori S, Pacilio M, et al. An investigation of the operating characteristics of two PTW diamond detectors in photon and electron beams. *Med Phys.* 2002;29:248-254.

168. Heydarian M, Hoban PW, Beckham WA, Borchardt IA, Beddoe AH. Evaluation of a PTW diamond detector for electron beam measurements. *Phys Med Biol.* 1993;38:1035-1042.

169. Laub WU, Kaulich TW, Nusslin F. A diamond detector in the dosimetry of high-energy electron and photon beams. *Phys Med Biol.* 1999;44(9):2183-2192.

170. Planskoy B. Evaluation of diamond radiation dosemeters. *Phys Med Biol.* 1980;25(3):519-532.

171. Vatnitsky S, Järvinen H. Application of natural diamond detector for the measurement of relative dose distributions in radiotherapy. *Phys Med Biol.* 1993;38:173-184.

172. Das IJ. Diamond Detector. In: Cyglar R, ed. *Clinical Dosimetry Measurements in Radiotherapy.* Madison, WI: Medical Physics Publishing; 2009:891-912.

173. Mobit PN, Sandison GA. A Monte Carlo comparison of the response of the PTW-diamond and the TL-diamond detectors in megavoltage photon beams. *Med Phys.* 1999;26(11):2503-2507.

174. De Angelis C, Casati M, Bruzzi M, Onori S, Bucciolini M. Present limitations of CVD diamond detectors for IMRT applications. *Nucl Instrum Methods Phys Res A.* 2007;583(1):195-203.

175. Ciancaglioni I, Marinelli M, Milani E, et al. Dosimetric characterization of a synthetic single crystal diamond detector in clinical radiation therapy small photon beams. *Med Phys.* 2012;39(7):4493-4501.

176. Marsolat F, Tromson D, Tranchant N, et al. A new single crystal diamond dosimeter for small beam: comparison with different commercial active detectors. *Phys Med Biol.* 2013;58(21):7647-7660.

177. Das IJ, Francescon P. Comments on the TRS-483 Protocol on Small field Dosimetry. *Med Phys.* 2018;45(12):5666-5668.

178. Casar B, Gershkevitsh E, Mendez I, Jurkovic S, Huq MS. A novel method for the determination of field output factors and output correction factors for small static fields for six diodes and a microdiamond detector in megavoltage photon beams. *Med Phys.* 2019;46(2):944-963.

179. Mancosu P, Reggiori G, Stravato A, et al. Evaluation of a synthetic single-crystal diamond detector for relative dosimetry on the Leksell Gamma Knife Perfexion radiosurgery system. *Med Phys.* 2015;42(9):5035-5041.

180. Veselsky T, Novotny Jr J, Pastykovaa V, Koniarova I. Determination of small field synthetic single-crystal diamond detector correction factors for CyberKnife, Leksell Gamma Knife Perfexion and linear accelerator. *Phys Med.* 2017;44:66-71.

181. Alhakeem E, Zavgorodni S. Output and ([Formula: see text]) correction factors measured and calculated in very small circular fields for microDiamond and EFD-3G detectors. *Phys Med Biol.* 2018;63(15):155002.

182. Looe HK, Poppinga D, Kranzer R, et al. The role of radiation-induced charge imbalance on the dose-response of a commercial synthetic diamond detector in small field dosimetry. *Med Phys.* 2019;46(6):2752-2759.

183. Beddar AS, Mackie TR, Attix FH. Water-equivalent plastic scintillation detectors for high energy beam dosimetry: II. Properties and measurements. *Phys Med Biol.* 1992;37(10):1901-1913.

184. Beddar AS, Mason DJ, O'Brien PF. Absorbed dose perturbation caused by diodes for small field photon dosimetry. *Med Phys.* 1994;21(7):1075-1079.

185. Gagnon JC, Theriault D, Guillot M, et al. Dosimetric performance and array assessment of plastic scintillation detectors for stereotactic radiosurgery quality assurance. *Med Phys.* 2012;39(1):429-436.

186. Wang LL, Beddar S. Study of the response of plastic scintillation detectors in small-field 6 MV photon beams by Monte Carlo simulations. *Med Phys.* 2011;38(3):1596-1599.

187. Beddar AS, Briere TM. Plastic Scintillation Detectors. In: Rogers DWO, Cygler JE, eds. *Clinical Dosimetry Measurements in Radiotherapy.* Madison, WI: Medical Physics Publishing; 2009:891-912.

188. Morin J, Beliveau-Nadeau D, Chung E, et al. A comparative study of small field total scatter factors and dose profiles using plastic scintillation detectors and other stereotactic dosimeters: the case of the CyberKnife. *Med Phys.* 2013;40(1):011719.

189. Pasquino M, Cutaia C, Radici L, et al. Dosimetric characterization and behaviour in small X-ray fields of a microchamber and a plastic scintillator detector. *Br J Radiol.* 2017;90(1069):20160596.

190. Francescon P, Kilby W, Satariano N. Monte Carlo simulated correction factors or output factor measurement with the CyberKnife system—results for new detectors and correction factor dependence on measurement distance and detector orientation. *Phys Med Biol.* 2014;59:N11-N17.

191. Carrasco P, Jornet N, Jordi O, et al. Characterization of the Exradin W1 scintillator for use in radiotherapy. *Med Phys.* 2015;42(1):297-304.

192. Galavis PE, Hu L, Holmes S, Das IJ. Characterization of the plastic scintillation detector Exradin W2 for small field dosimetry. *Med Phys.* 2019;46(5):2468-2476.

193. Debnath SBC, Fauquet C, Tallet A, et al. High spatial resolution inorganic scintillator detector for high-energy X-ray beam at small field irradiation. *Med Phys.* 2020;47(3):1364-1371.

194. Niroomand-Rad A, Blackwell CR, Coursey BM, et al. Radiographic film dosimetry: Recommendations of AAPM Radiation Therapy Committee Task Group 55. *Med Phys.* 1998;25(11):2093-2115.

195. Das IJ. Radiographic Film. In: Rogers DW, Cyglar J, eds. *Clinical Dosimetry Measurements in Radiotherapy.* Madison, WI: Medical Physics Publishing; 2009:865-890.

196. Pai S, Das IJ, Dempsey JF, et al. TG-69: Radiographic Film for Megavoltage Beam Dosimetry. *Med Phys.* 2007;34(6):2228-2258.

197. Niroomand-Rad A, Chiu-Tsao ST, Grams MP, et al. Report of AAPM Task Group 235 Radiochromic Film Dosimetry: An Update to TG-55. *Med Phys.* 2020; 47(12):5986-6025.

198. Mack A, Scheib SG, Major J, et al. Precision dosimetry for narrow photon beams used in radiosurgery-determination of Gamma Knife output factors. *Med Phys.* 2002;29(9):2080-2089.

199. Devic S, Seuntjens J, Hegyi G, et al. Dosimetric properties of improved GafChromic films for seven different digitizers. *Med Phys.* 2004;31(9):2392-2401.

200. Devic S, Vuong T, Moftah B. Advantages of inflatable multichannel endorectal applicator in the neo-adjuvant treatment of patients with locally advanced rectal cancer with HDR brachytherapy. *J Appl Clin Med Phys.* 2005;6(2):44-49.

201. Massillon JLG, Cueva-Procel D, Diaz-Aguirre P, Rodriguez-Ponce M, Herrera-Martinez F. Dosimetry for small fields in stereotactic radiosurgery using gafchromic MD-V2-55 film, TLD-100 and alanine dosimeters. *PloS one.* 2013;8(5):e63418.

202. Larraga-Gutierrez JM, Garcia-Hernandez D, Garcia-Garduno OA, Galvan de la Cruz OO, Ballesteros-Zebadua P, Esparza-Moreno KP. Evaluation of the Gafchromic((R)) EBT2 film for the dosimetry of radiosurgical beams. *Med Phys.* 2012;39(10):6111-6117.

203. Gonzalez-Lopez A, Vera-Sanchez JA, Lago-Martin JD. Small fields measurements with radiochromic films. *J Med Phys.* 2015;40(2):61-67.

204. Garcia-Garduno OA, Larraga-Gutierrez JM, Rodriguez-Villafuerte M, Martinez-Davalos A, Celis MA. Small photon beam measurements using radiochromic film and Monte Carlo simulations in a water phantom. *Radiother Oncol.* 2010;96(2):250-253.

205. Morales JE, Butson M, Crowe SB, Hill R, Trapp JV. An experimental extrapolation technique using the Gafchromic EBT3 film for relative output factor measurements in small x-ray fields. *Med Phys.* 2016;43(8):4687.

206. McCaw TJ, Micka JA, DeWerd LA. Development and characterization of a three-dimensional radiochromic film stack dosimeter for megavoltage photon beam dosimetry. *Med Phys.* 2014;41(5):052104.

207. Kry SF, Alvarez P, Cygler JE, et al. AAPM TG 191: Clinical use of luminescent dosimeters: TLDs and OSLDs. *Med Phys.* 2020;47(2):e19-e51.

208. Horowitz YS. The theoretical and microdosimetric basis of thermoluminescence and applications to dosimetry. *Phys Med Biol.* 1981;26:765-824.

209. Alvarez P, Kry SF, Stingo F, Followill D. TLD and OSLD dosimetry systems for remote audits of radiotherapy external beam calibration. *Radiat Meas.* 2017;106:412-415.

210. Davis SD, Ross CK, Mobit PN, Van der Zwan L, Chase WJ, Shortt KR. The response of lif thermoluminescence dosemeters to photon beams in the energy range from 30 kV x rays to ^{60}Co gamma rays. *Radiat Prot Dosimetry.* 2003;106(1):33-43.

211. Kirby TH, Hanson WF, Johnston DA. Uncertainty analysis of absorbed dose calculations from thermoluminescence dosimeters. *Med Phys.* 1992;19(6):1427-1433.

212. Moignier C, Huet C, Makovicka L. Determination of the KQclinfclin,Qmsr fmsr correction factors for detectors used with an 800 MU/min CyberKnife((R)) system equipped with fixed collimators and a study of detector response to small photon beams using a Monte Carlo method. *Med Phys.* 2014;41(7):071702.

213. Aaki F, Ishidoya T, Ikegami T, Moribe N, Yamashita Y. Application of a radiophotoluminescent glass plate dosimeter for small field dosimetry. *Med Phys.* 2005;32(6):1548-1854.

214. Arakia F, Moribe N, Shimonobou T, Yamashita Y. Dosimetric properties of radiophotoluminescent glass rod detector in high-energy photon beams from a linear accelerator and cyber-knife. *Med Phys.* 2004;31(7):1980-1986.

215. Perks J, Gao M, Smith V, Skubic S, Goetsch S. Glass rod detectors for small field, stereotactic radiosurgery dosimetric audit. *Med Phys.* 2005;32(3):726-732.

216. Yukihara EG, McKeever SW. Optically stimulated luminescence (OSL) dosimetry in medicine. *Phys Med Biol.* 2008;53(20):R351-R379.

217. Jursinic PA. Characterization of optically stimulated luminescent dosimeters, OSLDs, for clinical dosimetric measurements. *Med Phys.* 2007;34(12):4594-4604.

218. Kerns JR, Kry SF, Sahoo N, Followill DS, Ibbott GS. Angular dependence of the nanoDot OSL dosimeter. *Med Phys.* 2011;38(7):3955-3962.

219. Kim DW, Chung WK, Shin DO, et al. Dose response of commercially available optically stimulated luminescent detector, Al_2O_3:C for megavoltage photons and electrons. *Radiat Prot Dosimetry.* 2012;149(2):101-108.

220. McJury M, Oldham M, Cosgrove VP, et al. Radiation dosimetry using polymer gels: methods and applications. *Br J Radiol.* 2000;73(873):919-929.

221. Oldham M. 3D dosimetry by optical-CT scanning. *J Phys.* 2006;56:58-71.

222. Baldock C, De Deene Y, Doran S, et al. Polymer gel dosimetry. *Phys Med Biol.* 2010;55(5):R1-R63.

223. Oldham M, Siewerdsen JH, Shetty A, Jaffray DA. High resolution gel-dosimetry by optical-CT and MR scanning. *Med Phys.* 2001;28(7):1436-1445.

224. Pantelis E, Antypas C, Petrokokkinos L, et al. Dosimetric characterization of CyberKnife radiosurgical photon beams using polymer gels. *Med Phys.* 2008;35(6):2312-2320.

225. Pappas E, Maris TG, Papadakis A, et al. Experimental determination of the effect of detector size on profile measurements in narrow photon beams. *Med Phys.* 2006;33(10):3700-3710.

226. Clift C, Thomas A, John A, Chang Z, Das I, Oldham M. Toward acquiring comprehensive radiosurgery field commissioning data using the PRESAGE®/ optical-CT 3D dosimetry system. *Phys Med Biol.* 2010;55(5):1279-1293

227. Adamovics J, Maryanski MJ. Characterisation of PRESAGE: A new 3-D radiochromic solid polymer dosemeter for ionising radiation. *Radiat Prot Dosimetry.* 2006;120(1-4):107-112.

228. Sakhalkar H, Sterling D, Adamovics J, Ibbott G, Oldham M. Investigation of the feasibility of relative 3D dosimetry in the Radiologic Physics Center Head and Neck IMRT phantom using presage/optical-CT. *Med Phys.* 2009;36(7):3371-3377.

229. Kelly RG, Jordan KJ, Battista JJ. Optical CT reconstruction of 3D dose distributions using the ferrous-benzoic-xylenol (FBX) gel dosimeter. *Med Phys.* 1998;25(9):1741-1750.

230. Babic S, McNiven A, Battista J, Jordan K. Three-dimensional dosimetry of small megavoltage radiation fields using radiochromic gels and optical CT scanning. *Phys Med Biol.* 2009;54(8):2463-2481.

231. Newton J, Oldham M, Thomas A, et al. Commissioning a small-field biological irradiator using point, 2D, and 3D dosimetry techniques. *Med Phys.* 2011;38(12):6754-6762.

232. Thomas A, Newton J, Adamovics J, Oldham M. Commissioning and benchmarking a 3D dosimetry system for clinical use. *Med Phys.* 2011;38:4846-4857.

233. Xua Y, Wuu C-S, Maryanski MJ. Determining optimal gel sensitivity in optical CT scanning of gel dosimeters. *Med Phys.* 2003;30(8):2257-2263.

234. Crop F, Reynaert N, Pittomvils G, et al. The influence of small field sizes, penumbra, spot size and measurement depth on perturbation factors for microionization chambers. *Phys Med Biol.* 2009;54(9):2951-2969.

235. McEwen MR. Measurement of ionization chamber absorbed dose k(Q) factors in megavoltage photon beams. *Med Phys.* 2010;37(5):2179-2193.

236. Akino Y, Okamura K, Das IJ, et al. Technical Note: Characteristics of a microSilicon X shielded diode detector for photon beam dosimetry. *Med Phys.* 2021;48(4):2004-2009.

237. Wilcox EE, Daskalov GM. Evaluation of GAFCHROMIC EBT film for CyberKnife dosimetry. *Med Phys.* 2007;34(6):1967-1974.

238. Wilcox EE, Daskalov GM. Accuracy of dose measurements and calculations within and beyond heterogeneous tissues for 6 MV photon fields smaller than 4 cm produced by CyberKnife. *Med Phys.* 2008;35(6):2259-2266.

239. Fontanarosa D, Orlandini LC, Andriani I, Bernardi L. Commissioning Varian enhanced dynamic wedge in the PINNACLE treatment planning system using Gafchromic EBT film. *Med Phys.* 2009;36(10):4504-4510.

240. Poppinga D, Kranzer R, Ulrichs AB, et al. Three-dimensional characterization of the active volumes of PTW microDiamond, microSilicon, and Diode E dosimetry detectors using a proton microbeam. *Med Phys.* 2019;46(9):4241-4245.

241. Larraga-Gutierrez JM, Ballesteros-Zebadua P, Rodriguez-Ponce M, Garcia-Garduno OA, de la Cruz OO. Properties of a commercial PTW-60019 synthetic diamond detector for the dosimetry of small radiotherapy beams. *Phys Med Biol.* 2015;60(2):905-924.

242. Akino Y, Gautam A, Coutinho L, Wurfel J, Das IJ. Characterization of a new commercial single crystal diamond detector for photon- and proton-beam dosimetry. *J Radiat Res.* 2015;56(6):912-918.

243. Francescon P, Beddar S, Satariano N, Das IJ. Variation of k(fclin,fmsr, Qclin, Qmsr) for the small-field dosimetric parameters percentage depth dose, tissue-maximum ratio, and off-axis ratio. *Med Phys.* 2014;41(10):101708.

244. Das IJ, Francescon P. Small-field dosimetry in photon beams. In: Mijnheer BJ, ed. *Clinical 3D Dosimetry in Modern Radiation Therapy.* Boca Raton, FL: CRC press| Taylor & Francis Group; 2017:229-254.

245. Akino Y, Gibbons JP, Neck DW, Chu C, Das IJ. Intra- and intervariability in beam data commissioning among water phantom scanning systems. *J Appl Clin Med Phys.* 2014;15(4):251-258.

246. Cheng CW, Cho SH, Taylor M, Das IJ. Determination of zero field size percent depth doses and tissue maximum ratios for stereotactic radiosurgery and IMRT dosimetry: Comparison between experimental measurements and Monte Carlo simulation. *Med Phys.* 2007;34:3149-3157.

247. Sauer OA, Wilbert J. Functional representation of tissue phantom ratios for photon fields. *Med Phys.* 2009;36(12):5444-5450.

248. Li S, Rashid A, He S, Djajaputra D. A new approach in dose measurement and error analysis for narrow photon beams (beamlets) shaped by different multileaf collimators using a small detector. *Med Phys.* 2004;31(7):2020-2032.

249. TomoTherapy. *Hi Art System Dosimetry Analysis Guide, T-PHY-HB1400A-1204.* TomTherapy, Inc, Madison, WI2004.

250. de Chavez R, Jones CE, Charles PH. Integral small field output factor measurements using a transmission ionisation chamber. *Australas Phys Eng Sci Med.* 2019;42(1):235-244.

251. Azcona JD, Barbes B, Moran V, Burguete J. Commissioning of small field size radiosurgery cones in a 6-MV flattening filter-free beam. *Med Dosim.* 2017;42(4):282-288.

252. Czarnecki D, Wulff J, Zink K. The influence of linac spot size on scatter factors. *Metrologia.* 2012;49:S215-S218.

253. Serago CF, Houdek PV, Hartmann GH, Saini DS, Serago MS, Kaydee A. Tissue maximum ratios (and other parameters) of small circular 4, 6, 10, 15 and 24 MV x-ray beams for radiosurgery. *Phys Med Biol.* 1992;37(10):1943-1956.

254. Sharma SC, Ott JT, Williams JB, Dickow D. Commissioning and acceptance testing of a CyberKnife linear accelerator. *J Appl Clin Med Phys.* 2007;8:119-125.

255. Knutson NC, Schmidt MC, Belley MD, et al. Technical Note: Direct measurement of continuous TMR data with a 1D tank and automated couch movements. *Med Phys.* 2017;44(7):3861-3865.

256. BJR Suppl 25. *Central Axis Depth Dose Data for Use in Radiotherapy.* London: British Institute of Radiology; 1996.

257. Bedford JL, Hansen VN, Webb S. The derivation of tissue-maximum ratio from percentage depth dose requires peak scatter factor to be considered a function of source-to-surface distance. *Br J Radiol.* 1998;71(848):876-881.

258. van Battum LJ, Essers M, Storchi PR. Conversion of measured percentage depth dose to tissue maximum ratio values in stereotactic radiotherapy. *Phys Med Biol.* 2002;47(18):3289-3300.

259. Bjärngard BE, Zhu TC, Ceberg C. Tissue-phantom ratios from percentage depth doses. *Med Phys.* 1996;23(5):629-634.

260. Xiao Y, Altschuler MD, Bjarngard BE. Quality assurance of central axis dose data for photon beams by means of a functional representation of the tissue phantom ratio. *Phys Med Biol.* 1998;43:2195-2206.

261. Yang JN, Pino R. Analytical calculation of central-axis dosimetric data for a dedicated 6-MV radiosurgery linear accelerator. *Med Phys.* 2008;35:4333-4341.

262. Garcia LIR, Almansa JF. An algorithm to calculate the tissue phantom ratio from depth dose in radiosurgery. *Med Phys.* 2011;38(5):2359-2365.

263. Haider TK, el-Khatib EE. Measurements of phantom scatter factors for small field sizes in high energy x rays. *Med Phys.* 1994;21(5):663-666.

264. Ding GX, Krauss R. An empirical formula to obtain tissue-phantom ratios from percentage depth-dose curves for small fields. *Phys Med Biol.* 2013;58(14):4781-4789.

265. Yan G, Fox C, Liu C, Li JG. The extraction of true profiles for TPS commissioning and its impact on IMRT patient-specific QA. *Med Phys.* 2008;35(8):3661-3670.

266. Sahoo N, Kazi AM, Hoffman M. Semi-empirical procedures for correcting detector size effect on clinical MV x-ray beam profiles. *Med Phys.* 2008;35(11):5124-5133.

267. Higgins PD, Sibata CH, Siskind L, Sohn JW. Deconvolution of detector size effect for small field measurement. *Med Phys.* 1995;22:1663-1666.

268. Sibata CH, Mota HC, Beddar AS, Higgins PD, Shin KH. Influence of detector size in photon beam profile measurements. *Phys Med Biol.* 1991;36:621-631.

269. Wegener S, Sauer OA. Energy response corrections for profile measurements using a combination of different detector types. *Med Phys.* 2018;45(2):898-907.

270. Pittet P, Esteves J, Galvan JM, et al. SciFi detector and associated method for real-time determination of profile and output factor for small fields in stereotactic radiotherapy. *Med Phys.* 2020;47(4):1930-1939.

271. Lindsay P, Rink A, Ruschin M, Jaffray D. Investigation of energy dependence of EBT and EBT-2 gafchromic film. *Med Phys.* 2010;37(2):571-576.

272. Andres C, del Castillo A, Tortosa R, Alonso D, Barquero R. A comprehensive study of the Gafchromic EBT2 radiochromic film. A comparison with EBT. *Med Phys.* 2010;37(12):6271-6278.

273. Liu PZ, Suchowerska N, McKenzie DR. Can small field diode correction factors be applied universally? *Radiother Oncol.* 2014;112(3):442-446.

274. Fraass B, Doppke K, Hunt M, et al. American Association of Physicists in Medicine Radiation Therapy Committee Task Group 53: quality assurance for clinical radiotherapy treatment planning. *Med Phys.* 1998;25(10):1773-1829.

275. IAEA. *TRS 430: Commissioning and quality assurance of computerized planning systems for radiation treatment of cancer.* Vienna: International Atomic Energy Agency, ISBN 0074-1914; 2004.

276. Smilowitz JB, Das IJ, Feygelman V, et al. AAPM Medical Physics Practice Guideline 5.a.: Commissioning and QA of Treatment Planning Dose Calculations - Megavoltage Photon and Electron Beams. *J Appl Clin Med Phys.* 2015;16(5):14-34.

277. Chetty IJ, Curran B, Cygler JE, et al. Report of the AAPM Task Group No. 105: Issues associated with clinical implementation of Monte Carlo-based photon and electron external beam treatment planning. *Med Phys.* 2007;34(12):4818-4853.

278. Lief EP, Lutz WR. Determination of effective electron source size using multislit and pinhole cameras. *Med Phys.* 2000;27(10):2372-2375.

279. Zhu TC, Bjarngard BE. The head-scatter factor for small field sizes. *Med Phys.* 1994;21(1):65-68.

280. Sawkey DL, Faddegon BA. Determination of electron energy, spectral width, and beam divergence at the exit window for clinical megavoltage x-ray beams. *Med Phys.* 2009;36(3):698-707.

281. LoSasso T, Chui CS, Ling CC. Physical and dosimetric aspects of a multileaf collimation system used in the dynamic mode for implementing intensity modulated radiotherapy. *Med Phys.* 1998;25(10):1919-1927.

282. Mei X, Nygren I, Villarreal-Barajas JE. On the use of the MLC dosimetric leaf gap as a quality control tool for accurate dynamic IMRT delivery. *Med Phys.* 2011;38(4):2246-2255.

283. Yao W, Farr JB. Determining the optimal dosimetric leaf gap setting for rounded leaf-end multileaf collimator systems by simple test fields. *J Appl Clin Med Phys.* 2015;16(4):65-77.

284. Han Z, Hacker F, Killoran J, Kukluk J, Aizer A, Zygmanski P. Optimization of MLC parameters for TPS calculation and dosimetric verification: application to single isocenter radiosurgery of multiple brain lesions using VMAT. *Biomed Phys Eng Express.* 2020;6(1):015004.

285. Koger B, Price R, Wang D, Toomeh D, Geneser S, Ford E. Impact of the MLC leaf-tip model in a commercial TPS: Dose calculation limitations and IROC-H phantom failures. *J Appl Clin Med Phys.* 2020;21(2):82-88.

286. Chen S, Yi BY, Yang X, Xu H, Prado KL, D'Souza WD. Optimizing the MLC model parameters for IMRT in the RayStation treatment planning system. *J Appl Clin Med Phys.* 2015;16(5):322-332.

287. Boyer AL, Li S. Geometric analysis of light-field position of a multileaf collimator with curved ends. *Med Phys.* 1997;24(5):757-762.

288. Zhou D, Zhang H, Ye P. Rounded leaf end effect of multileaf collimator on penumbra width and radiation field offset: an analytical and numerical study. *Radiol Oncol.* 2015;49(3):299-306.

289. Azimi R, Alaei P, Higgins P. The effect of small field output factor measurements on IMRT dosimetry. *Med Phys.* 2012;39(8):4691-4694.

290. Younge KC, Roberts D, Janes LA, Anderson C, Moran JM, Matuszak MM. Predicting deliverability of volumetric-modulated arc therapy (VMAT) plans using aperture complexity analysis. *J Appl Clin Med Phys.* 2016;17(4):124-131.

291. Younge KC, Matuszak MM, Moran JM, McShan DL, Fraass BA, Roberts DA. Penalization of aperture complexity in inversely planned volumetric modulated arc therapy. *Med Phys.* 2012;39(11):7160-7170.

292. Ahnesjö A. Collapsed cone convolution of radiant energy for photon dose calculation in heterogeneous media. *Med Phys.* 1989;16:577-592.

293. Dawson DJ, Harper JM, Akinradewo AC. Analysis of physical parameters associated with the measurement of high-energy x-ray penumbra. *Med Phys.* 1984;11:491-497.

294. Ahnesjö A, Aspradakis MM. Dose calculations for external photon beams in radiotherapy. *Phys Med Biol.* 1999;44:R99-R155.

295. Kry SF, Feygelman V, Balter P, et al. AAPM Task Group 329: Reference dose specification for dose calculations: Dose-to-water or dose-to-muscle? *Med Phys.* 2020;47(3):e52-e64.

296. Akino Y, Das IJ, Cardenes HR, Desrosiers CM. Correlation between target volume and electron transport effects affecting heterogeneity corrections in stereotactic body radiotherapy for lung cancer. *Journal of radiation research.* 2014;55(4):754-760.

297. Xiao Y, Papiez L, Paulus R, et al. Dosimetric evaluation of heterogeneity corrections for RTOG 0236: stereotactic body tadiotherapy of inoperable stage I-II non–small-cell lung cancer. *Int J Radiat Oncol Biol Phys.* 2009;73(4):1235-1242.

298. Sterpin E, Salvat F, Olivera G, Vynckier S. Monte Carlo evaluation of the convolution/superposition algorithm of Hi-Art tomotherapy in heterogeneous phantoms and clinical cases. *Med Phys.* 2009;36(5):1566-1575.

299. Martens C, Reynaert N, De Wagter C, et al. Underdosage of the upper-airway mucosa for small fields as used in intensity-modulated radiation therapy: a comparison between radiochromic film measurements, Monte Carlo simulations, and collapsed cone convolution calculations. *Med Phys.* 2002;29(7):1528-1535.

300. Reckwerdt PJ, Mackie TR. Superposition/convolution speed improvements using run-length raytracing. *Med Phys.* 1992;19(3):784.

301. Bedford JL, Childs PJ, Nordmark Hansen V, Mosleh-Shirazi MA, Verhaegen F, Warrington AP. Commissioning and quality assurance of the Pinnacle(3) radiotherapy treatment planning system for external beam photons. *Br J Radiol.* 2003;76(903):163-176.

302. Craig J, Oliver M, Gladwish A, Mulligan M, Chen J, Wong E. Commissioning a fast Monte Carlo dose calculation algorithm for lung cancer treatment planning. *J Appl Clin Med Phys.* 2008;9(2):2702.

303. Rangel A, Ploquin N, Kay I, Dunscombe P. Towards an objective evaluation of tolerances for beam modeling in a treatment planning system. *Phys Med Biol.* 2007;52(19):6011-6025.

304. Fippel M, Haryanto F, Dohm O, Nusslin F, Kriesen S. A virtual photon energy fluence model for Monte Carlo dose calculation. *Med Phys.* 2003;30(3):301-311.

305. Aspradakis MM, Lambert GD, Steele A. Elements of commissioning step-and-shoot IMRT: delivery equipment and planning system issues posed by small segment dimensions and small monitor units. *Med Dosim.* 2005;30(4):233-242.

306. Smilowitz JB, Das IJ, Feygelman V, et al. AAPM Medical Physics Practice Guideline 5.a.: Commissioning and QA of Treatment Planning Dose Calculations - Megavoltage Photon and Electron Beams. *J Appl Clin Med Phys.* 2016;16(5):14-34.

307. Tang WL, Khan FM, Gerbi BJ. Validity of lung correction algorithms. *Med Phys.* 1986;13(5):683-686.

308. Saxena R, Higgins P. Measurement and evaluation of inhomogeneity corrections and monitor unit verification for treatment planning. *Med Dosim.* 2010;35(1):19-27.

309. Zietman AL, Palta JR, Steinberg ML. *Safety Is No Accident: A Framework for Quality Radiation Oncology and Care.* ASTRO; 2019.

310. Moran JM, Dempsey M, Eisbruch A, et al. Safety considerations for IMRT: Executive summary. *Pr Radiat Oncol.* 2011;1(3):190-195.

311. Molineu A, Hernandez N, Nguyen T, Ibbott G, Followill D. Credentialing results from IMRT irradiations of an anthropomorphic head and neck phantom. *Med Phys.* 2013;40(2):022101.

312. Kry SF, Alvarez P, Molineu A, Amador C, Galvin J, Followill DS. Algorithms used in heterogeneous dose calculations show systematic differences as measured with the Radiological Physics Center's anthropomorphic thorax phantom used for RTOG credentialing. *Int J Radiat Oncol Biol Phys.* 2013;85(1):e95-e100.

313. Haider TK, El-Khatib EE. Differential scatter integration in regions of electronic non-equilibrium. *Phys Med Biol.* 1995;40:31-43.

314. Krieger T, Sauer OA. Monte Carlo- versus pencil-beam-/collapsed-cone-dose calculation in a heterogeneous multi-layer phantom. *Phys Med Biol.* 2005;50(5):859-868.

315. Carrasco P, Jornet N, Duch MA, et al. Comparison of dose calculation algorithms in slab phantoms with cortical bone equivalent heterogeneities. *Med Phys.* 2007;34(8):3323-3333.

316. Carrasco P, Jornet N, Dutch MA, et al. Comparison of dose calculation algorithms in phantoms with lung equivalent heterogeneities under conditions of lateral electronic disequilibrium. *Med Phys.* 2004;31(10):2899-2911.

317. Fogliata A, Vanetti E, Albers D, et al. On the dosimetric behaviour of photon dose calculation algorithms in the presence of simple geometric heterogeneities: comparison with Monte Carlo calculations. *Phys Med Biol.* 2007;52(5):1363-1385.

318. Paelinck L, Reynaert N, Thierens H, De Neve W, De Wagter C. Experimental verification of lung dose with radiochromic film: comparison with Monte Carlo simulations and commercially available treatment planning systems. *Phys Med Biol.* 2005;50(9):2055-2069.

319. Vanderstraeten B, Reynaert N, Paelinck L, et al. Accuracy of patient dose calculation for lung IMRT: A comparison of Monte Carlo, convolution/superposition, and pencil beam computations. *Med Phys.* 2006;33(9):3149-3158.

320. Li T, Scheuermann R, Lin A, et al. Impact of multi-leaf collimator parameters on Head and Neck plan quality and delivery: A comparison between Halcyon and Truebeam(R) treatment delivery systems. *Cureus.* 2018;10(11):e3648.

321. JCGM-Joint Committee for Guides in Metrology. *Evaluation of measurement data - Guide to the expression of uncertainty in measurement JCGM 100:2008.* Vol 100. Cedex FRANCE: BIPM: Bureau International des Poids et Mesures; 2008.

322. Bassinet C, Huet C, Derreumaux S, et al. Small fields output factors measurements and correction factors determination for several detectors for a CyberKnife(R) and linear accelerators equipped with microMLC and circular cones. *Med Phys.* 2013;40(7):071725.

323. Mirzakhanian L, Bassalow R, Huntzinger C, Seuntjens J. Extending the IAEA-AAPM TRS-483 methodology for radiation therapy machines with field sizes down to 10×2 cm^2. *Med Phys.* 2020;47(10):5209-5221.

324. Wulff J, Heverhagen JT, Zink K, Kawrakow I. Investigation of systematic uncertainties in Monte Carlo-calculated beam quality correction factors. *Phys Med Biol.* 2010;55(16):4481-4493.

325. Bouchard H, Seuntjens J, Kawrakow I. A Monte Carlo method to evaluate the impact of positioning errors on detector response and quality correction factors in nonstandard beams. *Phys Med Biol.* 2011;56(8):2617-2634.

326. Andreo P, Burns DT, Salvat F. On the uncertainties of photon mass energy-absorption coefficients and their ratios for radiation dosimetry. *Phys Med Biol.* 2012;57(8):2117-2136.

327. Looe HK, Busing I, Tekin T, et al. The polarity effect of compact ionization chambers used for small field dosimetry. *Med Phys.* 2018;45(12):5608-5621.

328. Larraga-Gutierrez JM. Experimental determination of field factors ([Formula: see text]) for small radiotherapy beams using the daisy chain correction method. *Phys Med Biol.* 2015;60(15):5813-5831.

329. Verhaegen F, Das IJ, Palmans H. Monte Carlo dosimetry study of 6 MV stereotactic radiosurgery unit. *Phys Med Biol.* 1998;43:2755-2768.

330. Reynolds M, Fallone BG, Rathee S. Dose response of selected solid state detectors in applied homogeneous transverse and longitudinal magnetic fields. *Med Phys.* 2014;41(9):092103.

331. Followill DS, Kry SF, Lihong Q, et al. The Radiological Physics Center's standard dataset for small field size output factors. *J Appl Clin Med Phys.* 2012;13(5):782-289.

332. Followill DS. Erratum: "The Radiological Physics Center's standard dataset for small field size output factors". *J Appl Clin Med Phys.* 2014;15(2):4757.

333. del Mar Espinosa M, Nunez L, Muniz JL, Lagares JI, Embid M, Gomez-Ros JM. Postal dosimetry audit test for small photon beams. *Radiother Oncol.* 2012;102(1):135-141.

Table I. Reference and minimum collimator settings available on radiotherapy treatment units delivering small photon fields. See main text for the definition of machine-specific-reference field.

Treatment unit	**Delivery technique**	**Minimum field size**	**Machine-specific-reference (*msr*) field (cm^2)**	**Relevant Task Group report**
Linac	IMRT/VMAT	0.1 x 0.1 cm^2	10 × 10	Ref.[20,65]
Linac	SRS	0.5 cm diameter cone	10 × 10	Ref.[6,10,66]
Linac*	SBRT	0.1 x 0.5 cm^2	10 × 10	TG-101[8,67]
Tomotherapy	IMRT	1 × 40 cm^2	5 × 40	TG-148[68]
CyberKnife (CK)**	IMRT	0.5 cm diameter	6.0 cm diameter	TG-135[11]
Gamma Knife	SRS	0.4 cm diameter	1.6 or 1.8 cm diameter cone	Ref.[6,7]

*Within their planning and delivery systems, each institution is able to administratively control their preferred smallest field setting for commissioning of the MLC/microMLC for SRS/SBRT techniques.

**For CK, the current minimum clinically used cone diameter is 4 mm (@ 65 cm SAD for trigeminals). The new generation of MLC-shaped CK machines include the capability of 10x10 cm^2 field size as noted in the Canadian report on CK by Vandervoort et al.[69]

Table II. Values of r_{LCPE} for various beams calculated with the Monte Carlo method, where r_{LCPE} is the minimum beam radius to achieve complete lateral electron equilibrium in water.[21]

Beam	$TPR_{20,10}$	$\%dd(10\text{ cm})_x$	r_{LCPE} (cm)		
			$TPR_{20,10}$ (Eq. 6)	$\%dd(10\text{ cm})_x$ (Eq. 7)	d_{max} (Eq. 9)
Co^{60}	0.579	58.7	0.5	0.5	0.5
6 MV	0.670	66.2	1.2	1.1	1.1
10 MV	0.732	73.5	1.7	1.6	1.7
15 MV	0.765	77.9	2.0	2.0	2.0
24 MV	0.805	83.0	2.4	2.4	2.5

Figure 1

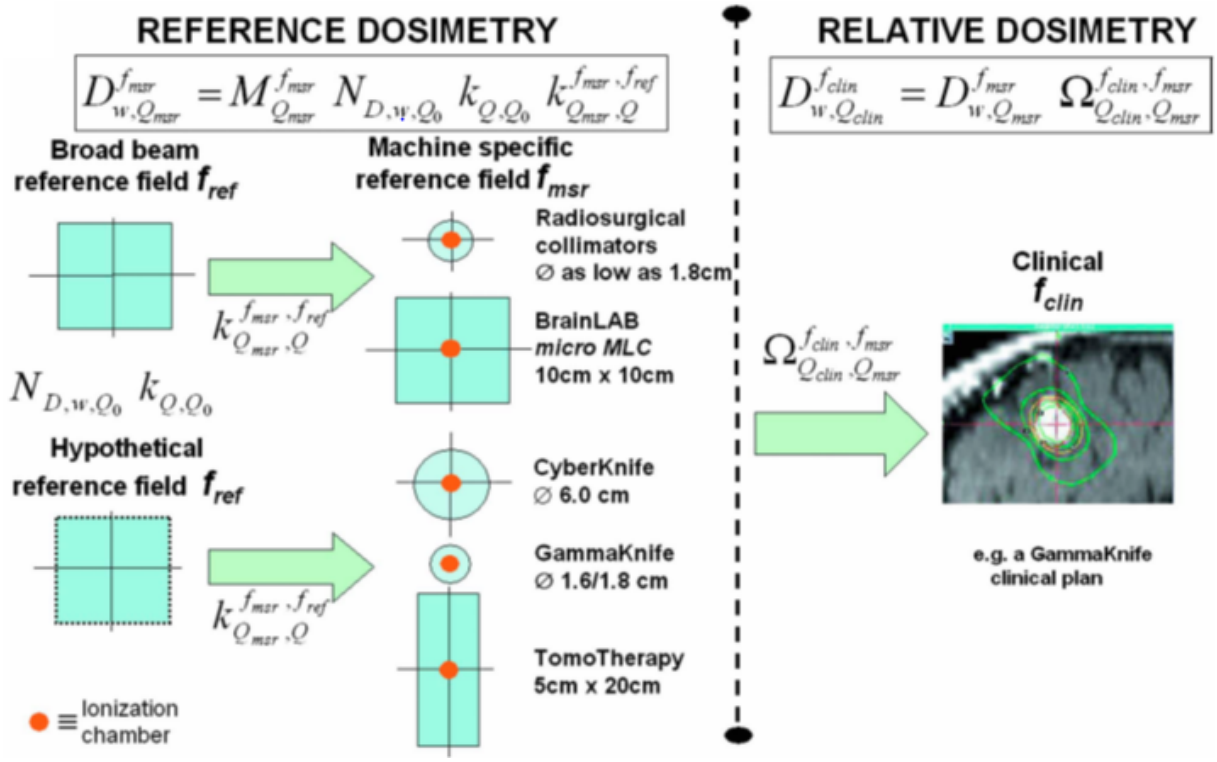
REFERENCE DOSIMETRY
$D^{f_{msr}}_{w,Q_{msr}} = M^{f_{msr}}_{Q_{msr}} N_{D,w,Q_0} k_{Q,Q_0} k^{f_{msr},f_{ref}}_{Q_{msr},Q}$
RELATIVE DOSIMETRY
$D^{f_{clin}}_{w,Q_{clin}} = D^{f_{msr}}_{w,Q_{msr}} \Omega^{f_{clin},f_{msr}}_{Q_{clin},Q_{msr}}$
Broad beam reference field f_{ref}
Machine specific reference field f_{msr}
Radiosurgical collimators ∅ as low as 1.8cm
BrainLAB micro MLC 10cm x 10cm
$k^{f_{msr},f_{ref}}_{Q_{msr},Q}$
N_{D,w,Q_0} k_{Q,Q_0}
Hypothetical reference field f_{ref}
CyberKnife ∅ 6.0 cm
GammaKnife ∅ 1.6/1.8 cm
TomoTherapy 5cm x 20cm
≡ Ionization chamber
$\Omega^{f_{clin},f_{msr}}_{Q_{clin},Q_{msr}}$
Clinical f_{clin}
e.g. a GammaKnife clinical plan

Figure 2

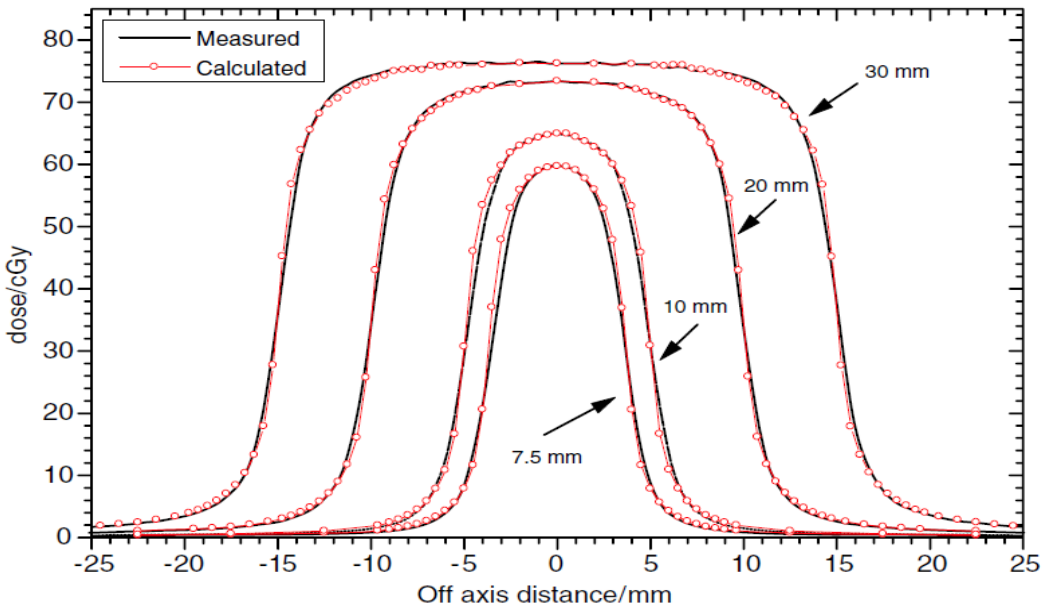
Measured
Calculated
30 mm
20 mm
10 mm
7.5 mm
dose/cGy
Off axis distance/mm
0
10
20
30
40
50
60
70
80
-25
-20
-15
-10
-5
0
5
10
15
20
25

Figure 3

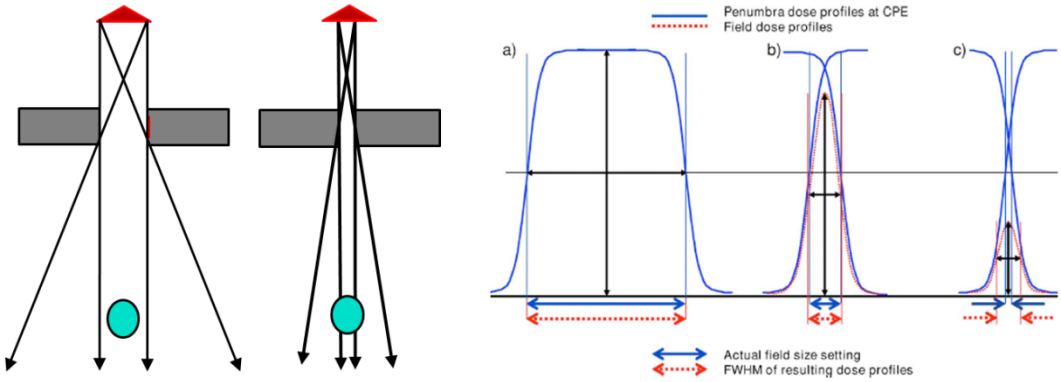
Penumbra dose profiles at CPE
Field dose profiles
a)
b)
c)
Actual field size setting
FWHM of resulting dose profiles

Figure 4

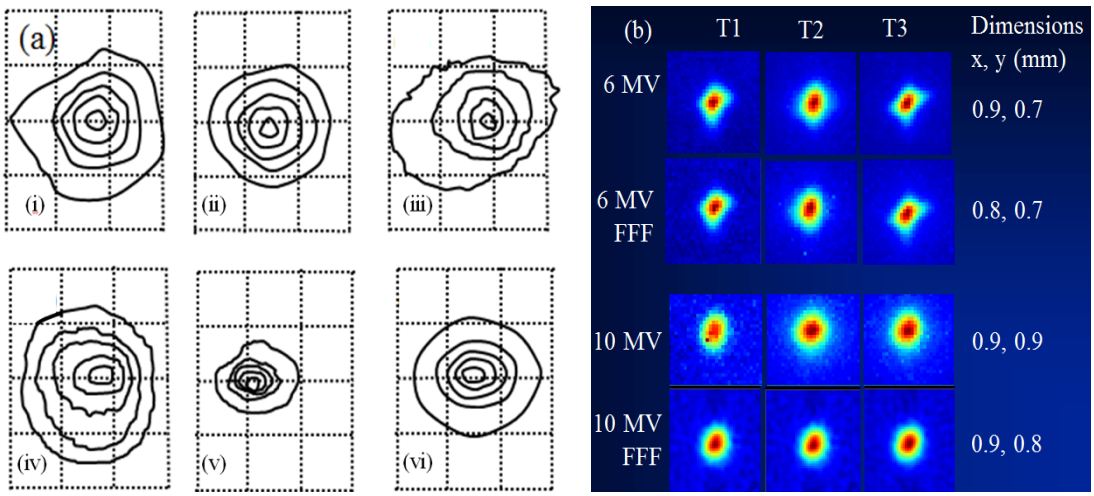
(a)
(i)
(ii)
(iii)
(iv)
(v)
(vi)
(b)
T1
T2
T3
Dimensions
x, y (mm)
6 MV
0.9, 0.7
6 MV
FFF
0.8, 0.7
10 MV
0.9, 0.9
10 MV
FFF
0.9, 0.8

Figure 5

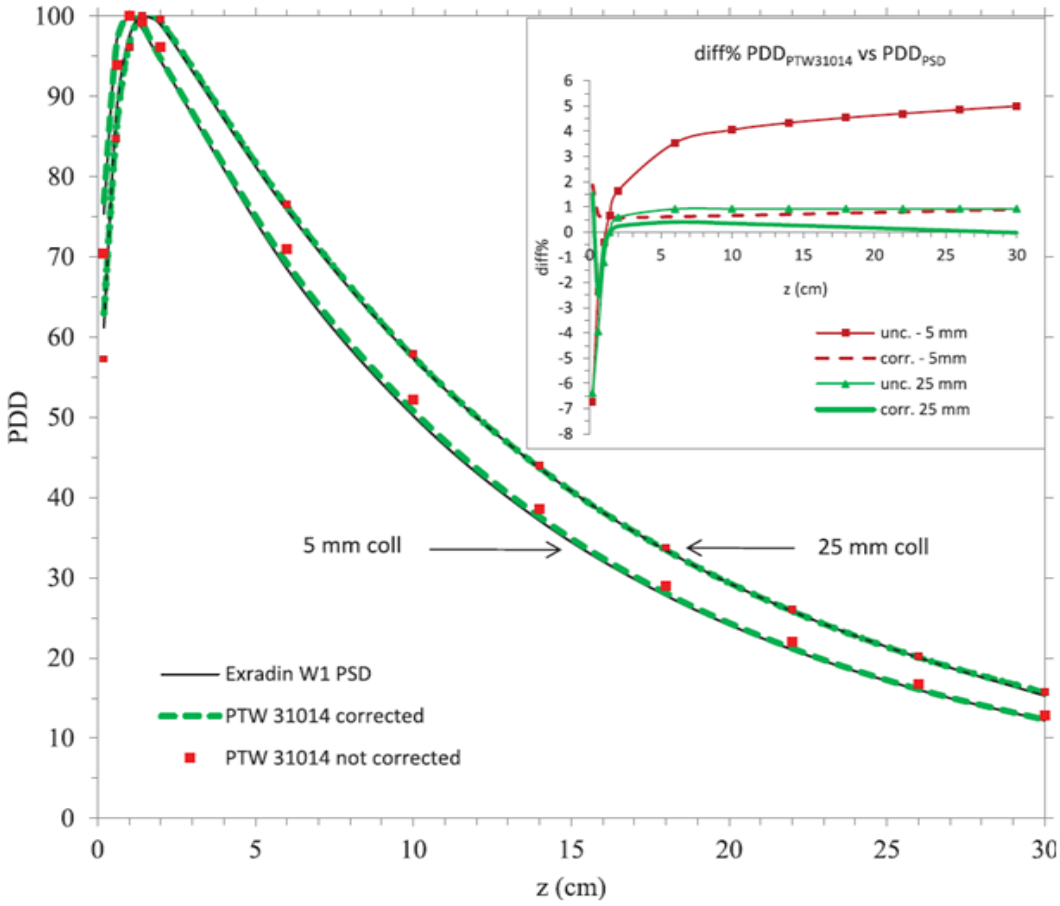
PDD
z (cm)
5 mm coll
25 mm coll
Exradin W1 PSD
PTW 31014 corrected
PTW 31014 not corrected
diff% PDD$_{PTW31014}$ vs PDD$_{PSD}$
diff%
unc. - 5 mm
corr. - 5mm
unc. 25 mm
corr. 25 mm

Figure 6

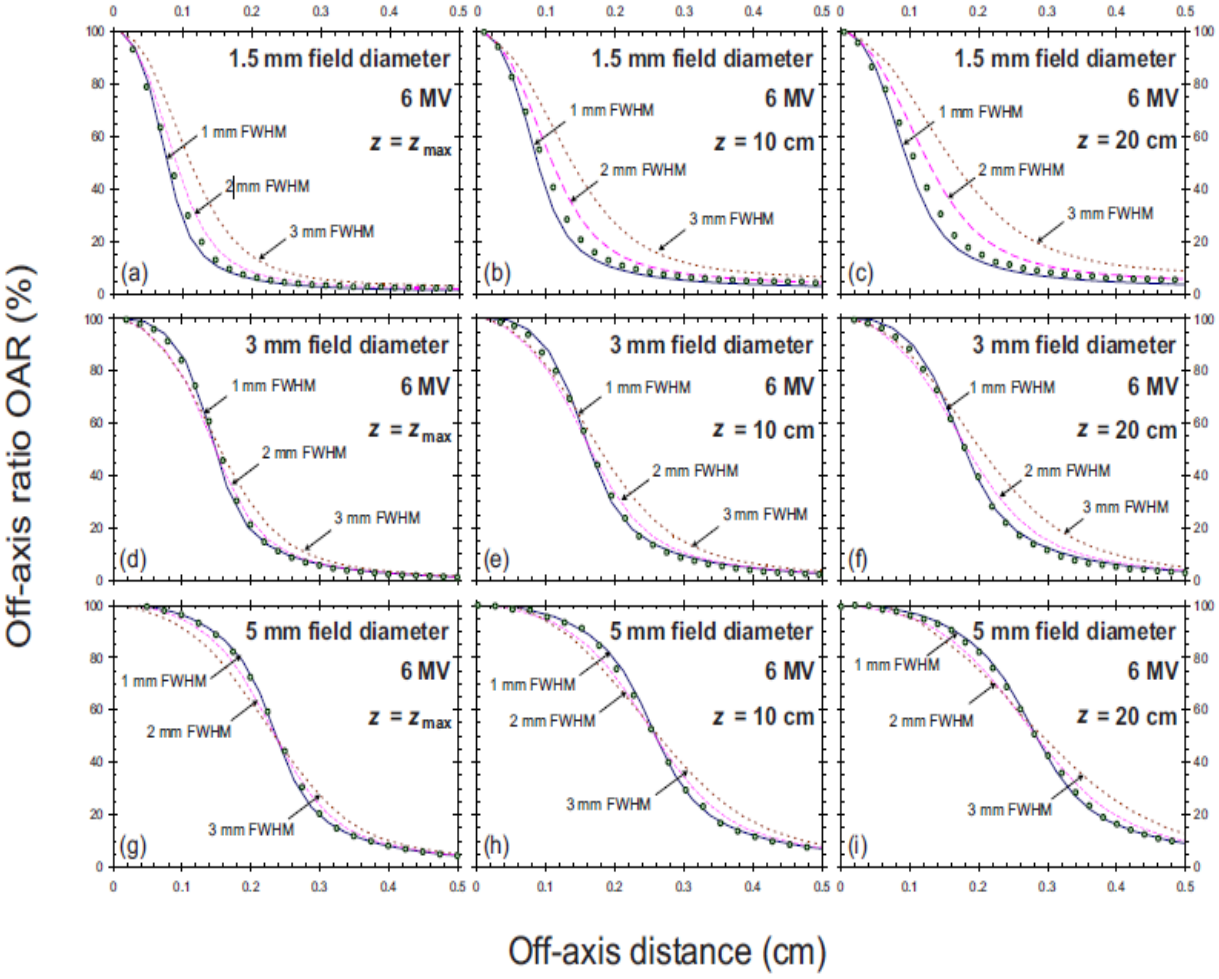
1.5 mm field diameter
6 MV
z = z max
1 mm FWHM
2 mm FWHM
3 mm FWHM
(a)
1.5 mm field diameter
6 MV
z = 10 cm
1 mm FWHM
2 mm FWHM
3 mm FWHM
(b)
1.5 mm field diameter
6 MV
z = 20 cm
1 mm FWHM
2 mm FWHM
3 mm FWHM
(c)
3 mm field diameter
6 MV
z = z max
1 mm FWHM
2 mm FWHM
3 mm FWHM
(d)
3 mm field diameter
6 MV
z = 10 cm
1 mm FWHM
2 mm FWHM
3 mm FWHM
(e)
3 mm field diameter
6 MV
z = 20 cm
1 mm FWHM
2 mm FWHM
3 mm FWHM
(f)
5 mm field diameter
6 MV
z = z max
1 mm FWHM
2 mm FWHM
3 mm FWHM
(g)
5 mm field diameter
6 MV
z = 10 cm
1 mm FWHM
2 mm FWHM
3 mm FWHM
(h)
5 mm field diameter
6 MV
z = 20 cm
1 mm FWHM
2 mm FWHM
3 mm FWHM
(i)
Off-axis ratio OAR (%)
Off-axis distance (cm)

Figure 7

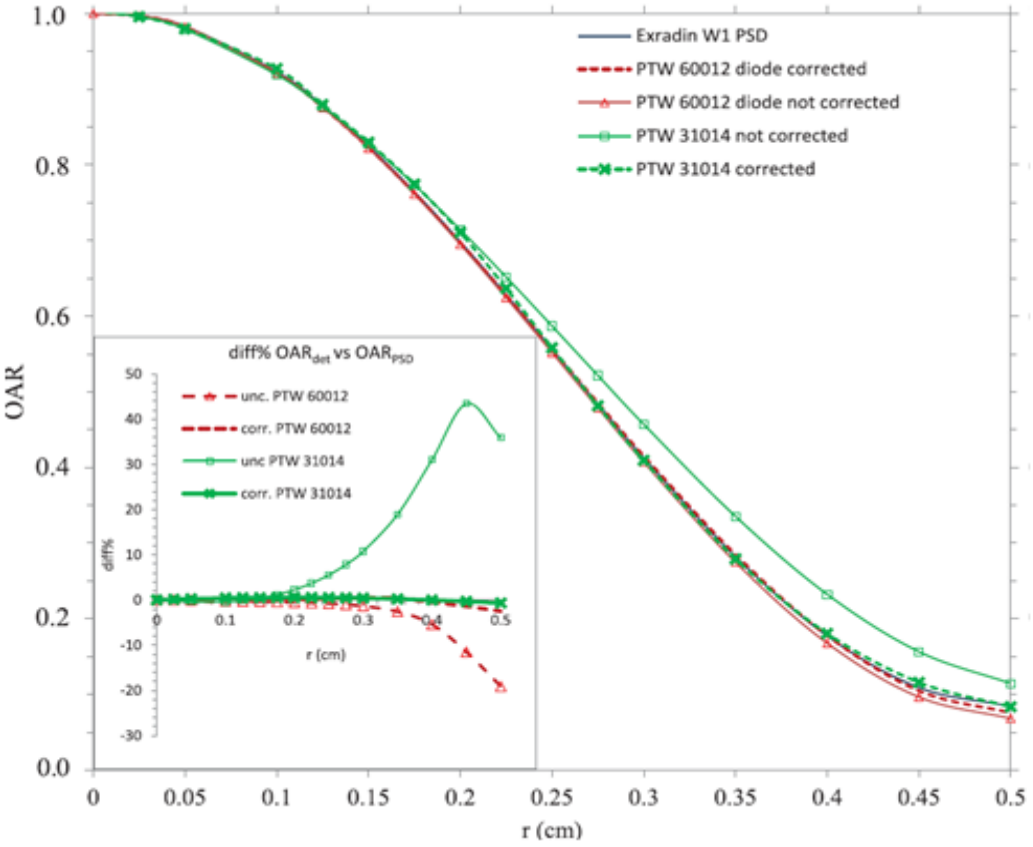
Exradin W1 PSD
PTW 60012 diode corrected
PTW 60012 diode not corrected
PTW 31014 not corrected
PTW 31014 corrected
OAR
r (cm)
diff% OAR_det vs OAR_PSD
unc. PTW 60012
corr. PTW 60012
unc PTW 31014
corr. PTW 31014
diff%
r (cm)

Figure 8

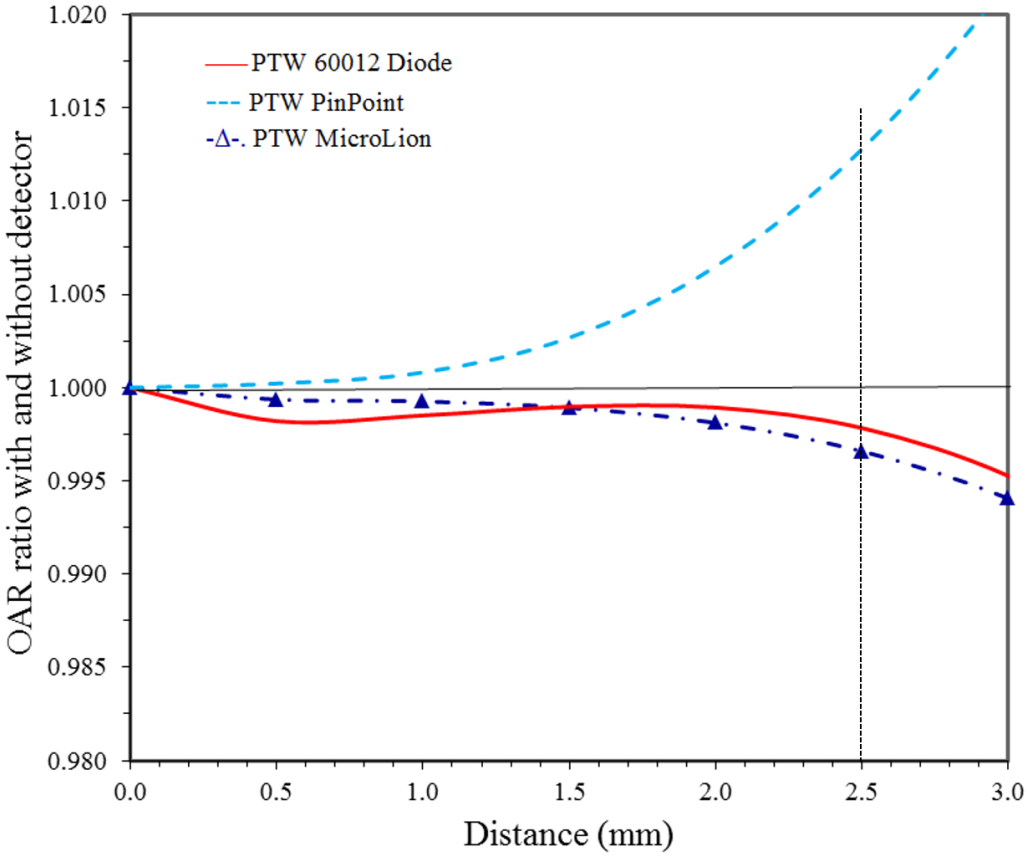
PTW 60012 Diode
PTW PinPoint
PTW MicroLion
OAR ratio with and without detector
1.020
1.015
1.010
1.005
1.000
0.995
0.990
0.985
0.980
0.0
0.5
1.0
1.5
2.0
2.5
3.0
Distance (mm)

Figure 9

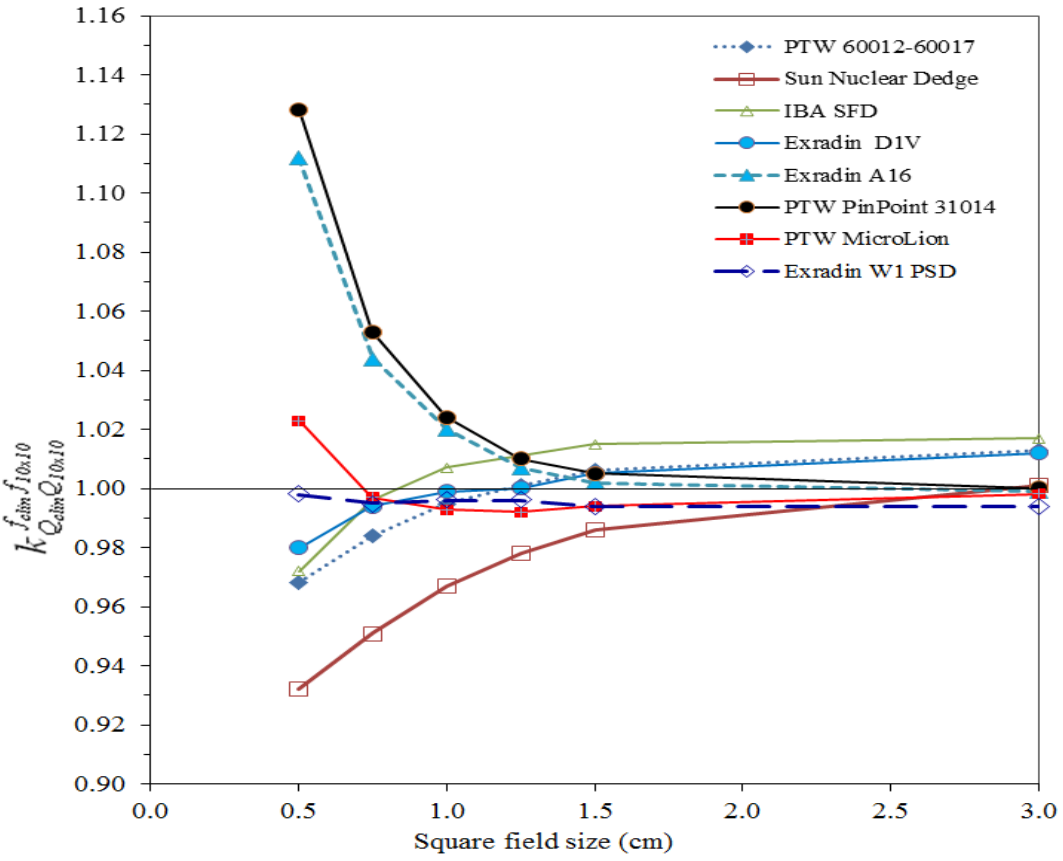
PTW 60012-60017
Sun Nuclear Dedge
IBA SFD
Exradin D1V
Exradin A16
PTW PinPoint 31014
PTW MicroLion
Exradin W1 PSD
1.16
1.14
1.12
1.10
1.08
1.06
1.04
1.02
1.00
0.98
0.96
0.94
0.92
0.90
0.0
0.5
1.0
1.5
2.0
2.5
3.0
Square field size (cm)

Figure 10

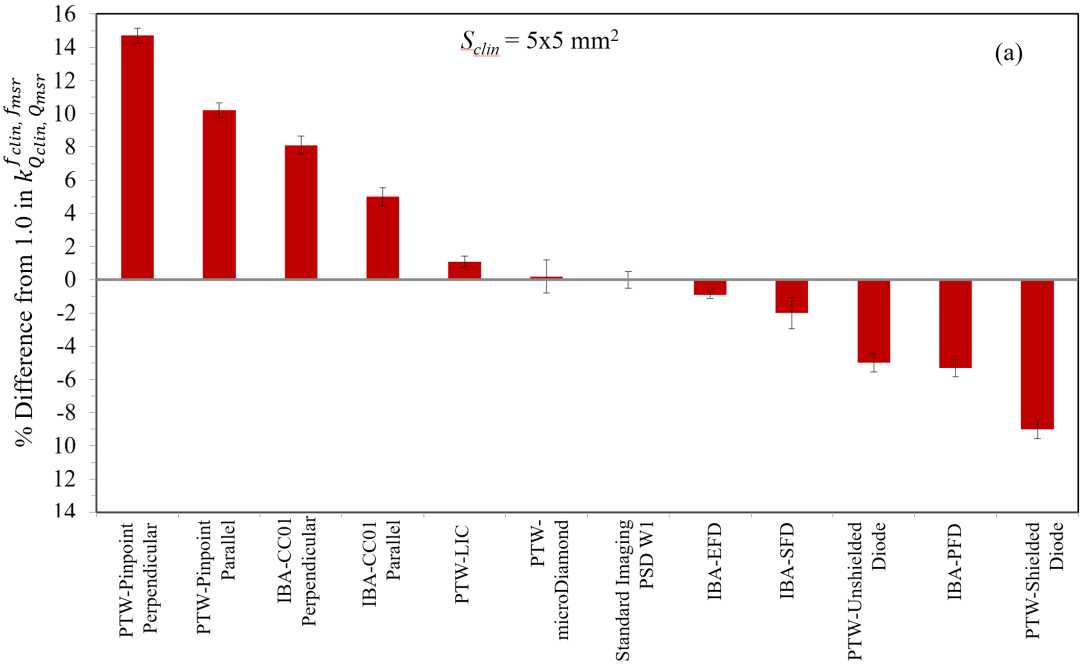
S_{clin} = 5x5 mm^2
(a)
% Difference from 1.0 in $k^{f_{clin},f_{msr}}_{Q_{clin},Q_{msr}}$
16
14
12
10
8
6
4
2
0
-2
-4
-6
-8
10
12
14
PTW-Pinpoint Perpendicular
PTW-Pinpoint Parallel
IBA-CC01 Perpendicular
IBA-CC01 Parallel
PTW-LIC
PTW-microDiamond
Standard Imaging PSD W1
IBA-EFD
IBA-SFD
PTW-Unshielded Diode
IBA-PFD
PTW-Shielded Diode

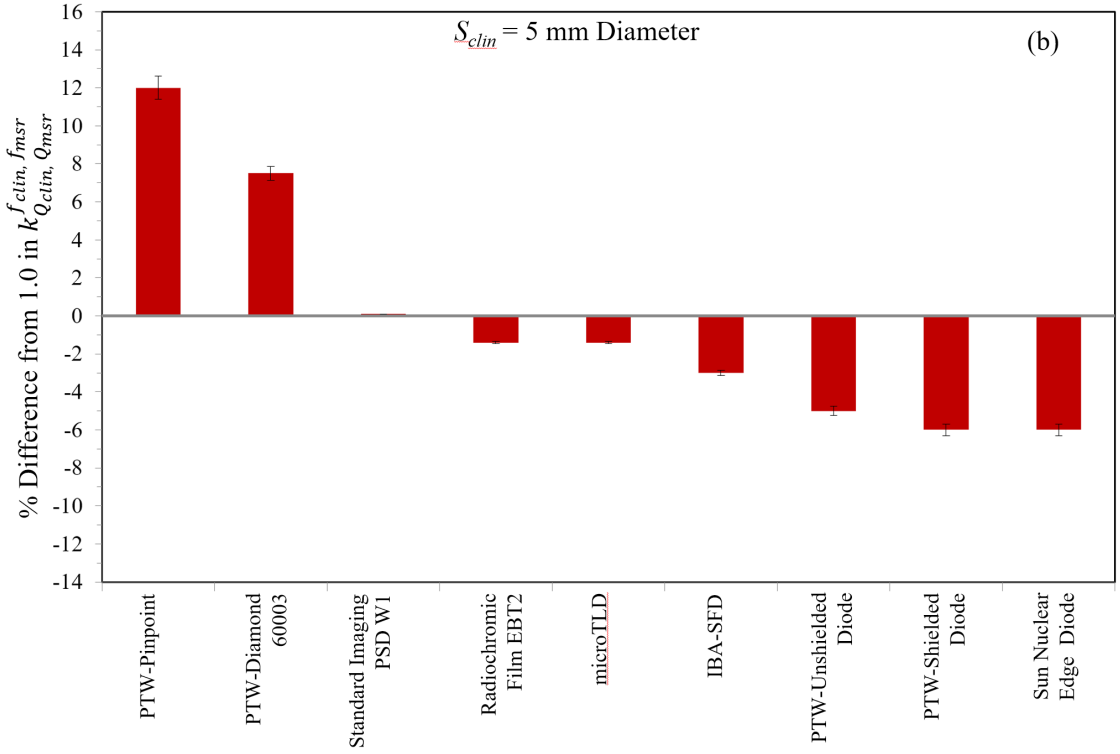
S_{clin} = 5 mm Diameter
(b)
% Difference from 1.0 in $k^{f_{clin},f_{msr}}_{Q_{clin},Q_{msr}}$
16
14
12
10
8
6
4
2
0
-2
-4
-6
-8
-10
-12
-14
PTW-Pinpoint
PTW-Diamond 60003
Standard Imaging PSD W1
Radiochromic Film EBT2
microTLD
IBA-SFD
PTW-Unshielded Diode
PTW-Shielded Diode
Sun Nuclear Edge Diode

Figure 11

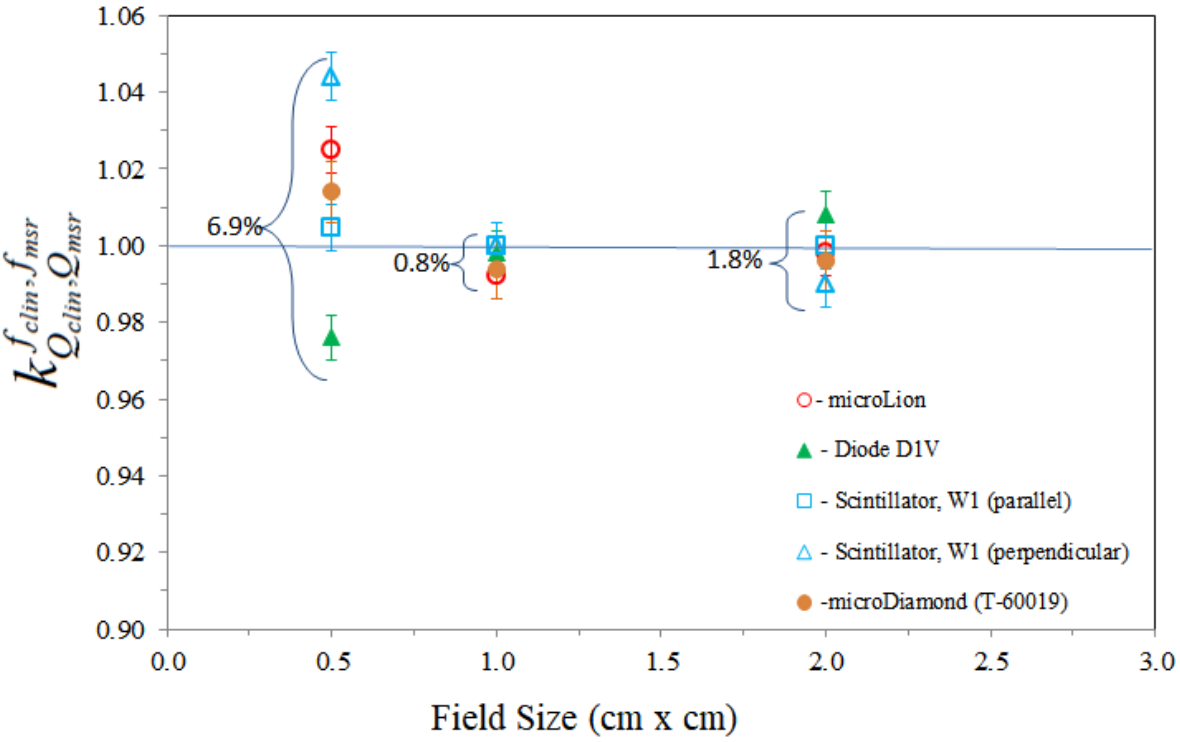
1.06
1.04
1.02
1.00
0.98
0.96
0.94
0.92
0.90
$k_{Q_{clin},Q_{msr}}^{f_{clin},f_{msr}}$
6.9%
0.8%
1.8%
0.0
0.5
1.0
1.5
2.0
2.5
3.0
Field Size (cm x cm)
- microLion
- Diode D1V
- Scintillator, W1 (parallel)
- Scintillator, W1 (perpendicular)
-microDiamond (T-60019)

Figure 12

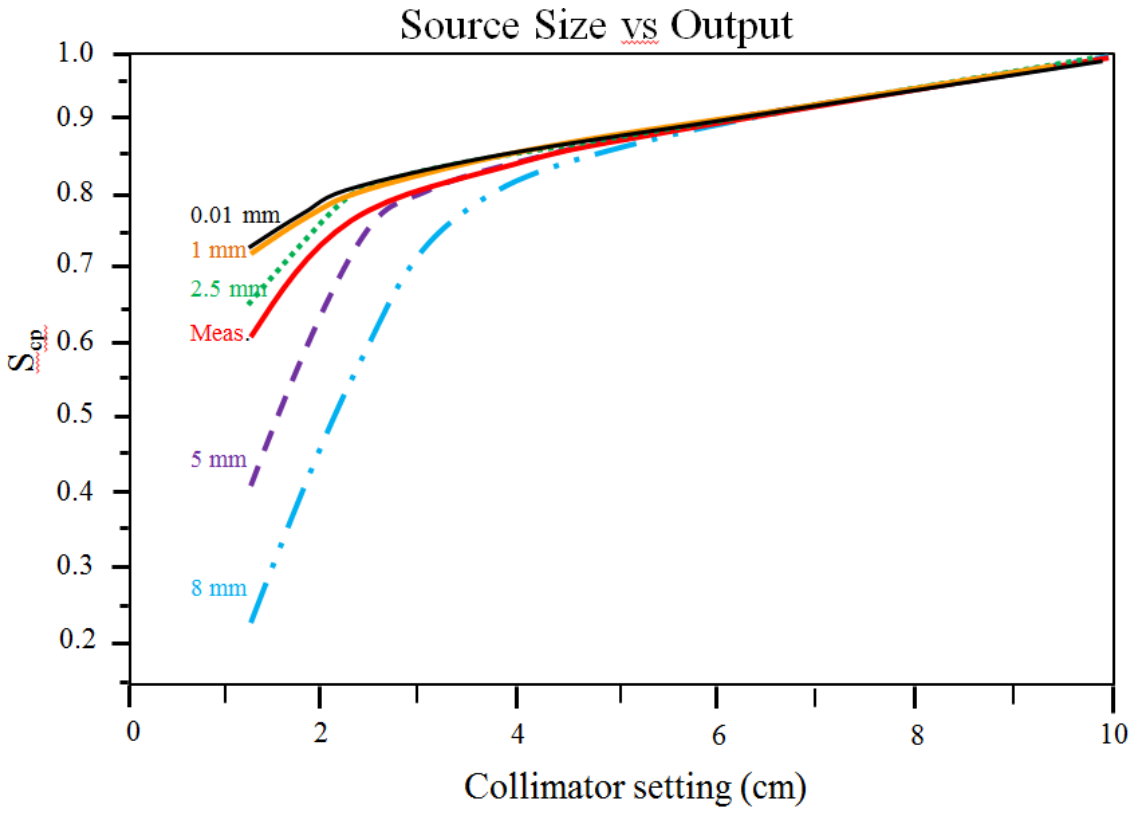
Source Size vs Output
1.0
0.9
0.8
0.7
0.6
0.5
0.4
0.3
0.2
S_{cp}
0.01 mm
1 mm
2.5 mm
Meas.
5 mm
8 mm
0
2
4
6
8
10
Collimator setting (cm)

Figure 13

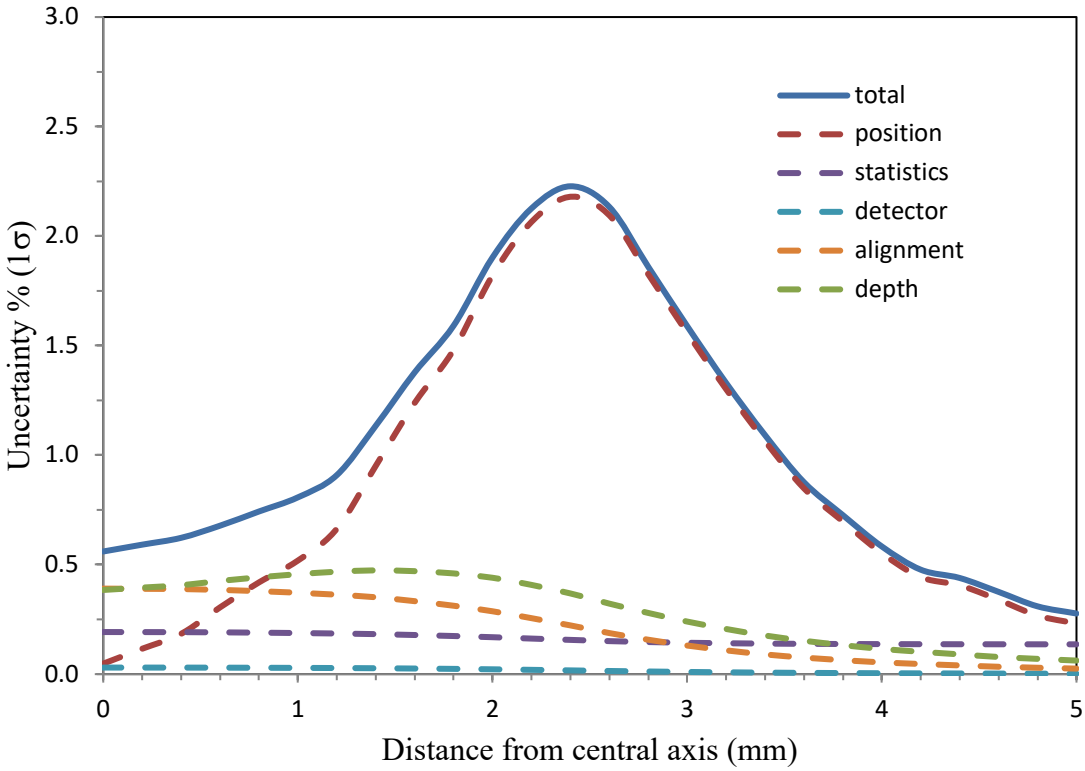
3.0
2.5
2.0
1.5
1.0
0.5
0.0
Uncertainty % (1σ)
0
1
2
3
4
5
Distance from central axis (mm)
total
position
statistics
detector
alignment
depth